KIF11 Silencing and Inhibition Induces Chromosome Instability in Human Cells

by

Yasamin Asbaghi

A Thesis submitted to the Faculty of Graduate Studies of
The University of Manitoba
in partial fulfillment of the requirements of the degree of

MASTER OF SCIENCE

Department of Biochemistry and Medical Genetics
University of Manitoba
Winnipeg

TABLE OF CONTENTS

ABSTRACT

Chromosome Instability (CIN) is defined as an increase in the rate at which whole chromosomes or large parts are gained or lost. CIN is not only associated with virtually all tumor types, but it is associated with aggressive tumors, tumor recurrence, acquisition of multidrug resistance and poor patient prognosis. However, the genes and molecular defects that contribute to CIN are poorly understood. I hypothesize that *KIF11* is an essential gene for chromosomes integrity during mitosis and therefore any defect in *KIF11* expression or function will induce CIN and contribute to tumorigenesis. Accordingly, *KIF11* was either silenced using siRNA or inhibited using monastrol within two distinct human cell lines and was investigated for CIN associated phenotypes. Here, I have identified and validated *KIF11* as a novel CIN gene. This study represents the first steps necessary to identify and develop novel treatments design to target origins of CIN in CIN associated cancers.

ACKNOWLEDGMENTS

First and foremost, I wish to express my sincere gratitude to Dr. Kirk J. McManus for his excellent supervision and for giving me the opportunity to train and study under his guidance. I would also like to thank him for his continues advice and support over the years of gathering data and writing this thesis. His extensive knowledge with his time facilitated this research project and allowed me to accomplish this degree. I feel truly privileged to have been a member in his laboratory.

I acknowledge and thank my committee members Dr. Sabine Hombach-Klonisch and Dr. R. Daniel Gietz for their helpful suggestions and valuable time during my studies at the University of Manitoba.

I would especially like to thank the following individuals who have been particularly helpful and supportive throughout this thesis: Zelda Lichtensztejn, Laura Thompson, Brent Guppy, and Sajesh Babu. Thanks to Erin McAndrew, Lucile Jeusset and Amy Cisyk for being more than a teammate for me and for being always there when I needed someone to talk to. Additionally, I would like to thank all other members of the McManus lab both past and present including Nicole Wilkinson, Tarik Leylek, Allison Baergen, Megan Neufeld, Signe Penner-Goeke, and Aaron MacAulay.

To my mother and brother, I wish to express my warmest gratitude for all the support they have given me throughout my life even when they are thousand kilometres away. I must thank Hamid for his love and support without which I would not be where I am today. Finally, this is for my late father who is in my heart forever.

This research was funded through operating grants from Natural Sciences and Engineering Research Council (NSERC) and CancerCare Manitoba Foundation. Additional funding for graduate studies was provided by the University of Manitoba through the Graduate Enhancement of Tri-Council Stipends (GETS) program, International Graduate Student Entrance Scholarship (IGSES), and the Presidents Graduate Scholarship in Human Genetics.

LIST OF TABLES

LIST OF FIGURES

LIST OF ABBREVIATIONS

~	Approximately
ºC	Degrees Celsius
2D	Two dimensional
3D	Three dimensional
aa	Amino acids
APC/C	Anaphase promoting complex/cyclosome
ATM	Ataxia telangiectasia mutated
ATR	Ataxia telangiectasia and Rad3 related
BCA	Bicinchoninic acid
CCD	Charge-coupled device
CDC25	Cell division cycle 25
CDK4/6	Cyclin dependent kinase 4/6
CHK2	Checkpoint kinase 2
CIN	Chromosome instability
cm	Centimetre
CPTS	Copper phthalocyanine 3, 4', 4'', 4'''-tetrasulfonic acid tetrasodium salt
CRC	Colorectal cancer
Cy3	Cyanine 3
DAPI	4',6-diamidino-2-phenylindole
DMEM	Dulbecco's modified Eagle's medium
DMSO	Dimethyl sulfoxide
DNA	Deoxyribonucleic acid
DSB	Double strand break
EDTA	Ethylenediaminetetraacetic Acid
FBS	Fetal bovine serum
FC	Flow cytometry
G	Goat
G1-pm	G1-postmitotic
G1-ps	G1-pre S phase
GCR	Gross chromosomal rearrangement
GFP	Green florescent protein
h	Hour(s)
HNPCC	Hereditary nonpolyposis colon cancer
HRP	Horseradish peroxidase
IC_{50}	Inhibitory concentration 50
IIF	Indirect immunofluorescence
kb	Kilo base
kDa	Kilo Dalton
KIF11	Kinesin family member 11

KS	Kolmogorov-Smirnov
M	Mouse
MCC	Mitotic checkpoint complex
MCS	Mitotic chromosome spread
mg	Milligram (weight)
min	Minute(s)
mL	Millilitre (volume)
mM	Millimolar (concentration)
MMR	Mismatch repair
MN	Micronucleus
MNF	Micronucleus formation
MS	Mitotic spread
MSI	Microsatellite instability
MYT1	Myelin Transcription Factor 1
n	Number of technical replicates
N	Number of biological replicates
N/A	Not applicable
NA	Nuclear area
Neck9	NIMA related kinase 9
nM	Nanomolar
PBS	Phosphate buffered saline
Pg.	Page
PLK1	Polo like kinase 1
PVDF	Polyvinylidene difloride
R	Restriction
RB	Retinoblastoma
Rb	Rabbit
RFP	Red florescent protein
RNA	Ribonucleic acid
RTCA	Real-time cellular analyses
SAC	Spindle assembly checkpoint
SD	Standard deviation
SDS/DTT	Sodium dodecyl sulfate/dithiothreitol
siRNA	Small interfering RNA
SL	Synthetic lethal
SSB	Single strand break
t	Time(s)
TBST	Tris-Buffered saline and Tween 20
TCGA	The cancer genome atlas
TERT	Telomerase reverse transcriptase
TP53	Tumor protein 53

WB	Western blot
ɤ-TuRC	ɤ-tubulin ring complex
µL	Microliter (volume)
µm	Micrometer
µM	Micromolar (concentration)

CHAPTER 1: INTRODUCTION

1.1 Introduction

Cancer is one of the major causes of mortality worldwide, yet despite the extensive efforts there is no effective cure for most patients. Due to defects within numerous genes and cellular pathways that contribute to oncogenesis, there is no single treatment that can be applied to all cancer patients. However, since genome instability is a well-established driving force in tumorigenesis, it could perhaps be exploited for therapeutic benefit. Accordingly, understanding and characterizing the aberrant origins underlying genome instability is a critical first step required to develop therapeutic treatments against that may be applicable in a large proportion of cancers.

Genome instability is a general term that most frequently refers to aberrant events that impact genome integrity and includes high mutation rates, chromosomal rearrangements, and chromosomal gains and/or losses[1]. While genome instability is estimated to be prevalent in up to 95% of all cancers, it is arguably best understood in the context of colorectal cancer (CRC)[2]. In general, there are two types of genome instability; 1) small scale changes involving short segments of nucleotides stemming from defect in mismatch repair and referred to as microsatellite instability (MSI)[3], and 2) large scale changes that reflect changes in chromosome numbers or large chromosomal fragments which is referred to as chromosome instability (CIN)[4]. Of these two types of genome instability, CIN is the predominant form, and occurs in up to 85% of sporadic, or randomly arising CRCs, whereas MSI only occurs in ~15%[5]. Moreover, while the aberrant molecular events causing MSI are well known and arise from defects in the DNA mismatch repair (MMR) pathway, the mutated genes and aberrant pathways giving rise to CIN remain largely unknown. Accordingly, identifying and characterizing the mutated genes and aberrant pathways driving CIN (i.e. the pathogenic origins) are critical and essential first steps in the development of

novel therapeutic strategies and targets that exploit those abnormal origins. This thesis begins to address the pathogenic origins of CRC by identifying and validating a novel CIN gene, *KIF11* (Kinesin Family Member 11) that is normally required for genome integrity.

1.2 Microsatellite Instability

MSI arises due to aberrant expression or function of four members (MSH2, MLH1, PMS2, MSH6) of the MMR pathway. Inactivation of any of these genes (*e.g. MLH1*) typically occurs via gene mutation (premature truncation) or promoter hypermethylation[6,7]. The MMR proteins are responsible for recognizing and repairing base mismatches or short deletions or insertions arising as a result of slipped strand mispairing that occurs during DNA replication. Cells with defective MMR are unable to effect appropriate repair and therefore accumulate errors that lead to DNA sequence changes at microsatellites, but also within genes such as tumor suppressor genes. Germline mutations in MMR genes (e.g. *MSH2, MLH1, PMS1, and PMS2*) are associated with a predisposition to develop hereditary nonpolyposis colon cancer (HNPCC) or Lynch Syndrome[8], but MMR gene mutations and *MLH1* promoter hypermethylation also occur in up to 15% of all sporadic CRCs[5].

The MMR pathway is evolutionary conserved from prokaryotes to eukaryotes. Although the pathway in eukaryotes is not completely understood, it is well characterized in prokaryotes especially in *Escherichia coli.* In general, there are a number of proteins involved in MMR responsible for mismatch recognition, DNA excision, and DNA replication. MutS heterodimer complex is responsible for recognition of DNA mismatch in both prokaryotes and eukaryotes[9]. In eukaryotes, there are generally two types of MutS complexes, MutSα containing MSH2 and MSH6 proteins, and MutSβ containing MSH2 and MSH3 proteins[10]. While the MutSα complex is responsible for recognition of single-nucleotide insertion/deletion mismatches, base-base

mispairs, and insertion/deletion of up to 2-8 nucleotides in length, the MutSβ complex is responsible for recognition of insertion/deletion of longer stretches of insertions/deletions (2-8 nucleotides and beyond) and thus its function is only partially redundant with MutSα[11]. Following the recognition of the mismatch nucleotide(s), the MutS complex recruits MutLα (MLH1 and PMS2) in an ATP dependent fashion. In *E. coli* MutL acts as a structural matchmaker between MutS and MutH an additional protein required for efficient MMR. In prokaryotes, MutH functions in strand discrimination and functions to distinguish the methylated template strand from the unmethylated, nascently synthesized daughter strand. Interestingly, there is no MutH equivalent in higher eukaryotes, and thus it is currently unclear how strand discrimination is accomplished in humans. Nevertheless, strand discrimination of the nascently synthesized strand in *E. coli* is accomplished based on the hemi-methylation status and therefore is called methyl-directed MMR[12]. More specifically, DNA is methylated at 5′-GATC-3′ sequences, however, immediately following DNA synthesis, there is a short gap where the newly synthesized strand is not methylated[12]. The MMR machinery in *E. coli* use this non-methylated strand as a guide to discern the newly synthesized strand from the parental/template strand[12]. MutH recognizes this methylated region and nicks the newly synthesized strand for the entry of excision enzymes[13]. However, in eukaryotes lacking MutH, MutL plays the role of the matchmaker between MutS and other components of MMR system[10]. Although, the precise mechanism strand discrimination has yet to be elucidated in higher eukaryotes, evidence suggest that the presence of a nick in the newly synthesized strand containing nucleotide mispairs is sufficient for initiation of the MMR pathway[14]. Accordingly, in eukaryotes, MMR is also referred to as nick-directed MMR. Although the origin of this nick *in vivo* is unknown, it may be induced with an unknown enzymatic protein responsible for strand discrimination in eukaryotes.

1.3 Chromosome Instability

CIN is defined as an increase in rate at which whole chromosomes or large chromosomal fragments are gained or lost[4]. In general, there are two types of CIN, numerical and structural. Numerical CIN refers to the gain or loss of whole chromosomes, whereas structural CIN refers to the gain or loss of large chromosomal segments and may arise due to gross chromosomal rearrangements (GCRs)[15]. CIN is a frequent characteristic of virtually all human cancers, particularly solid tumors, where it occurs in up to 80% of all cancers[16]. CIN is proposed to provide a selective growth advantage to promote oncogenesis by increasing or decreasing the number of oncogenes and tumor suppressor genes, respectively[17]. Furthermore, because CIN produces a heterogeneous population of cancer cells with differing genetic compositions stemming from gain or losses of random chromosomes, it is proposed to promote the rapid adaption of cancer cells to various selective pressures[18]. These observations perhaps explain why CIN is frequently associated with aggressive cancers[19], the acquisition of multidrug resistance[20], and poor patient prognosis[21].

Studies in unicellular organisms, including *Saccharomyces cerevisiae* (budding yeast), have provided us with a greater understanding of the genes and pathways that are normally required for genome stability. For example, much of our current understanding of MSI and aberrant genes and pathways that contribute to MSI in humans were first identified in unicellular organisms, such as prokaryotes and eukaryotes including *S. cerevisiae*[22]. Similarly, extensive genetic and biochemical studies performed in *S. cerevisiae* have identified many of the genes and pathways required to maintain chromosome stability under normal conditions. Due to the evolutionarily conserved nature of many of these genes and pathways (*e.g.* DNA replication and repair, chromosome segregation, and cell cycle control), much of our current insight into human biology has been derived through cross-species candidate gene approaches. In particular, these

cross-species approaches have provided us with a greater understanding of human CIN genes (*i.e.* genes whose diminished function induces CIN). For example, it is known that *S. cerevisiae* have ~6,000 total genes[23], and a recent study showed that 692 (~11.5% of all yeast genes) are CIN genes[24]. By extrapolation alone, it is estimated that as many as 2,300 CIN genes (~11.5%) may exist amongst the ~20,000 genes contained within the human genome[25]. Interestingly however, despite the potential high prevalence of CIN genes in humans, fewer than 150 CIN genes have been identified and characterized to date. Of those identified, many encode functions within biological pathways that are predominantly involved in mitosis[26] including cell cycle checkpoint regulation[27,28], centrosome amplification[29], kinetochore structure[30], sister chromatid cohesion[31], telomere maintainance[32], and cytokinesis[33]. Accordingly, based on the extensive evolutionarily conserved nature of these essential biological pathways, we predict that many additional CIN genes exist that encode functions within these evolutionarily conserved pathways.

There are multiple pathways within human cells that normally function to maintain chromosome stability, and conceptually, mutation of any of the genes encoding functions within those pathways may induce CIN. Perhaps the two best characterized pathways that when altered give rise to CIN are the cell cycle checkpoint (see *Section* 1.3.1, pg. 6) and sister chromatid cohesion (see *Section* 1.3.2, pg. 14) pathways. In general, cell cycle checkpoints function to protect genome integrity by ensuring a cell does not prematurely enter the next stage of cell cycle prior to completing all essential processes within the current stage. During mitosis for example, the lack of proper kinetochore/microtubule attachments activates the spindle assembly checkpoint (SAC) to prevent premature metaphase into anaphase transition, which could result in inaccurate chromosome segregation into daughter cells (detailed further in *Section* 1.3.1.3, pg. 9)[34]. However, there are some types of abnormal kinetochore attachments that can satisfy components of the SAC

and do induce CIN (detailed in *Section* 1.3.1.3, pg. 9). Beyond cell cycle checkpoints, aberrant sister chromatid cohesion is another process that can lead to CIN. In essence, cohesion functions in a ring-like manner to tether nascently synthesized chromatids together to prevent entanglement and/or premature segregation from occurring. During the metaphase to anaphase transition, cohesion is cleaved and each sister chromatid is segregated to opposite poles[35]. Cells with aberrant cohesion are unable to properly regulate sister chromatid segregation and are therefore prone to chromosome missegregation events and CIN (detailed in *Section* 1.3.2, pg. 14).

1.3.1 Cell Cycle Checkpoints

A primary function of cell cycle checkpoints is to maintain genome integrity. This function is regulated by many proteins and pathways that are evolutionary conserved from organisms ranging from yeast to humans[36]. In essence, these pathways function by temporarily halting cell cycle progression, particularly when the genome is compromised (*i.e.* when DNA is damaged). Generally speaking, there are three cell cycle checkpoints, all of which have the potential to impact genome stability – two checkpoints, G1/S and G2/M checkpoints, function in response to DNA damage and monitor the G1/S and the G2/M transitions, respectively[37], while the third checkpoint, the SAC, regulates the metaphase to anaphase transition by ensuring proper kinetochore-microtubule attachments prior to chromosome segregation[38]. When a checkpoint becomes dysfunctional due to mutations within the underlying genes (as frequently occurs during oncogenesis), a cell may potentially escape a checkpoint and re-enter the cell cycle even in the presence of DNA damage or abnormal kinetochore attachment, and will ultimately lead to the formation of daughter cells with aberrant chromosome structure or DNA content. Below are brief descriptions of the three cell cycle checkpoints that are designed only to highlight the function and regulation of each checkpoint.

1.3.1.1 The G1/S checkpoint

G1 is the first phase of the cell cycle and is separated into a post-mitotic (G1-pm) and a pre-S phase (G1-ps) sub-phases by a restriction (R) point. In order that cells pass through the G1-pm, they need to continuously receive mitogenic signals from outside the cell. However, when passed the R point, cells are committed to the cell cycle and growth stimulating signals are no longer needed for progression through cell cycle[39]. Early in G1, the transcriptional repressor protein RB (retinoblastoma) binds to the E2F transcription factors (E2F1, E2F2, and E2F3) to effectively halt cell cycle progression[40]. E2Fs are a family of functionally related proteins that normally target the promotor region of genes required for cell cycle progression, such as *C-Myc* (i.e. Cyclin E transcription activator)[40]. The E2F family of transcriptional regulators is comprised of two groups, namely transcriptional activators and repressors[41]. During G1-pm the level of Cyclin D-CDK4/6 (cyclin dependent kinase 4/6) gradually rises until it reaches a point that can target RB for phosphorylation and therefore triggers R transition[40,42]. Phosphorylated RB can no longer inhibit the transcriptional activities of E2Fs, and thus cells alter their gene expression patterns in a manner that promotes transition into S-phase. For instance, E2F1 promotes cyclin E expression[43], which complexes with CDK2 to promote G1/S transition[44]. While cells are transitioning from G1 to S phase, Cyclin E-CDK2 kinase activity initiates the formation of the pre-replication complex[45]. In the meantime, Cyclin A expression increases and competes with Cyclin E to form a Cyclin A-CDK2 complex[45]. When the abundance of the Cyclin A-CDK2 complex reaches a threshold, pre-replication complex assembly is terminated and DNA replication is initiated[45].

The G1 checkpoint functions to temporarily arrest cells in G1 when DNA damage including both single strand breaks (SSBs) and/or double strand breaks (DSBs) are present and

sensed by the DNA damage response system (reviewed by Bartek and Lukas (2001)[44]). In general, the presence of SSBs and DSBs induces ATR (ataxia telangiectasia and Rad3 related) or ATM (ataxia telangiectasia mutated) activation, two master DNA damage response kinases that activate CHK1 (checkpoint kinase 1) and CHK2, respectively[46,44]. Activated CHK1 and CHK2 phosphorylate TP53 (tumor protein 53), a transcription factor that in turn promotes the expression of P21[47]. P21 inhibits the Cyclin E-CDK2 complex to prevent cell cycle progression and induce a G1 arrest[48]. If the DNA damage is extensive and results in a prolonged G1 arrest, P53 can potentiate the activities of pro-apoptotic proteins to induce programmed cell death to effectively remove deleterious cells from the population[47]. However, if the DNA damage is effectively repaired, the 'stop' signal is no longer produced and the G1 checkpoint will be satisfied. Thus, cells will continue to proliferate and eventually transition from G1 into S phase. In cancer, however, genes controlling the G1/S transition are frequently mutated or dysregulated. For example, overexpression of *Cyclin D* or somatically inactivation of *RB* has been seen in various cancers and is reviewed by Massagué (2004)[49]. Accordingly, cancer cells frequently lack a functional cell cycle checkpoint and therefore are not able to prevent cell proliferation when DNA is damaged. Thus, these cancer cells are susceptible to induce genome instability and/or CIN.

1.3.1.2 The G2/M Checkpoint

Following DNA replication in S phase, cells transition into G2 phase where they prepare their components for entry into mitosis. More specifically, during G2, Cyclin B level increases until it peaks by the end of G2[50]. During this time, the WEE1 and MYT1 (Myelin Transcription Factor 1) kinases[51] function to maintain the Cyclin B-CDK1 complex in an inactivated (phosphorylated) form within the cytoplasm[52]. When Cyclin B levels become maximal, it is activated by CDC25 (cell division cycle 25) and translocated from the cytoplasm into the

nucleus[52]. The activated Cyclin B-CDK1 complex maintains its activity by negatively regulating its inhibitor (WEE1) and positively regulating its activator (CDC25)[53]. An additional molecular component that regulates this process is PLK1 (polo-like kinase 1), which functions to further inhibit WEE1 and MYT1 and activate CDC25[54]. Activation of Cyclin B-CDK1 regulates G2/M transition and initiates the onset of mitosis[55].

As with the G1/S checkpoint, the G2/M checkpoint generally functions to halt the progression of cells harboring DNA damage. In an analogous fashion to G1/S checkpoint, DNA damage followed by DNA replication in S phase activates the master DNA damage response kinases, ATM and ATR, that subsequently activate CHK2 and CHK1, respectively. However, unlike the G1 checkpoint, CHK1 and CHK2 are now responsible for activating WEE1 and MYT1 and deactivating CDC25[56,47,57]. These simultaneous events result in the deactivation of the Cyclin B-CDK1 complex and arrests cells in G2 until all DNA damage is repaired and the checkpoint is satisfied. Accordingly, the G2/M checkpoint plays an important role in preventing cells with damaged DNA from entering mitosis. However, similar to the G1/S checkpoint, the genes encoding functions within the G2/M checkpoint have also been found mutated or dysregulated in a number of cancers. For example, *CDC25* is frequently overexpressed in different cancer types and its overexpression is associated with aggressive disease and poor patient prognosis[58]. Therefore, these cancers are also unable to prevent cell progression when DNA is damaged or when it is not properly replicated and thus have a high potential to cause genome instability and/or CIN.

1.3.1.3 The Spindle Assembly Checkpoint (Mitotic Checkpoint)

Another important cell cycle checkpoint is the SAC, which functions during mitosis to ensure the proper segregation of genetic material (i.e. chromosomes) into daughter cells (reviewed

by Musacchio and Salmon (2007)[34]). As noted above, mitosis is initiated by the Cyclin B-CDK1 complex activation. Cyclin B-CDK1 complex remains activated until the anaphase at which the sudden decline in Cyclin B-CDK1 levels initiates chromosome segregation to opposite centrosomes[59]. Although Cyclin B is important for entry and the initial stages of mitosis, its degradation is required for transition into the anaphase and mitotic exit[60]. High Cyclin B-CDK1 level induces APC/C (anaphase promoting complex/cyclosome) phosphorylation, which is necessary for APC/C complex recognition by its activator, CDC20[61]. When complexed with CDC20, the APC/C^{CDC20} becomes a functional E3 ubiquitin ligase[62] that targets Cyclin B and Securin for proteolytic degradation via the 26S proteasome. While Cyclin B activates CDK1 which is essential for maintaining mitosis, Securin is a negative regulator of Separase, a protease that cleaves sister chromatid cohesion to facilitate chromosomes segregation[63].

In general, there are two principal elements associated with the SAC checkpoint, kinetochore attachments and tension. To satisfy the SAC requires that all sister chromatids have bipolar attachments (*i.e.* amphitelic attachment; see Figure 1-1), that is, the two kinetochores of a given chromosome (1 per sister chromatid) must capture microtubules emanating from opposite centrosomes[64]. Of particular note, is that the presence of a single unattached kinetochore will activate the SAC and prevent premature completion of mitosis. Unattached kinetochores contains MAD1-MAD2 complexes which triggers the assembly of MCC (mitotic checkpoint complex)[65]. MCC is the inhibitor of APC/C^{CDC20} complex and is formed from MAD2, MAD3, BUB3, and CDC20 (i.e. co-activator subunit of APC/C) proteins[66]. When APC/C is inhibited, sustained Cyclin B level maintain CDK1 activity and arrests cells in mitosis. Upon binding of the kinetochore microtubules to the kinetochores, MAD1-MAD2 complex is released and the assembly of MCC complex can no longer be triggered[65].

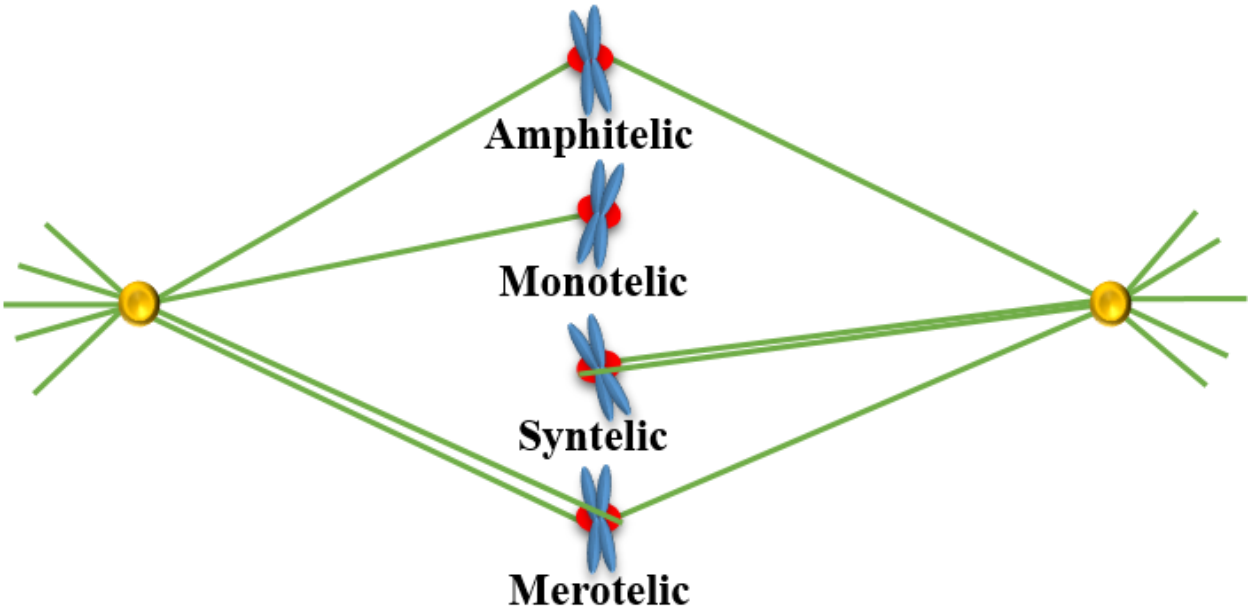

Figure 1-1: Different Types of Kinetochore Attachments
A schematic depicting the four types of kinetochore attachments. Centrosomes are shown in yellow, microtubules in green, kinetochores in red, and chromosomes/chromatids in blue. Microtubules bound to kinetochores are kinetochore-microtubules. Amphitelic attachments result in both bipolar attachment and tension and thus satisfy the SAC permitting cells to progress through mitosis. Monotelic attachments fail to produce bipolar attachment and tension, while syntelic attachments only satisfy the bipolar attachment component of the SAC. Merotelic attachments produce both bipolar attachment and tension and will satisfy the SAC to allow cells to transition into anaphase, however, merotelic attachments may induce aberrant chromatid segregation and CIN.

The second factor required to satisfy the SAC is tension, and is conferred by the microtubule/kinetochore interactions and the poleward/retrograde movement of the microtubules that is counterbalanced by cohesion. The absence of tension activates the SAC to arrest cells in mitosis[67]. Therefore, the occupation of both sister chromatid kinetochores by microtubules is not sufficient to satisfy the SAC, but these microtubules must emanate from opposite centrosomes to generate tension on sister chromatids. For example, when both sister chromatid kinetochores are captured by microtubules emanating from a single centrosome this attachment has no tension on

sister chromatids and cannot satisfies the SAC (i.e. syntelic attachment, Figure 1-1). It is suggested that tension between sister chromatids can be sensed by the activity of Aurora B which localizes within the inner kinetochore[68]. Aurora B is a kinase responsible for the phosphorylation of a number of proteins localized within the outer kinetochore, such as the Ncd80 complex[68]. The Ncd80 complex is responsible for kinetochore attachment to the microtubules. Phosphorylation of the Ndc80 complex by Aurora B has been shown to negatively regulate microtubule binding to the kinetochores[69]. However, tension on sister chromatids stretches the structure of inner kinetochore[70] and create a gap between the Aurora B and its substrates. It is suggested that the generated gap prevents the phosphorylation of Aurora B substrates and stabilizes the kinetochore-microtubule attachment (reviewed by Lampson and Cheeseman (2011)[68]). In agreement with this hypothesis, the ability of Aurora B to phosphorylate its substrates depends directly on its distance from these substrates[68]. In contrast, in the absence of tension, the Aurora B kinase, destabilizes incorrect kinetochore attachments so that a given pair of chromatids will have proper bipolar attachments (*i.e.* amphitelic attachment)[68].

Proper SAC function is critical to ensure chromosome segregation fidelity. Chromosomes with abnormal kinetochore attachments can cause chromosome missegregation events during mitosis, which in turn produces daughter cells with unequal chromosome complements. As shown in Figure 1-1, in addition to the requisite amphitelic (*i.e.* bipolar) kinetochore attachment, there are three abnormal kinetochore attachments that are referred to as monotelic, syntelic, and merotelic attachments[71]. Briefly, monotelic attachments occur when only one of the kinetochores located on sister chromatids is occupied by microtubules emanating from a single centrosome. However, when both kinetochores are occupied with microtubules emerging from a single centrosome, it is called a syntelic attachment. Finally, when a given kinetochore is occupied by microtubules

emanating from both centrosomes it is defined as a merotelic attachment[71]. As there is no bipolar attachment or tension produced by monotelic and syntelic attachments, these two type of attachments cannot deactivate the SAC signals and therefore they prevent cell cycle progression. However, merotelic attachments produce both bipolar attachment and tension, so it satisfies the SAC and cells can progress through mitosis. Studies have shown that kinetochores with merotelic attachments do not label with Mad2 or 3F3/2 (the SAC markers) antibodies[72] indicating the SAC has been satisfied. As this abnormal kinetochore attachment satisfies the SAC, it can induce chromosome missegregation events[72] and lead to lagging chromatids that may induce the formation of micronuclei, or small extra-nuclear bodies that are found outside of the primary nucleus.

1.3.1.4 Checkpoint Defects, CIN, and Cancer

Cancer is a genetic disease that arises due to the accumulation of mutations in genes, including those that control cell growth and proliferation. Generally speaking, these genes are known as proto-oncogenes which promote cell proliferation, and tumor suppressor genes which inhibit cell cycle progression. Checkpoint associated genes are frequently mutated in cancer and thus cancer cells often propagate genome instability due to the lack of functional cell cycle checkpoints[73]. For example, *TP53* is a classical tumor suppressor gene that is mutated in up to 60% of all cancers, and a critical component of cell cycle checkpoints and the DNA damage response[74]. There are other components of cell cycle checkpoints mutation in which is frequently reported in different cancers, such as *ATM* and *RB* (tumor suppressor genes)[75,76]. Mutated *RB* found in cancers deregulate the expression of E2F family members, which directly target *MAD2* and affect its expression[77]. Recall, MAD2 is a component of MCC complex and is a SAC protein whose overexpression induces aneuploidy and is associated with tumorigenesis[78]. Moreover, Cahill et

al.[79] showed that a large number of CRCs exhibiting CIN have a somatic mutation in their *BUB1* and *MAD3* genes (the SAC components). Hence, while mutations in genes encoding functions within the SAC frequently occur in different cancers and is associated with CIN[79], mutations of genes encoding functions within the remaining checkpoints have also been identified in CIN cancers. Overall, cells lacking functional cell cycle checkpoints are unable to prevent cell cycle progression when the integrity of the DNA is in danger, and thus, these cells can continue to proliferate with abnormal DNA content and/or structure.

1.3.2 Sister Chromatid Cohesion, CIN, and Cancer

Following DNA replication during S phase, sister chromatids are held together by a protein complex called cohesin. Cohesin is comprised of four core subunits called SMC1, SMC3, RAD21, and STAG1/2/3 and effectively regulates sister chromatid cohesion. Collectively, cohesin forms a ring-like structure that tethers nascently synthesized chromatids together to prevent entanglement and/or premature segregation. Apart from the core cohesin components, there are additional proteins important for cohesion regulation, including those involved in cohesin loading onto the DNA (NIPBL and MAU2), cohesion establishment during S-phase (ESCO1/2, PDS5A/B, WAP1, and Sororin), and cohesion removal during mitosis (PLK1, CDK1, Aurora B, and Separase) (reviewed by Peters and Nishiyama (2012)[35]).

Sister chromatid cohesion is especially important for chromosome congression to the metaphase plate during metaphase and chromosome segregation during anaphase. During the early stage of mitosis, sister chromatid cohesion is cleaved along the lengths of the chromosome arms by a protease called Separase, but is preserved at the centromeres with a protein called SGO1[80]. Early in anaphase SGO1 is polyubiquitinated by APC/C^{CDC20} complex for degradation[81] and

therefore the remaining centromeric cohesion is also cleaved by Separase leading to sister chromatid segregation[82].

In general, timely and accurate separation of sister chromatids, relies on sister chromatid cohesion. In fact, mutation in genes encoding functions within sister chromatid cohesion is associated with CIN cancers and therefore these mutations are suggested to have a causative role in oncogenesis[83]. For example, Barber et al.[84] identified somatic mutations in 4 cohesion genes (*SMC1*, *SMC3*, *NIPBL*, and *STAG3*) in CRC cancers. Additionally, this group demonstrated that down regulation of these genes induced cohesion defects and contributed to CIN[84]. There are more studies (reviewed by Barbero (2012)[85]) supporting the role of cohesion interacting genes (e.g. *PLK1* and *Aurora B*) mutations in tumorigenesis. Beyond a role in sister chromatid cohesion and segregation, cohesion is also required for efficient DNA DSB repair[85,86], and is involved in gene expression[87].

1.4 Microtubules and Microtubule Motor Proteins

Microtubules are highly dynamic cylinders formed by polymerization of α- and β-tubulin dimers (Figure 1-2). Each microtubule is comprised of 13 protofilaments assembled around a hollow core[88]. Microtubule filaments have a plus-end which has the β-subunit exposed and a minus-end which has the α-subunit exposed[89]. This orientation of microtubules provides them with a structural polarity essential for their biological function. Mitotic spindle microtubules are nucleated from a structure called the centrosome[90]. The centrosome is comprised of a core γ-tubulin ring complex (γ-TuRC) which acts as a scaffold and template for α- and β-tubulins during microtubule nucleation[91]. In general, microtubules contain a minus-end and a plus-end. While the end of microtubule associated with centrosome and γ-TuRC complex is the minus-end, the

opposite end is the plus-end. Microtubules are important structures required for different cellular processes such as, organelles transportation, cell structure organization, and more importantly mitotic spindle assembly[92].

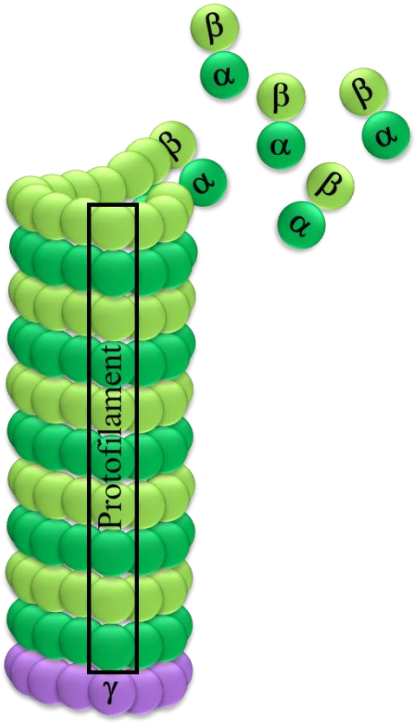

Figure 1-2: Microtubule Structure
Schematic illustrating the organization of α-tubulin (dark green balls) and β-tubulin (light green balls) dimers within a microtubule. α- and β-tubulin dimers employ γ–tubulins (purple balls) as a template for microtubule nucleation. 13 protofilaments assemble around a hollow core to form a microtubule filament.

Microtubules are the main components of mitotic spindle apparatus, which is the structure formed during mitosis to promote the distribution of sister chromatids between two daughter cells. In general, there are three types of microtubules that together form the mitotic spindle apparatus,

including astral microtubules, kinetochore microtubules, and interpolar microtubules[93] (Figure 1-3). Astral microtubules emerge from centrosomes and expand towards the cell periphery. The main function of astral microtubules is to interact with cell membrane to orientate the spindle apparatus. Kinetochore microtubules emerge from the centrosomes and contact the kinetochore of sister chromatids to align them in the metaphase plate. Later in anaphase, these microtubules participate in sister chromatid segregation to opposite poles. Interpolar microtubules emanate from the two opposite centrosomes and expand towards the middle of the cell where they interact with each other. These microtubules provide a suitable surface for movement of microtubule motor proteins essential for the assembly of the bipolar spindle apparatus[93] (see *Section* 1.5.3, pg. 24).

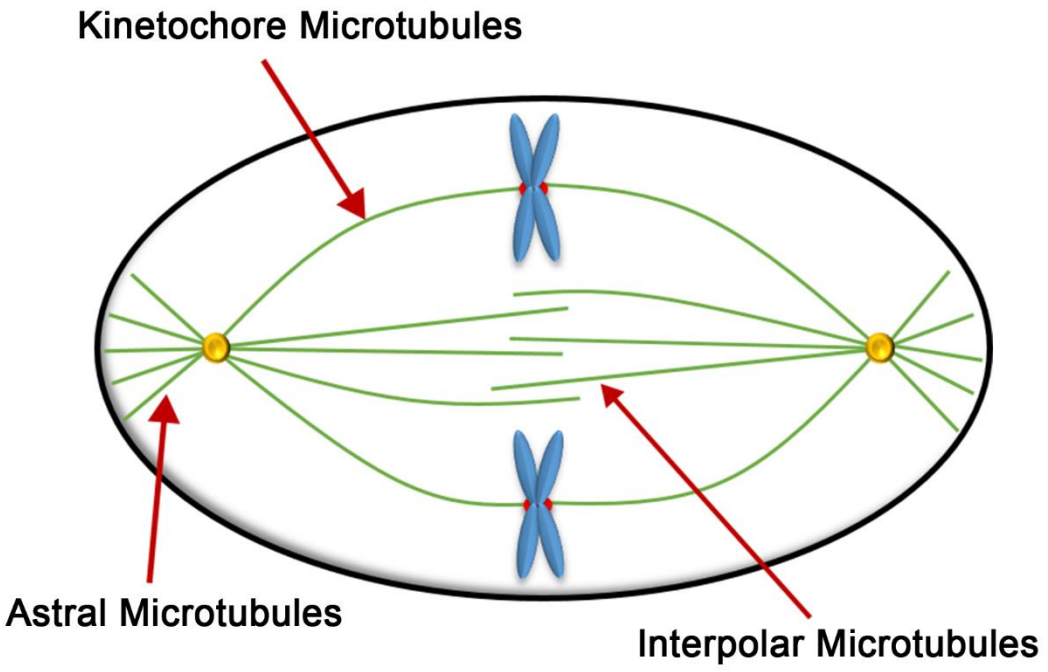

Figure 1-3: Mitotic Spindle Apparatus
Schematic presenting the three classes of microtubules that together form the mitotic spindle apparatus. Chromosomes are shown in blue, kinetochores in red, centrosomes in yellow, and microtubules in green.

Microtubule motor proteins are a class of molecular proteins that utilize ATP hydrolysis as an energy source to migrate along microtubule tracks. In general, there are two classes of microtubule motor proteins that are collectively referred to as dyneins and kinesins. While dyneins are minus-end directed motor proteins[94], the kinesins, including KIF11, are typically plus-end directed motor proteins[95] (detailed below). In general, kinesins function in various cellular processes ranging from transport of cellular components (e.g. vesicles, organelles, chromosomes, protein complexes, and ribonucleoproteins)[96,97], to mitotic spindle assembly[98].

In total, there are 14 kinesin subfamilies named Kinesin-1 through Kinesin-14[96]. Like all motor proteins, kinesins are comprised of three main domains, called the head, the stalk, and the tail domains (detailed in *Section* 1.5.1, pg. 19). With the exception of two kinesin subfamilies (kinesin-13 and -14), all kinesins have N-terminal head domain that makes them a plus-ended directed motor protein. The kinesin-14 subfamily has a C-terminal head domain and therefore moves toward the minus-end of microtubules, while the kinesin-13 subfamily has a head domain in the middle of the protein that generally functions as a microtubule depolymerizing unit[99].

KIF11 is an evolutionary conserved protein found in organisms ranging from yeast to humans. In fact, orthologs have been identified in at least 69 different species including Kif11 in *Mus musculus* (79.7% sequence identity with human KIF11), Kif11 in *Danio rerio* (48.9% sequence identity with KIF11), bmk-1 in *Caenorhabditis elegans* (34.0% sequence identity with KIF11), and CIN8 in *S. cerevisiae* (28.0% sequence identity with KIF11)[100,101]. KIF11 and its orthologs all belong to Kinesin-5 subfamily of Kinesins, but KIF11 is the only member of Kinesin-5 subfamily found in humans. Below are descriptions of the KIF11 homotetrameric structure and its important function during mitosis.

1.5 KIF11

1.5.1 *KIF11* Encodes a Homotetrameric Microtubule Motor Protein

KIF11, also known as Eg5, KSP, and Human Kinesin-5, was first identified as a plus-end directed microtubule motor protein in *Xenopus laevis*[102]. KIF11 is encoded by a gene spanning approximately 62 kb[103] of chromosome 10q24.1[104]. KIF11 is a bipolar homotetrameric protein with 1056 amino acids (aa) in length[105] and a molecular mass of 119kDa[105]. Similar to all kinesins, KIF11 consists of a head, a stalk, and a tail domain (Figure 1-4A), with four KIF11 monomers self-assembling to produce a functional homotetrameric unit[106] (Figure 1-4B).

The head domain, also known as the motor domain, is the catalytic portion of the protein and is located at the N-terminus rendering KIF11 a plus-end directed microtubule motor protein[99]. The head domain is responsible for hydrolysing the chemical energy of ATP and converting it to the mechanical energy. Accordingly, the head domain consists of a catalytic core and a neck linker[107]. More specifically, the catalytic core contains two nucleotide binding sites including a microtubule binding site that keeps the protein attached to the microtubule and an ATP binding site[108]. The role of these sites is further explained in *Section* 1.5.2 (pg. 22). The neck linker is located at the C-terminal end of the head domain and is required for plus-end directed movement along microtubules (see *Section* 1.5.2, pg. 22). The neck linker is evolutionary conserved between kinesins with 18 aa length in kinesin-5 family[109]. In general, ATP hydrolysis of the catalytic core domain triggers conformational changes in the head domain, and in particular the neck linker, to facilitate movement of the KIF11 homotetramer along microtubules[109]. The neck linker is also responsible for transmitting the mechanical tension from one head to another head contained within the KIF11 homotetramer[109]. In other kinesins, the neck linker is either parallel to the catalytic core of the protein or is disordered. However, in KIF11, the neck linker is perpendicular

to catalytic core[110]. This specific structural feature is proposed to help its specific function, which is cross-linking with antiparallel microtubules[111] (see below).

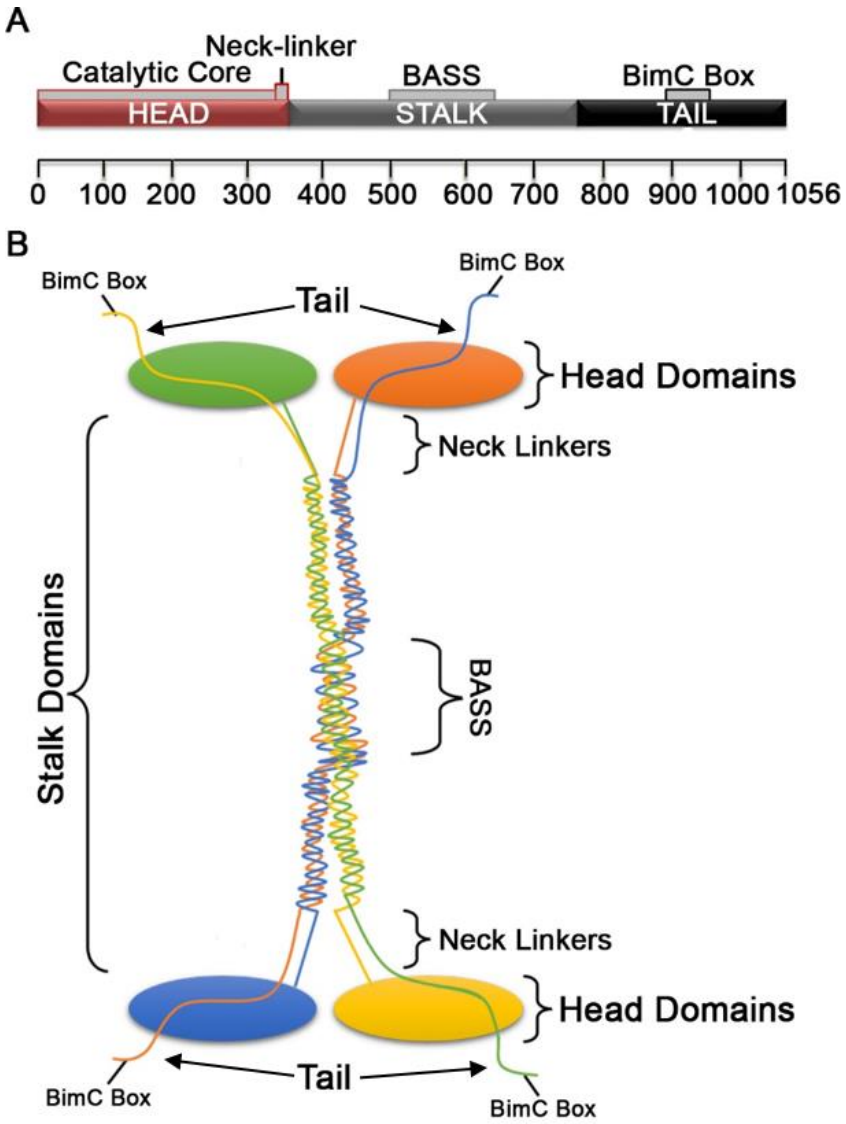

Figure 1-4: KIF11 Domains and Structural Motifs
(A) A schematic depiction of the KIF11 protein with its various domains and subdomains indicated. For reference purposes, the aa positions are indicated below the schematic. ***(B)*** Schematic depicting a model of homotetrameric KIF11 structure. For simplicity, each monomer is represented by a single color (green, orange, blue, or yellow). The three main domains of KIF11 (the head, the stalk and the tail domains) and three subdomains (the Neck-linker, the BASS and the BimC Box) are labelled accordingly. Head catalytic cores are shown with ovals.

The C-terminal portion of KIF11 is referred to as the tail domain, and is responsible for maintaining KIF11 on microtubules. Thus, like the head domain, the tail domain also contains a microtubule binding site[112]. This binding site ensures the interaction of the protein with microtubules without having any inhibitory effect on KIF11 migration along microtubules[113]. In fact, Weinger et al.[113] suggest that the KIF11 head domain microtubule binding site is insufficient to maintain constant protein-microtubule interactions. They show that the tail domain mediates the KIF11 walking process along microtubules by ensuring that the protein remains bound to microtubules. Overall, they show that for appropriate cross-linking to occur between microtubules, each KIF11 homotetramer requires eight microtubule binding sites, one located within the head and tail domains of each monomer. At the extreme C-terminal portion of KIF11, there is a conserved sequence of 40 aa between the kinesin-5 subfamily members that is called BimC box[114]. This conserved sequence is vital for association of KIF11 with microtubules[115]. Phosphorylation of Thr927 within BimC box is essential for KIF11 localization to the centrosomes early in mitosis (see *Section* 1.5.4, pg. 27)[115].

Finally, the central domain of KIF11 is referred to as the stalk domain, and is required for homotetramerization. Evidence shows that the stalk domain is sufficient for homo-tetramerization, as deletion of either the head domain or the tail domain does not interrupt this process[113]. The BASS subdomain located within the stalk domain is specifically shown to regulate the tetramerization process[116]. In addition, the BASS subdomain is suggested to be required for transferring the forces generated with catalytic head domain between the four monomers, which is essential for ability of the protein in sliding the antiparallel microtubules against each other[117] (see below).

1.5.2 The KIF11 Mechanochemical Cycle

In general, there are two modes of motion for KIF11, an ATP-independent diffusive mode and an ATP-dependent directional mode[118]. Within the cytoplasm, homotetrameric KIF11 moves randomly in its diffusive mode containing one ADP molecule bound to each of its catalytic cores. When a KIF11 head domain encounters a microtubule binding site, the KIF11 catalytic core binds firmly to the adjacent microtubule. When bound to the microtubule, KIF11 remains in diffusive mode until the opposite head domain binds to an antiparallel microtubule. Once KIF11 is cross-linked between two microtubules, its migration shifts from diffusive to directional mode[118,113]. This shift in mode only occurs when KIF11 is cross-linked between two anti-parallel microtubules presumably so that KIF11 can regulate ATP consumption to conserve energy[118].

Once directional mode is initiated, a series of conformational changes occur within the KIF11 head domain that releases ADP[119]. ATP rapidly replaces ADP and triggers subsequent conformational changes that alter the position of neck linker and position it next to the catalytic core subdomain[119]. This motion throws the adjacent head forward to the next binding site on the microtubule. The trailing head hydrolyzes ATP to weaken its attachment to the microtubule, so that the neck linker can return to its original position[120,121]. Thus, when the leading neck linker docks to the catalytic core, it throws the trailing head forward and the cycle repeats itself (Figure 1-5). The simultaneous motion of KIF11 on antiparallel microtubules serves to slide the microtubules in opposite directions (i.e. towards centrosomes) while KIF11 appears to remain stationary[110]. In fact, the motion of KIF11 on interpolar microtubules can be envisioned to be similar to walking on a treadmill.

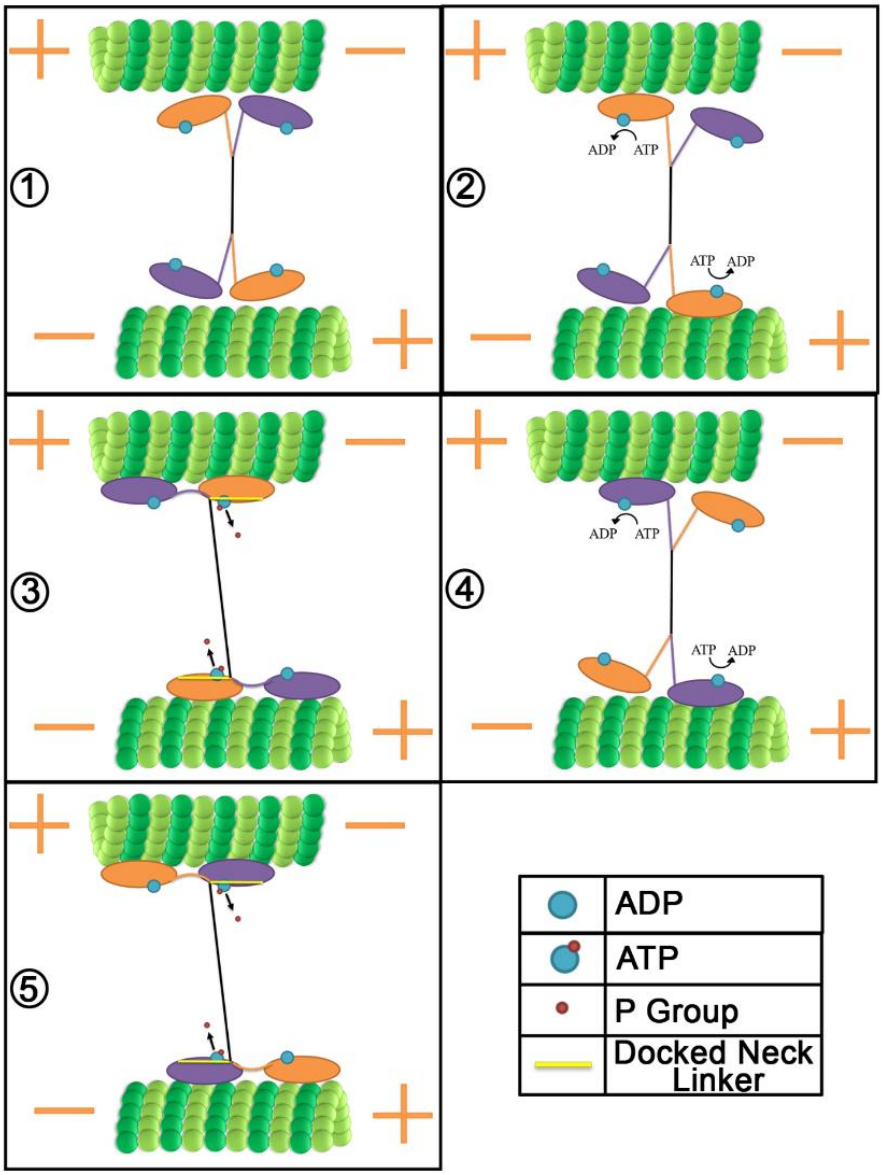

Figure 1-5: The KIF11 Mechanochemical Cycle
A schematic depicting the directional motion of KIF11 between two interpolar microtubules. ***(1)*** KIF11 homotetrameric protein moves randomly within the cell until one head domain encounters a microtubule binding site. ***(2)*** Binding of the KIF11 head domain to the microtubule induces conformational changes that releases ADP to facilitate ATP binding. ***(3)*** ATP binding to the head domain triggers another series of conformational changes that docks the neck linker down to the catalytic core. The docking of the leading neck linker to the catalytic core throws the trailing head forward to the next microtubule binding site. ***(4)*** The trailing head utilizes the ATP molecule and the neck linker shifts to its original position. The presence of ADP weakens the connection between the trailing head and the microtubule. ***(5)*** The leading head exchanges ADP with ATP, and the neck linker docks to the core domain and the trailing head is thrown forward and the cycle repeats itself.

1.5.3 KIF11 is an Important Microtubule Motor Protein Required for Centrosome Separation and Chromosome Segregation

Unlike conventional kinesins, KIF11 does not transport cargo but rather forms a bridge between two adjacent and antiparallel microtubules to facilitate their movement in opposite directions. KIF11 converts energy from ATP hydrolysis into a power stroke that propels KIF11 in a plus-end directed manner[122]. KIF11, like all kinesin-5 super-family members, have a conserved function during mitosis, they are all required to generate a bipolar spindle in early prophase and to assist in chromosome segregation during the later stages of mitosis (i.e. anaphase to telophase)[123,114]. Early in prophase, duplicated centrosomes migrate to opposite poles to form a bipolar spindle, which is orchestrated primarily by the activity of KIF11[124]. Throughout prometaphase and into metaphase, KIF11 continues to push centrosomes apart when the bipolar spindle is formed and chromosomes are aligned to the metaphase plate. Following transition into anaphase, when sister chromatids begin segregating toward opposite poles, KIF11 continues to function by forcing centrosomes further apart to assist in spindle elongation and chromosome segregation[125] (Figure 1-6).

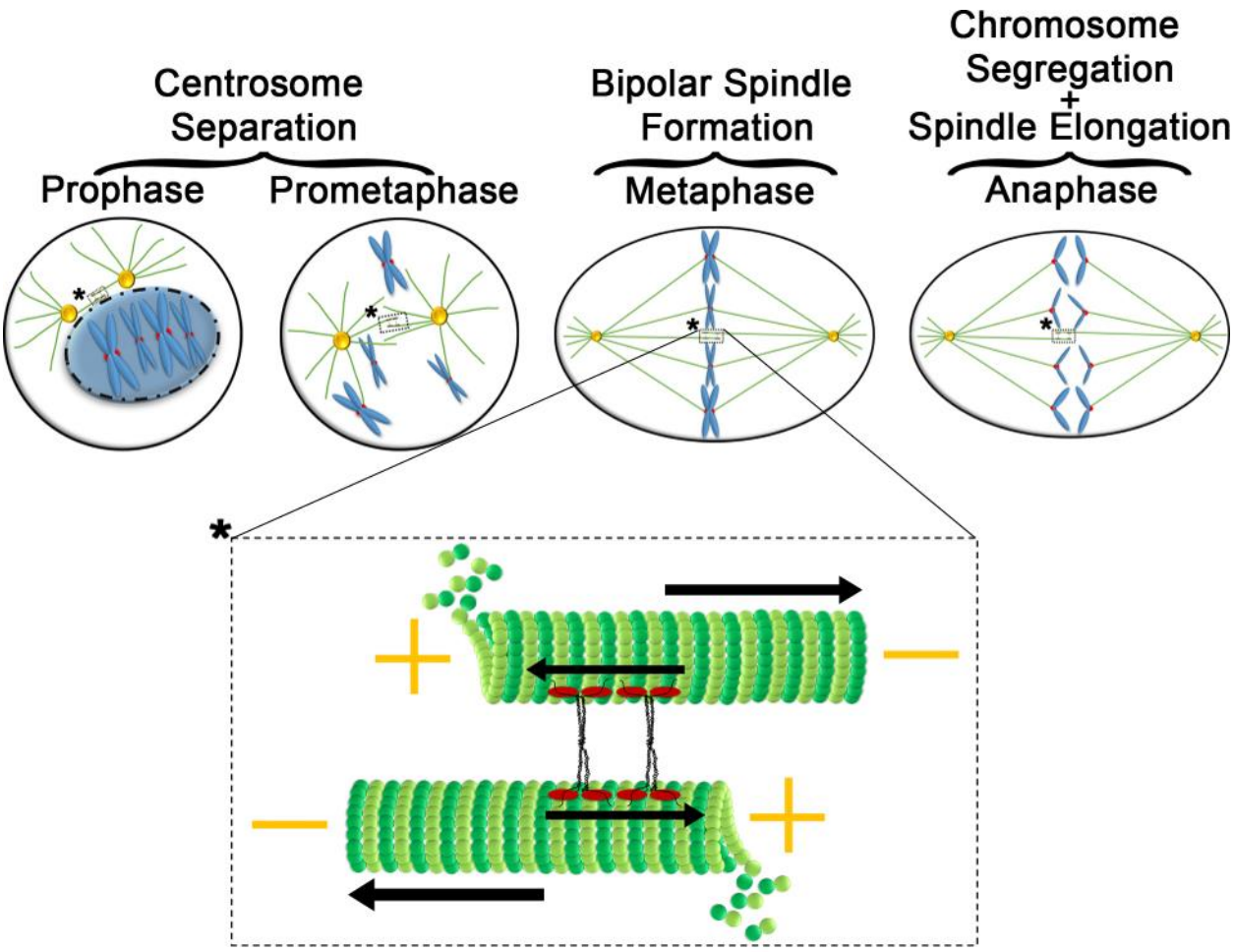

Figure 1-6: KIF11 is Required for Bipolar Spindle Assembly and Chromosome Segregation
A schematic depicting KIF11 function in different mitotic phases. A bounding box (indicated with *) is presented within each phase of the cell cycle for which a high-resolution schematic is included that details KIF11 function. The plus-end directed motion of KIF11 is shown with small black arrows, while the poleward direction of the microtubules is shown with large black arrows. In general, plus-end directed motion of KIF11 on interpolar microtubules makes a power stroke that slides microtubules in opposite directions while KIF11 remains relatively stationary. This poleward movement of microtubules in early stages of mitosis separates centrosomes to produce a bipolar spindle in metaphase when chromosomes are aligned at the metaphase plate. Further motion of KIF11 on microtubules during anaphase results in spindle elongation and facilitates mitotic chromosome segregation.

KIF15 and nuclear envelope-associated dynein are two additional motor proteins that participate in bipolar spindle assembly and chromosome segregation[126,127]. KIF11, KIF15 and dynein work together to balance the forces that form the bipolar spindle. For example, the power and directionality imparted by KIF11 is counterbalanced by the power and directionality of dynein, which results in a slow and non-accelerating separation of antiparallel microtubules[112]. KIF15 is a kinesin required for maintaining the bipolar spindle during metaphase[128]. Although, *KIF11* silencing or inhibition typically prevents bipolar spindle assembly and cells generally form a monopolar spindle (see *Section* 1.5.5, pg. 28), it has been reported that in some KIF11 inhibited cells, KIF15 overexpression can partially reconstitute KIF11 function to generate spindle bipolarity and function in centrosome separation[128]. Despite the previous reports that KIF15 functions as a dimer[129], it has recently been reported that at physiological ionic strength, KIF15 actually exists as a tetramer[130]. This recent insight into KIF15 structure may explain how KIF15 can functionally substitute for diminished KIF11 function.

Apart from the central role during mitosis, KIF11 also functions in a number of additional cellular processes including axonal branching[131], growth cone motility[132], neuronal migration[133], and protein translation and polypeptide synthesis regulation[134]. In general, due to KIF11 being a 'slow' motor protein, it limits the effects of other motor proteins[132]. Briefly, KIF11 functions in post mitotic neurons by promoting axonal branching and growth by organizing microtubule dynamics[135,131], while during neuronal migration, KIF11 functions as a brake on microtubules to govern neuronal migration rate and directionality[133]. Finally, KIF11 is suggested to regulate protein translation efficiency by binding ribosomes to microtubules and moving them along microtubule tracks[134]. Despite the important roles of KIF11 in the above noted processes, further discussion of these processes is beyond the scope of this thesis.

1.5.4 The Regulation of KIF11 Function by Other Proteins

KIF11 function and localization is regulated by a number of phosphorylation sites located along its length. During the early stages of mitosis, CyclinB-Cdk1 phosphorylates KIF11 on Thr927 to effectively targets KIF11 to centrosomes[115]. Thr927 is located within the BimC box and its phosphorylation is important for protein localization to the microtubules[115]. Moreover, PLK1 inhibition has been shown to be associated with decreased localization of KIF11 to the centrosomes, suggesting PLK1 kinase activity may be required for centrosome localization as well[136]. In fact, Mardin and Schiebel showed that following PLK1 inhibition, KIF11 failed to accumulate at centrosomes and was associated with errors in centrosome separation[137]. Bertran et al.[138] showed that PLK1 indirectly regulates KIF11 localization to the centrosomes by phosphorylating and activating Neck9 (NIMA related kinase 9). Activated Neck9 targets Neck6/7 which phosphorylates KIF11 at Ser1033. Ser1033 phosphorylation is required for KIF11 localization to centrosomes[138]. Interestingly, Nek6 overexpression in interphase cells is associated with early centrosome separation[137] further implicating KIF11 function in centrosome dynamics.

KIF11 activity and function are also regulated by TPX2[139], an important component of spindle assembly machinery. TPX2 is normally expressed during S phase, G2, and mitosis, but it is rapidly degraded as cells enter G1[140]. In *X. laevis,* TPX2 is associated with α- and β-importins during mitosis and disassociates from this complex through RanGTP activity[141]. TPX2 binds to microtubules and contributes at spindle assembly by recruiting additional proteins important to spindle assembly, so these proteins together form a stable bipolar spindle. KIF11 is one of the proteins that is targeted to microtubules by TPX2[142]. KIF11 binding to TPX2 regulates KIF11 localization to spindle microtubules but not centrosomes[142]. Other than localization, TPX2 also regulates KIF11 activity[142]. In cells expressing TPX2 lacking the KIF11 interaction domain,

hyperactivity of KIF11 results in the generation of imbalanced forces and consequently formation of abnormal spindles[142]. TPX2 regulates minus-end transport of KIF11 toward centrosomes by linking KIF11 to Dyneins and Dynactins (dynein activator complexes)[143].

1.5.5 Monopolar Spindle Formation Following *KIF11* Silencing or Inhibition

Recall that KIF11 is required during mitosis for bipolar spindle formation and that *KIF11* silencing and inhibition is associated with monopolar spindle formation[144,145]. Monopolar spindles form when centrosomes fail to separate and migrate to opposite poles and are seen as a single centrosome in the middle of astral microtubules (Figure 1-7). Due to the lack of tension on sister chromatids in monopolar spindles, these cells will normally be arrested in mitosis due to the SAC activation. In agreement with this possibility, Kapoor et al.[146] showed the localization of MAD2 (MCC protein) to the kinetochores of mitotic cells treated with monastrol (i.e. KIF11 selective inhibitor), indicating SAC activation. Although, monopolar spindle formation and mitotic arrest following *KIF11* silencing or inhibition is reported with numerous studies, the ultimate fate of many of these cells is not well understood. Therefore, more studies are required to identify the effect *KIF11* silencing or inhibition has on the fate of these cells.

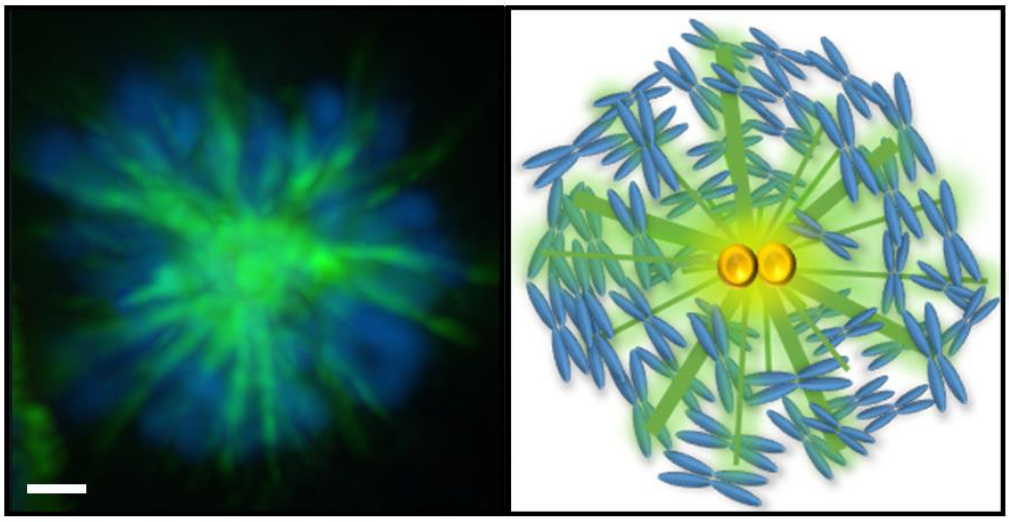

Figure 1-7:KIF11 Silencing or Inhibition Induces Monopolar Spindle Assembly
(A) Representative 3D projections of Immunofluorescent labelled cell showing the effect of KIF11 silencing on monopolar spindle assembly. DAPI (4',6-diamidino-2-phenylindole) and α-Tubulin are pseudo-colored blue and green, respectively. (Scale bar = 2 μm) ***(B)*** Schematic depicting a mitotic cell with failed centrosome separation and monopolar spindle formation. Centrosomes are shown in yellow, microtubules in green, and chromosomes in blue.

1.5.6 Using KIF11 Inhibitors as Anticancer Drugs

Uncontrolled cell proliferation is a hallmark of cancer cells which distinguishes these cells from non-cancerous cells[147]. Accordingly, anticancer drugs directly targeting this feature of cancer cells (i.e. antimitotic drugs) are attractive therapeutic options that are currently under investigation. In fact, there are a number of antimitotic drugs that have been proven effective in a number of cancer types. For example, Vinca alkaloids (inhibitor of microtubule polymerization), paclitaxel and taxanes (inhibitors of microtubule depolymerization) are three examples of successful anticancer drugs[148]. However, these drugs target microtubules that are the main component of mitosis, but also function in a number of important cellular processes (e.g. organelles transportation[92]). Thus, despite the cytotoxic effects imparted by these drugs on cancer cells, their

use is also associated with numerous off-target effects and the acquisition of multi-drug resistance[149]. Recently, a new class of anticancer drugs are under investigation that rather than targeting microtubules, target other components of the mitotic machinery that are not typically expressed or are often non-functional in non-proliferating cells. Some of these newly developing targets are Aurora A, Aurora B, PLK1, and most importantly KIF11[150].

In 1999, monastrol was identified as the first small molecule inhibitor of KIF11, and was discovered in a screen seeking to identify antimitotic drugs that do not disrupt microtubules dynamics[151]. Due in part to the high inhibitory concentration of monastrol (IC_{50} = 30μM)[152], a number of additional KIF11 inhibitors have been identified, developed and evaluated as novel anticancer compounds. The various types of these inhibitors are reviewed by Huszar et al. (2009)[153] and include STLC, HR22C6, ispinesib, AZ4877, HHPQ, and K858. To date, a number of KIF11 inhibitors have been entered in phase I and II clinical trials as anticancer drugs[106], including those listed in Table 1-1. Ispinesib, is one of the most potent KIF11 inhibitors and was the first to enter clinical trials. Most recently, ispinesib entered phase II clinical trials[154], however, there is limited results and demonstrated efficacy to date[155]. For example, a phase II study of the effect of ipinesib on a cohort of 17 patients with malignant melanoma indicated that ispinesib does not appear to have any meaningful impact on metastatic melanoma[156]. Furthermore, additional phase II clinical trials also failed to show ipinesib efficacy in recurrent or metastatic head and neck squamous cell carcinoma[157], androgen independent docetaxel resistant prostate cancer[158], advanced renal cell carcinoma[159], platinum/taxane resistant relapsed ovarian cancer[160], and metastatic colorectal cancer[161], suggesting it may not have clinical efficacy. However, the underlying reason(s) accounting for the apparent failure of KIF11 inhibitors remains to be determined.

Table 1-1: KIF11 Inhibitors in Clinical Trials

Name[A]	Inhibitory Concentration (IC_{50})	Phase[B]
Ispinesib	1.2-9.5 nM[153]	I/II
AZD4877	2 nM[153]	I/II
Filanesib	0.3-5 nM[162]	I/II
Litronesib	___	I/II
SB-743921	___	I/II
Carfilzomib	6 nM[153]	I/II
MK0731	2.2 nM[153]	I

[A]Data adapted from Huszar et al. (2009)[153]
[B]Data adapted from clinicaltrials.gov[163]

1.6 A Recent High-Content Screen Identifies KIF11 as a Putative Human CIN Gene

As presented in *Section* 1.3 (pg. 4), cross-species candidate gene approaches suggest that the human genome may contain ~2,300 CIN genes, however, fewer than 150 have been identified to date. Recently, Stirling et al.[24] performed a systematic screen and identified a comprehensive list of 692 yeast CIN genes. To expand the number of CIN genes in humans and identify those genes that may contribute to CIN and oncogenesis, Ms. Laura Thompson (McManus laboratory) employed a cross-species candidate gene approach to identify a list of candidates to pursue in a human context. More specifically, a list of 164 candidate human CIN genes was identified that were subsequently interrogated for their role in CIN. Using reverse genetics (i.e. gene silencing) and image based microscopy, two phenotypes associated with CIN, namely changes in nuclear

areas (NA) and micronucleus (MN) formation were quantitatively assessed and compared with controls (*GAPDH*-silenced cells).

In general, changes in NA are typically associated with large scale changes in chromosome content, and are generally suggestive of numerical CIN[164], whereas micronuclei are extranuclear bodies found outside the primary nucleus that frequently arise due to chromosome segregation defects. Thus increases in the number of micronuclei are suggestive of small scale changes in chromosome content and are most likely representative of structural CIN[164]. Overall, the CIN screen was performed in two karyotypically stable cell lines with different cellular contexts; hTERT (an immortalized fibroblast cell line with modal chromosome number of 46[165]) and HT1080 (a transformed fibrosarcoma cell line with chromosome modal number of 46[166]). Overall this CIN screen identified 148 putative CIN genes, including *KIF11*, as determined by a statistically significant change relative to controls in at least one of the CIN-associated phenotypes (i.e. changes in NA or MN formation) in at least one cell line (Figure 1-8). *KIF11* was identified as a candidate CIN gene in hTERT, as diminished expression was associated with a 1.8-fold increase in NA, and a 5.3-fold increase in MN formation relative to the control (GAPDH). Furthermore, subsequent statistical analyses revealed these increases to be statistically significant (p-value <0.0001), identifying *KIF11* as a putative CIN gene within those cells. Interestingly, although *KIF11* silencing within HT1080 also resulted in statistically significant increases in NA and MN formation, it also induced extensive levels of cytotoxicity. In fact, fewer than 50 nuclei were enumerated within the HT1080 cells and thus these results were not included as they did not meet the minimum number of cells required (50 nuclei) for the study. Accordingly, these preliminary findings along with the mitotic-associated function, identify KIF11 as an excellent candidate CIN gene to pursue in subsequent validation assays.

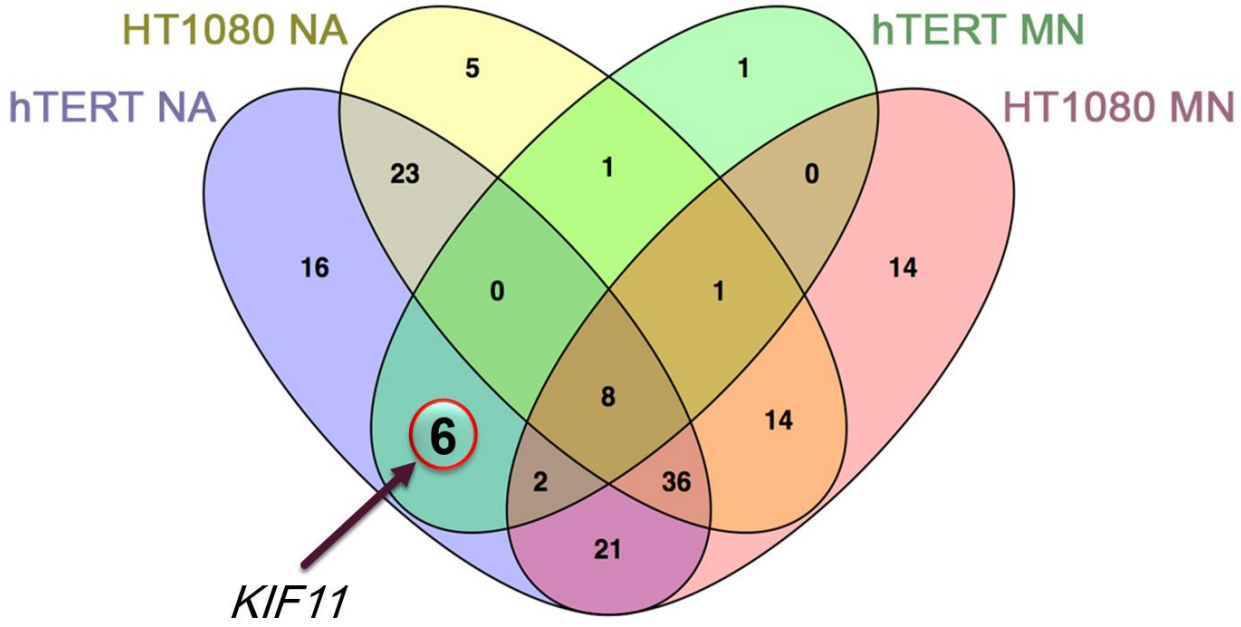

Figure 1-8: Cross-species Candidate Gene Approach Identified 148 Putative Human CIN Genes

Venn diagram presenting the results of a high-content, RNAi-based screen performed in HT1080 and hTERT cells that assessed two aberrant phenotypes associated with CIN, namely nuclear areas (NA) and micronucleus (MN) formation. Among 164 genes screened in this study, silencing of 148 genes induced CIN as was detected with at least one assay in at least one cell line. The red circle indicates the 6 genes identified in hTERT cell line with both assays, and includes *KIF11*. (Unpublished data of Laura L Thompson & Kirk J McManus).

CHAPTER 2: RATIONALE, HYPOTHESIS, RESEARCH AIMS, AND SIGNIFICANCE

2.1 Rationale

Understanding the aberrant pathways that contribute to oncogenesis and identifying the aberrant genes involved in these pathways is a critical first step to develop effective strategies to better combat cancer. CIN is a well-known aberrant phenotype occurs in ~80% of all cancer types and is associated with aggressive cancers, the acquisition of multi-drug resistance and consequently poor patient prognosis. However, despite these associations, the aberrant genes and molecular defects that cause CIN are only poorly understood. KIF11 is a microtubule motor protein that normally functions to maintain chromosome stability in human cells, and is an excellent candidate to pursue for *in vitro* study and validation for numerous reasons. First, *KIF11* is human ortholog of *CIN8*, an established budding yeast CIN gene[167]. Based on the evolutionary conserved nature of KIF11 function (see *Section* 1.4, pg. 15), I propose that normal *KIF11* expression and function are required to maintain chromosome stability under normal conditions in humans. Secondly, KIF11 is a plus-end microtubule motor protein that functions in bipolar spindle assembly in early mitosis to assist in chromosome segregation during anaphase (see *Section* 1.5.3, pg. 24). Thus, I propose diminished KIF11 expression and function will adversely impact bipolar spindle formation and chromosome segregation and underlie CIN. Thirdly, *KIF11* is somatically mutated and deleted in numerous cancer types, including CRC (Table 2-1). Finally, recent data obtained from a CIN screen performed in the McManus laboratory identified KIF11 as a putative CIN gene (see *Section* 1.6, pg. 31). Collectively, these data suggest KIF11 is a CIN gene and is an excellent candidate to pursue in both silencing and inhibition-based experiments.

Table 2-1: Frequency of Somatic *KIF11* Mutations and Deletions in Five Cancer Types

Cancer Type	Alteration Frequency[A]		Canadian New Cases[B]	USA New Cases[C]	Potential Canadian[D]	Potential American[D]
	Mutations	Deletions				
Prostate	0.8%	4.1%	21,600	180,890	1,058	8,863
Uterine	4.1%	0.4%	6,560	60,050	295	2,702
Colorectal	3.2%	0.5%	26,150	134,490	967	4,976
Lung	1.1%	1.7%	28,430	224,390	796	6,282
Breast	0.5%	0.2%	25,700	246,660	179	1,726

[A]Only The Cancer Genome Atlas (TCGA, Provisional)[168] data has been included as they are the most recent and comprehensive genome-wide, gene re-sequencing datasets available[169,170].
[B]The estimated incidence of newly diagnosed individuals in Canada in 2016[171].
[C]The estimated incidence of newly diagnosed individuals in USA in 2016[172].
[D]The potential number of Canadians and Americans with somatic *KIF11* mutations and deletions in 2016 are calculated by multiplying the *KIF11* mutation plus deletion frequency within a given caner type by the number of newly diagnosed individuals presented in column B and C.

2.2 Hypothesis

Based on the literature summary and preliminary findings from the McManus laboratory, I hypothesize that *KIF11* is a human CIN gene whose aberrant expression and function may contribute to oncogenesis. More specifically, I hypothesize that KIF11 silencing and inhibition will induce CIN phenotypes in two karyotypically stable cell line models. To test these hypothesis, I have formulated the following two Research Aims.

2.3 Research Aims

Aim 1: To Evaluate the Impact KIF11 Silencing has on Chromosome Instability

To evaluate the effect diminished expression has on CIN, KIF11 will be silenced using siRNAs (small interfering RNAs) in two karyotypically stable cell lines (HCT116 and hTERT). Changes in various phenotypes associated with CIN will be evaluated including NA, MN formation, DNA content and chromosome numbers, and statistically compared with controls.

Aim 2: To Evaluate the Impact KIF11 Inhibition has on Chromosome Instability

To determine the effect KIF11 inhibition has on CIN, two karyotypically stable cell lines (HCT116 and hTERT) will be treated with monastrol and various CIN phenotypes will be assessed including NA, MN formation, and chromosome numbers. To evaluate the effect KIF11 inhibition has on cell proliferation, real-time cellular analyses (RTCA) will be employed.

2.4 Significance

Our current knowledge pertaining to the molecular origins of CIN in cancer is extremely limited. Accordingly, much greater insight into the aberrant genes and abnormal pathways driving CIN and contributing to oncogenesis is needed. This thesis seeks to establish *KIF11* as a novel CIN gene by evaluating the impact diminished KIF11 expression and function have in two distinct,

yet karyotypically stable cellular contexts including a transformed CRC context (HCT116), and an immortalized fibroblast context (hTERT). Finally, because *KIF11* is altered in numerous cancer types beyond CRC, the findings I make will be of wide interest to those studying cancer in general.

CHAPTER 3: MATERIALS AND METHODS

3.1 Reagents

Appendix A contains a list of the solutions and the reagents used throughout this study (pg. 111). In general, all reagents were purchased through Corning, Thermo Scientific, Fisher Scientific, Fisherbrand, BioRad, Dharmacon, Life Technologies, Vector Laboratories, Roche, Gibco, Falcon, Sarstedt, Sigma-Aldrich and VWR.

3.2 Cell Culture

Two karyotypically stable and adherent human cell lines were employed throughout this study and include HCT116, a transformed colorectal cancer cell line, and hTERT[165], an immortalized fibroblast cell line. The general properties of each line are presented in Table 3-1. HCT116 cells were cultured in McCoy's 5A medium (Fisher Scientific) supplemented with 10% fetal bovine serum (FBS; Sigma-Aldrich), while hTERT cells were cultured in Dulbecco's modified Eagle's medium (DMEM; Fisher scientific) supplemented with 10% FBS. All cells were grown on 15 cm tissue culture dishes (Sarstedt) unless otherwise stated. Cells were maintained in a humidified incubator (Sanyo) at 37°C with 5% CO_2 until confluency reached ~80%, at which point cells were detached (see below) and reseeded as required.

A biological safety cabinet was used for all cell culture passaging and manipulations. For cell passaging, media was aspirated and cells were washed with 1×phosphate buffered saline (PBS) (Appendix A). This was followed by the addition of 2 mL of 0.05% trypsin containing ethylenediaminetetraacetic acid (EDTA; Fisher Scientific) for 5 minutes (min) for HCT116, or the addition of 3 mL of 0.05% trypsin containing EDTA for 10 min for hTERT. hTERT cells were incubated with trypsin at 37°C to increase the efficacy of detachment. Cells were monitored with

an inverted ID03 microscopy (Zeiss) using a 10× objective to ensure detachment from the plate. Following detachment, cells were collected in ~5 mL of PBS and transferred to a sterile 15 mL conical tube. Cells were pelleted by centrifugation at 140 xg for 5 min in a Thermo Scientific Legend XFR centrifuge. Supernatant was aspirated and the cell pellet was resuspended in 3 mL of 1×PBS, and 1 mL of the cells was dispensed into a 15 cm culture dish containing 20 mL of fresh medium.

Table 3-1: General Properties of the HCT116 and hTERT Cell Lines

	HCT116	**hTERT**
Organism	Homo sapiens	Homo sapiens
Tissue	Colon	Foreskin
Cell Type/Disease	Epithelial, CRC, transformed	Fibroblast, immortalized with hTERT
Culture Properties	Adherent	Adherent
Culture Medium	McCoy's 5A + 10% FBS	DMEM + 10% FBS
Approximate Doubling Time	22h	36h
Karyotype	45, XY	46, XY
Source	American Type Culture Collection	C. P. Case (University of Bristol, Bristol, UK)[173]

3.2.1 Cell Counting

To generate accurate live cell counts for cell seeding purposes, cells were harvested as detailed above, but were resuspended in ~6 mL of 1×PBS. To obtain a single cell suspension, HCT116 cells, which can form cellular aggregates, were passed through a 40 μm cell strainer –

hTERT were not strained as they do not form cellular aggregates. Next, a 40 μL aliquot of cells was mixed with an equal volume (40 μL) of 0.2% trypan blue stain (Gibco). Trypan blue is a vital dye that selectively colors dead cells blue due to its uptake resulting from the loss of membrane integrity, while live cells remain colorless as the intact membrane excludes the dye. Next, 10 μL of the cell/trypan blue solution was dispensed into a cell counter slide (Cedex Smart Slide, Roche) in duplicate and analyzed using a cell counter (Cedex XS, Roche). The Cedex XS employs an image-based approach to determine the total number of cells, and can easily distinguish between live and dead based on trypan blue staining. The average of two cell counts was employed to calculate the concentration of live cells within the solution from which appropriate dilutions (PBS or media) were made. Table 3-2 presents the total number of live cells employed (seeded) within each subsequent experiment detailed within this thesis.

Table 3-2: Cell Seeding Densities Employed in Each Experimental Approach

Treatment	Cell Line	Experimental Approach [A]	Plate Format	Cells/Well (Treatment)	Cells/Well (Controls)
siRNA	HCT116/hTERT	WB/NA/MNF	6-well plate	160×10^3	80×10^3
	HCT116/hTERT	IIF	6-well plate	80×10^3	5×10^3
	HCT116	FC	6-well plate	80×10^3	5×10^3
	hTERT	FC	6-well plate	80×10^3	8×10^3
	HCT116	MCS	6-well plate	40×10^3	5×10^3
	hTERT	MCS	6-well plate	80×10^3	40×10^3
Inhibitor	HCT116/hTERT	NA/MNF	96-well plate	4×10^3	1×10^3
	HCT116	MCS	24-well plate	40×10^3	5×10^3
	hTERT	MCS	24-well plate	80×10^3	5×10^3
	HCT116/hTERT	RTCA	16-well plate	4×10^3	4×10^3

[A]Abbreviations: WB (Western blot), IIF (indirect immunofluorescence), MNF (micronucleus formation), FC (flow cytometry), MCS (mitotic chromosome spread).

3.3 siRNA-based Silencing

ON-TARGETplus siRNA duplexes targeting KIF11 (si*KIF11*-1, -2, -3, -4), GAPDH (si*GAPDH*-Pool; negative control), and non-targeting siRNA (siNon-targeting; negative control) were purchased from Dharmacon. Duplexes were resuspended in 1×siRNA buffer (Dharmacon; Appendix A) to a final stock concentration of 20 μM or a working concentration of 10 μM. A pool (si*KIF11*-Pool) of the four individual siRNA duplexes targeting KIF11 was prepared by combining equal volumes of the four siRNA duplexes (4× 2.5 μM or 10 μM total). All siRNAs were stored at -80ºC in small aliquots to minimize freeze-thaw cycles.

For silencing purposes, the appropriate numbers of cells were seeded into various types of vessels depending on the experimental approach as indicated in Table 3-2. Cells were permitted to attach and grow for 24 hours (h) prior to transfection with individual or pooled siRNAs using lipid-based approaches (RNAiMax) as detailed by the manufacturer (Life Technologies). siRNAs and RNAiMAX concentrations were optimized to maintain viable cells and induce silencing as was measured with a morphological change in cells induced following *KIF11* silencing. Efficient *KIF11* silencing induces a mitotic arrest with monopolar spindles, a phenotype that can be observed through transmission microscope as rounded-up cells. The concentrations of siRNAs and RNAiMAX that induce this phenotype without excessive amount of death was identified to be 0.5 μL and 3 μL respectively for each 40,000 cells. Briefly, 0.5 μL of the siRNA duplexes (10 μM) and 3μL RNAiMAX were mixed in serum-free media and used to transfect 40,000 cells. Silencing efficiency was further confirmed by semi-quantitative Western blots as indicated below (*Section* 3.4, pg. 42). In general, a similar timeline was followed for each subsequent experiment (Figure 3-1); following transfection, cells were grown for 5 days at which point they were fixed, counterstained, imaged and analyzed as detailed below.

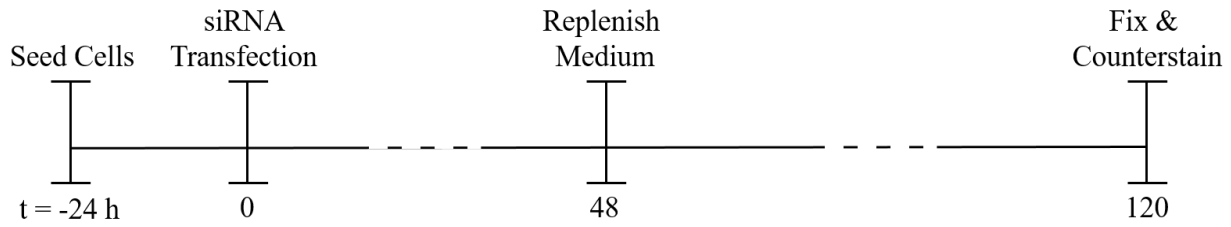

Figure 3-1: Experimental Timeline Employed for the Silencing Experiments
A schematic presenting the general timeline employed for the siRNA based silencing experiments. Cells were seeded, permitted to attach and grown for 24 h prior to transfection with appropriate siRNAs (time (t) = 0 h). Approximately 48 h post-transfection medium was replenished and cells were permitted to grow for an additional 3 days (t = 120) at which point they were fixed, counterstained, imaged and analyzed.

3.4 Protein Analysis with Western Blot

To harvest proteins for Western blots, medium was aspirated from each well of a 6-well plate, and cells were washed 3 times with cold (4ºC) 1×PBS. Depending on cell confluency, ~100-200 µL of RIPA (radioimmunoprecipitation assay) buffer (Appendix A) containing 4% Complete Protease Inhibitor Cocktail (25×; Roche) was added to each well in a cold room (4ºC). Cells were incubated at 4ºC for 5 min, collected using cell scrapers and transferred to micro-centrifuge tubes. Cells were sonicated two times using Sonifer Cell Disrupter (Branson Sonic Power Co.) with duty cycle of 50% and an output control setting of 6. To remove insoluble cellular debris, samples were centrifuged (Biofuge Fresco, Heraeus) at 15000 xg for 2 min at 4ºC. The supernatant containing soluble proteins was collected and stored at -20ºC for short-term storage (<2 weeks) or at -80ºC for long-term storage (>2 weeks).

Protein concentrations were determined using the Pierce™ BCA (bicinchoninic acid) Protein Assay Kit (Thermo Scientific) along with protein standards prepared according to the manufacturer (Pierce). Three replicates of appropriately diluted protein (protein:RIPA [1:5]) were

prepared and their concentrations were determined using the Cytation 3 plate reading function (BioTek). Briefly, the absorbance of the standards (and unknown protein samples) was read at 562 nm and employed to generate a standard curve from which the concentrations of the unknown protein samples were determined.

Samples were prepared for Western blot analyses by combining 20 μg of total protein/sample with 5× sodium dodecyl sulfate/dithiothreitol (SDS/DTT) Sample Buffer (Appendix A) to a maximum total volume of 30 μL. To denature proteins, samples were heated to 95ºC for 5 min in a Thermomixer R (Eppendorf) and immediately plunged into ice to prevent renaturation. Denatured samples were dispensed into pre-rinsed wells of a 4-20% mini-Protean TGX gel (BioRad) and placed in a Miniprotean tank (BioRad) containing 1× Running Buffer (Appendix A). Samples were electrophoresed at 140 V (300 W, 3 A) for 40 min using a standard power supply (PowerPac HC, BioRad). Following electrophoresis, proteins were transferred to polyvinylidene difloride (PVDF) membranes (Millipore; 0.45 μm pore size) using the Trans-Blot SD Semi-Dry Transfer Cell apparatus (BioRad). Briefly, PVDF membranes were pre-rinsed with methanol followed by three rinses with Milli-Q water. The transfer apparatus was assembled according to the manufacturer (BioRad) and proteins were transferred to the membranes in 1× Transfer Buffer (Appendix A) at 14 V for 40 min.

To visually confirm protein transfer and to identify appropriate regions to cut for subsequent blotting, membranes were stained with copper phthalocyanine 3, 4', 4'', 4'''-tetrasulfonic acid tetrasodium salt (CPTS; Appendix A). Membranes were cut such that the top half could be used to evaluate KIF11 (119 kDa) expression, while the bottom half could be used to assess the abundance of the loading control, Cyclophilin B (21 kDa). Membranes were destained in TBST (Tris-Buffered Saline and Tween 20; Appendix A) for 5 min at medium speed on a Belly

Dancer (Stovall Life Science, Inc), and were blocked with 5% non-fat milk (Appendix A) for 45 min with gentle rocking. Next, membranes were incubated with primary antibodies (KIF11 or Cyclophilin B) diluted in 5% non-fat milk at 4ºC overnight with gentle rocking. The following day, membranes were rinsed with TBST three times for 10 min each, and were incubated with an appropriate secondary antibody conjugated with horseradish peroxidase. Table 3-3 presents information pertaining to the primary and secondary antibodies employed in this study including sources, catalogue numbers and working dilutions. Membranes were then incubated for 1 h at room temperature with gentle rocking, and were subsequently washed 3 times with TBST as indicated above.

Table 3-3: Antibody List and Dilution Employed

Antibody[A]	**Catalogue Number**	**Source**	**Type[B]**	**Dilution (WB)**	**Dilution (IIF)**
KIF11	ab181981	Abcam	Rb	1:15000[C]	1:200
Cyclophilin-B	ab16045	Abcam	Rb	1:50000	---
Anti-Rabbit HRP	111-035-144	Jackson Immuno Research Labs	G	1:15000	---
α-Tubulin	ab7291	Abcam	M	---	1:3000
Anti-Rabbit Cy3	111-165-144	Jackson Immuno Research Labs	G	---	1:200
Anti-Mouse AlexaFluor 488	ab150117	Abcam	G	---	1:200

[A]HRP (Horseradish peroxidase), Cy3 (Cyanine 3)
[B]Ra (rabbit), M (mouse), G (goat)
[C]More concentrated KIF11 antibody (1:5000) was used for hTERT cells

To visualize protein expression, SuperSignal West Dura Extended Duration Substrate was used as indicated by the manufacturer (Thermo Scientific). Briefly, 1.0 mL of substrate was prepared per membrane and dispensed onto Saran wrap. Membranes were placed face down (i.e. protein-side down) onto the substrate and incubated at room temperature for 5 min. Following incubation, excess substrate was removed by dabbing the edge of the membranes with a Kimwipe, and the membrane was placed in a plastic page protector. Proteins were visualized using a My ECL imager (Thermo Scientific) with various exposure times acquired for each membrane. An optimal exposure time was identified for each blot and was defined as the time required to produce a strong signal with minimal pixel saturation (i.e. within the linear dynamic range of the camera).

3.5 Indirect Immunofluorescence Labelling and DAPI Counterstaining

Cells were seeded onto ethanol sterilized glass coverslips (18 × 18 mm; Fisherbrand) at the densities described in Table 3-2 (pg. 40) and allowed to attach (~20-24 h). Cells were transfected with siRNAs as indicated above (*Section* 3.3, pg. 41), and were fixed 5 days post-transfection with freshly prepared 4% paraformaldehyde (Appendix A) in 1×PBS for 10 min at room temperature. Paraformaldehyde was aspirated, cells were washed three times with 1×PBS, and cell membranes were permeablized with 0.5% Triton X-100 in PBS (Appendix A) for 10 min. Permeablized cells were washed two times with 1×PBS and the edges of coverslips were dabbed on a Kimwipe to remove excess PBS. Coverslips were inverted onto parafilm containing 30 μL of the appropriate primary antibody aliquot (see Table 3-3 [pg. 44] for working dilutions). Coverslips were left at room temperature overnight, but were maintained under a plastic lid to prevent desiccation. The following day, coverslips were returned to 6-wells plates and were permeablized with 0.1% Triton X-100 (30 seconds) and washed two times with PBS. Approximately 30 μL/coverslip of diluted secondary antibodies (Table 3-3) were dispensed onto parafilm and coverslips were dabbed with

a Kimwipe, gently inverted onto the secondary antibody, and incubated for 1 hr at room temperature while protected from the light. Cells were permeablized with 0.1% Triton X100 and were washed twice with PBS. Excess PBS was removed from coverslips with a Kimwipe and coverslips were inverted onto 7.4 μL (18mm × 18mm coverslips, 1.5 thickness) or 5 μL (12mm circular coverslips, 1.5 thickness) of mounting media containing DAPI (Vector Laboratories; Appendix A) on a microscope slide. To equilibrate DAPI across the cells, slides were incubated overnight at 4ºC and subjected to image acquisition as detailed below (*Section* 3.7).

3.6 Optimizing KIF11 Inhibitor (Monastrol) Concentration for Subsequent Treatments

Monastrol (Sigma 475879) was purchased from Sigma-Aldrich, resuspended to a stock concentration of 15mM in dimethyl sulfoxide (DMSO; Fisher Scientific) and stored at -80ºC. To identify the optimal monastrol concentrations to employ in subsequent KIF11 inhibitor studies, various concentrations were evaluated in both HCT116 and hTERT cells. In brief, 4,000 cells (in 200 μL of medium) were dispensed into each well of a 96 well-plate, permitted to attach and grow for 24 h. Cells were treated with a 10-fold serial dilution of monastrol ranging from 1 μM to 1000 μM in sextuplet with DMSO (0.6%) serving as the vehicle control. Based on published data showing increases in mitotic phenotypes (i.e. rounded-up cells) in cell populations treated with monastrol[144,145], HCT116 and hTERT cells were monitored for similar phenotypes using an inverted ID03 microscope (Zeiss) and 10× objective (Zeiss) for up to 24 h. The optimal concentration was identified to be 100 μM, as it was the concentration resulting in the greatest number of mitotic cells with minimal cytotoxicity. This concentration is in agreement with previous studies[174,175,176,177], and thus was employed in all subsequent studies.

3.7 Microscopy and Imaging

All images were acquired using either an Axio Imager.Z2 (Zeiss) epi-fluorescence microscope equipped with a 14-bit gray scale charge-coupled device (CCD) AxioCam HRm camera (Zeiss), or a Cytation 3 Cell Imaging Multi-Mode Reader (BioTek) equipped with 16-bit gray scale CCD camera (Sony). In general, all high-resolution images were acquired using the Imager.Z2, while quantitative (low-resolution) images were acquired using either the Imager.Z2 or the Cytation 3.

3.7.1 High-Resolution Indirect Immunofluorescence Microscopy

To validate the specificity of antibodies and reveal qualitative changes in the abundance of KIF11 following siRNA-based silencing, high-resolution indirect immunofluorescence imaging was employed. All 2D and 3D high-resolution images were acquired using a Zeiss Axio Imager.Z2 equipped with a 63× Plan-Apochromat oil immersion lens (numerical aperture [NA] = 1.4) and AxioVision 4.8 (Zeiss) software.

In general, DAPI, FITC and Texas Red filters were employed to collect multi-channel images of DAPI, Alexafluor488 and Cy3 fluorophores, respectively. Due to sample variability, the optimal exposure times for DAPI and Alexa488 channels were independently optimized for each image, and were defined as the exposure time producing maximum signal intensity without image saturation. However, to observe qualitative differences in KIF11 expression as represented by changes in KIF11 signal intensity, the Cy3 channel exposure time was first optimized using the control samples and then maintained constant throughout all subsequent imaging, including the *KIF11* silenced conditions. All images were imported to Imaris 7.7.2 software (Bitplane) for subsequent analyses and presentation purposes.

3.7.2 Quantitative Imaging Microscopy

Quantitative imaging microscopy was performed to assess NAs (*Section* 3.8, below), MN formation (*Section* 3.9, below) and mitotic chromosome enumeration (*Section* 3.11, below). In general, images were acquired using either an Axio Imager.Z2 equipped with a 20× Plan-Apochromat dry lens (NA = 0.5) or a 63× Plan-Apochromat oil immersion lens (NA = 1.4) using an AxioVision 4.8 software, or a Cytation 3 equipped with a 20× Olympus LUCPLFLN lens (NA = 0.45) using Gen5 (BioTek) software.

Generally, the Imager.Z2 was used to acquire images of DAPI counterstained DNA. In general, DAPI signal intensities were independently optimized for each mitotic chromosome spread so that chromosomes could be accurately enumerated. Images were saved as 16-bit Carl Zeiss (zvi) files and were analyzed using either Imaris or FIJI software. Data were imported into Prism v6.0 (GraphPad) where statistical analyses (see *Section* 3.13, below) were performed and graphs were generated. Similarly, the Cytation 3 equipped with DAPI filter was used to acquire images of Hoechst 33342 (Life Technologies) counterstained nuclei and micronuclei. Importantly, the exposure time was first optimized for Hoechst 33342 and maintained constant during image acquisition so that quantitative comparisons could be made. In general, nine non-overlapping images were acquired per well, and images were analysed using the Gen5 image analysis software (BioTek). All imaging data were imported into Prism v6.0 where statistical analyses (see *Section* 3.13, below) were performed and graphs were generated.

3.8 Nuclear Area Assay

In general, two approaches were employed for acquisition and analysis of the images for this section; 1) HCT116 and hTERT cells were silenced using siRNAs targeting *KIF11* or controls,

imaged using the Axio Imager.Z2 and analysed using Imaris software, or 2) HCT116 and hTERT cells were treated with monastrol, imaged using Cytation 3, and analysed using Gen5 software.

3.8.1 Quantification of Nuclear Areas Following siRNA-based Silencing

To quantify NAs following siRNA-based treatments, cells were fixed with freshly prepared paraformaldehyde (4%) in 1×PBS, permeablized with 0.1% Triton X100, washed two times with 1×PBS and mounted in mounting media containing DAPI. Images were acquired using the Imager.Z2 equipped with a 20× objective and were analysed using Imaris software. The DAPI channel exposure time was first optimized and then maintained constant so that quantitative comparisons could be made. All imaging data were imported into Imaris and the pixel dimensions were set to reflect the pixel dimensions of the camera and the 20× objective (x × y dimensions; 0.3225 μm × 0.3225 μm) employed. To ensure accurate quantification of NAs and exclude artefacts three different inclusion/exclusion criteria were employed; 1) an XY boundary exclusion filter was applied to eliminate partial nuclei located along the periphery of the image, 2) a minimum size inclusion filter was employed to eliminate cellular debris and apoptotic nuclei, and 3) a mean signal intensity threshold was applied to eliminate mitotic and/or apoptotic cells. All data were exported into Prism v6.0 where statistical analyses were performed and graphs were generated.

3.8.2 Quantification of Nuclear Areas Following Monastrol Treatment

To quantify NAs following monastrol treatment, cells were fixed with freshly prepared paraformaldehyde in 1×PBS (4%), washed two times with 1×PBS and were counterstained with Hoechst 33342 (300 ng/mL). Images were acquired using a Cytation 3 equipped with a 20× objective and were analysed using Gen5 software. As above, the DAPI channel was used to determine NAs. To ensure accurate quantification of NAs similar inclusion/exclusion criteria to

those listed above were employed. All data were exported into Prism v6.0 where statistical analyses were performed and graphs were generated.

3.9 Micronucleus Formation Assay

Quantitative imaging microscopy was performed to identify potential changes in the number of micronuclei following *KIF11* silencing or inhibition with monastrol. Similar to NA assay detailed above, two approaches were employed to quantify nuclei following siRNA-based silencing or monastrol treatments.

3.9.1 Quantification of Micronucleus Formation Following *KIF11* Silencing

To quantify MN formation following *KIF11* silencing, cells were fixed with freshly prepared paraformaldehyde (4%) in 1×PBS, permeablized with 0.1% Triton X100, washed two times with 1×PBS and mounted in mounting media containing DAPI. Images were acquired using the Imager.Z2 equipped with a 20x objective and were analysed using Imaris software. The DAPI channel was imported into Imaris and images were visually inspected for MN formation considering two critical parameters; 1) size; a MN was defined as a small extranuclear body with an area <1/3 the size of the primary nucleus, 2) intensity; to distinguish micronuclei from bright, highly fluorescent apoptotic bodies a maximum intensity threshold was employed. In general, a minimum of 100 nuclei were analysed for MN formation. All data were imported to Prism v6.0, where standard statistics and graphs were generated. In general, the frequency of cells with micronuclei was determined for each condition. Graphs were imported into Photoshop CS6 (Adobe) where figures were assembled.

3.9.2 Quantification of Micronucleus Formation Following Monastrol Treatment

To quantify MN formation following KIF11 inhibition, cells were fixed with freshly prepared paraformaldehyde (4%) in 1×PBS, washed two times with 1×PBS and were counterstained with Hoechst 33342. Images were acquired using a Cytation 3 microscope equipped with a 20× objective. Images were imported into Gen5 image analysis software and as above both size and signal intensity thresholds were employed to restrict the analysis to micronuclei and eliminate apoptotic bodies. A minimum of 100 nuclei were analysed for MN formation and restriction of the results to micronuclei was confirmed with careful visual inspection. All data were imported to Prism v6.0, where standard statistics and graphs were generated. In general, the frequency of cells with micronuclei was determined for each condition. Graphs were imported into Photoshop where figures were assembled.

3.10 Flow Cytometry Analysis of DNA Content

Flow cytometry was performed to evaluate potential changes in DNA content following *KIF11* silencing. Briefly, five days post-silencing cells were harvested, fixed and permeablized with ethanol, and labelled with Propidium Iodide (PI; Appendix A) in preparation for flow cytometry and DNA content analysis as detailed below.

3.10.1 Ethanol Fixation

Following silencing, cells were detached with trypsin (*Section* 3.2, pg. 38), pelleted by centrifugation (390 xg; 5 min), counted and resuspended in an appropriate volume of 1×PBS so that the final concentration of cells was 1×10^6 cells/mL. Cells were transferred into a 5 mL polystyrene round-bottom tube (Falcon) and were centrifuged (140 xg, 5 min). The supernatant was removed, and cells were fixed and permeablized with 1 mL ice-cold 70% ethanol (Appendix

A) that was added drop wise with continuous vortexing. Cells were fixed overnight at 4ºC prior to PI staining.

3.10.2 Propidium Iodide Staining

Following ethanol fixation, cells were pelleted by centrifugation (250 xg, 10 min, 4ºC), supernatant was removed and 1×10^6 cells were resuspended in 1 mL of 1×PBS containing 40 µL of PI and 10 µL RNase A (10 mg/mL; Fisher Scientific; Appendix A) and mixed well. Cells were incubated for 30 min at 37ºC to degrade any RNA present within the samples. Cells were centrifuged at 250 xg for 5 min, the supernatant was removed, the cells were resuspended in 500 µL of 1×PBS and flow cytometry was performed as detailed below.

3.10.3 Flow Cytometry

Flow cytometry was performed using a Becton Dickinson FACS Calibur equipped with BD CellQuest version 0.4.dfb. Prior to performing flow cytometry, HCT116 cells were briefly sonicated (duty cycle of 35%, output of 2.5, 3-5 pulses) to disrupt cellular aggregates and render a single cell suspension. Instrument settings were first optimized utilizing the untreated and negative control samples. Briefly, cells were gated based on SSC-H, FSC-H, FL2-A, and FL2-W and a total number of 10,000 gated events (i.e. cells) were acquired in triplicate. Gated events were subsequently analysed using FlowJo software version 10.0.5 and the proportion of cells with DNA content of 2C, 4C, and >4C was determined based on PI intensity.

3.11 Mitotic Chromosome Spreads and Chromosome Enumeration

To determine whether *KIF11* silencing or inhibition induces changes in chromosome numbers, mitotic chromosome spreads were generated and manually enumerated in both HCT116 and hTERT cells.

3.11.1 Generation of Mitotic Chromosome Spreads

To generate mitotic chromosome spreads, cells were seeded onto ethanol-sterilized coverslips according to the densities presented within Table 3-2 (pg. 40). Cells were silenced and grown for 5 days as indicated above (*Section* 3.3), and were mitotically enriched using KaryoMAX colcemid (10 μL/ mL of medium; Life Technologies) for either 2 h (HCT116) or 4 h (hTERT). Following colcemid treatment, medium was aspirated and HCT116 and hTERT cells were treated with hypotonic solution (75 mM KCl; Appendix A) for 16 and 8 min, respectively. Cells were fixed using three 10 min washes with 3:1 mixture of methanol:acetic acid (Appendix A). Cover slips were air dried and counterstained with mounting media containing DAPI. Slides were stored overnight at 4ºC and imaged the following day.

3.11.2 Chromosome Enumeration

Mitotic chromosome spreads were imaged using an Axio Imager.Z2 equipped with a 63× oil immersion lens as described above (*Section* 3.7.2). Images were acquired as TIF files and were imported into FIJI software where chromosomes from a total of 100 spreads/condition were manually enumerated. Chromosome counts were imported into Prism v6.0, where statistical analyses (see *Section* 3.13) and graphs were generated. All figures were assembled using Photoshop.

3.12 Real-Time Cellular Analyses

To determine whether monastrol treated samples continue to proliferate, RTCA was performed in E-plates using an RTCA-dual plate (RTCA-DP; Acea Biosciences) analyzer housed within a 37ºC incubator. The RTCA-DP system employs microelectrodes at the bottom of each E-plate well to measure increases or decreases in electrical impedance (termed cell index), which

reflects increases (cellular proliferation) and decreases (cellular death) in cell numbers, respectively. Briefly, 4000 cells were seeded into each well of the E-plate in quadruplicate and cell indices were monitored every 15 min. Approximately 24 h post seeding, 100 μL fresh media containing monastrol (100 μM) or DMSO (6%) was added to the appropriate wells, or an identical volume of fresh media was added to untreated wells and used as a control. Cells indices were monitored for 5 additional days, following which all data were imported into Prism and proliferation curves were plotted and visually compared between treatments. Graphs were generated and exported into Photoshop where figures were assembled.

3.13 Statistical Approaches and Analyses

Two different statistical analyses, namely Student's *t*-test and Kolmogorov-Smirnov (KS), were performed throughout this thesis to identify statistical significant differences between controls and silenced or monastrol treated conditions. Student's *t*-test is a parametric statistical test that compares the mean value of different conditions that are assumed to follow a normal distribution. Unlike Student's *t*-test, KS test is a nonparametric statistical test examining the null hypothesis that the distribution of all conditions follow the reference distribution (control). If the difference between the distribution of control and a treated sample is not statistically significant (p-value > 0.05), the null hypothesis is accepted. In contrast, if the null hypothesis is rejected (p-value < 0.05), it is assumed that the distribution of the silenced or monastrol treated sample is statistically different from the controls. A p-value of < 0.05 is considered statistically significant.

CHAPTER 4: RESULTS

4.1 Aim 1: To Evaluate the Impact *KIF11* Silencing has on Chromosome Instability

To determine whether *KIF11* silencing induces CIN, a variety of phenotypes associated with CIN were quantitatively assessed. These include changes in NA, MN formation, DNA content, and chromosome numbers[178,179,22]. In addition, to determine whether KIF11 exhibits a conserved role in maintaining chromosome stability, two distinct and karyotypically stable cell lines were employed throughout this thesis. Briefly, HCT116 is a transformed colorectal cancer cell line of epithelial origin with a modal number of 45 chromosomes, while hTERT is an immortalized fibroblast cell line with a modal number of 46 chromosomes. Both cell lines have been used extensively in the past to investigate other candidate CIN genes[83,180,181].

4.1.1 Establishing *KIF11* Silencing Efficiency in HCT116 and hTERT Cells

Before examining the effect diminished KIF11 expression has on surrogate markers of CIN, the silencing efficiencies of pooled siRNA (si*KIF11*-Pool) and four individual siRNAs (si*KIF11*-1, -2, -3, -4) were evaluated. Accordingly, cells were transfected, permitted to grow for 5 days, at which point proteins were harvested and Western blots were performed. Briefly, semi-quantitative Western blot analyses were performed by normalizing the KIF11 signal intensities to the corresponding signal intensities of the loading control (i.e. Cyclophilin-B), and are presented relative to the si*GAPDH* negative control. As shown in Figure 4-1, *KIF11* silencing by both pooled and individual siRNA approaches typically reduced expression to <11% and <16% of controls in HCT116 and hTERT, respectively. The three most efficient silencing conditions were similar in both cell lines and thus the si*KIF11*-Pool and the top two individual siRNA duplexes (si*KIF11*-1 and si*KIF11*-3) were selected and employed in subsequent experiments.

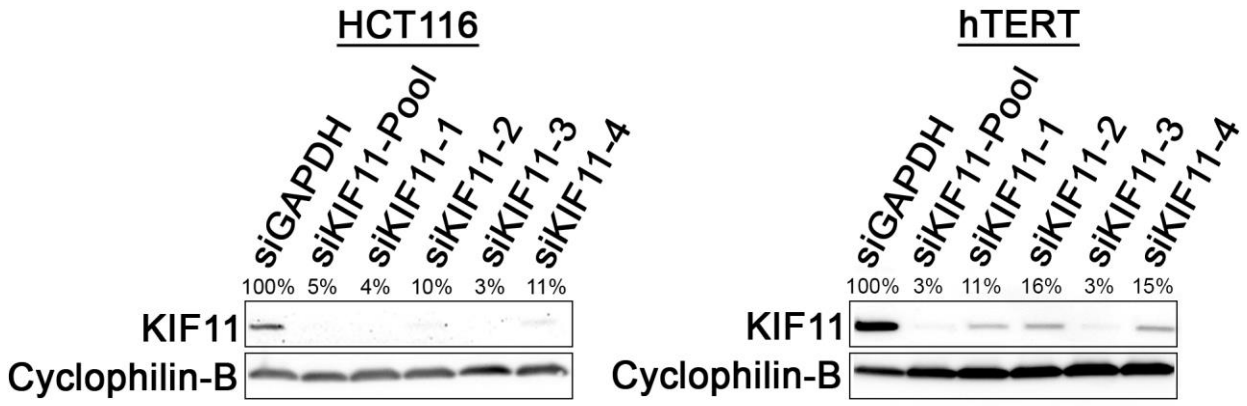

Figure 4-1: Evaluating KIF11 Expression within HCT116 and hTERT Cells
Western blot confirming the silencing efficiency of KIF11 siRNAs (si*KIF11*-Pool, -1, -2, -3, -4) in HCT116 (left) and hTERT (right) cells. Cyclophilin-B serves as the loading control, while si*GAPDH* serves as the negative control. The numbers represent the residual protein remaining following silencing and are presented relative to si*GAPDH*.

While monitoring the cells following silencing with transmitted light microscopy, it was noted that the cells began to round up, or become loosely attached to the vessels within a few hours post-transfection (Figure 4-2). This is an established phenotype that is observed following *KIF11* silencing or inhibition, and has been shown to occur due to a mitotic arrest (i.e. mitotic enrichment)[144,145]. To confirm that these rounded-up cells are arrested in mitosis and to further investigate the efficiency of silencing, IIF was performed. In general, IIF revealed a qualitative decrease in *KIF11* signal intensity within the silenced cells relative to the control cells where KIF11 labeling was predominantly associated with astral microtubules within mitotic cells (Figure 4-3). In fact, IIF shows that following *KIF11* silencing there is an increase in the proportion of cells exhibiting an aberrant mitotic phenotype that is reminiscent of a prometaphase-like state that likely stems from the lack of a bipolar spindle assembly (i.e. monopolar spindle)[115,182].

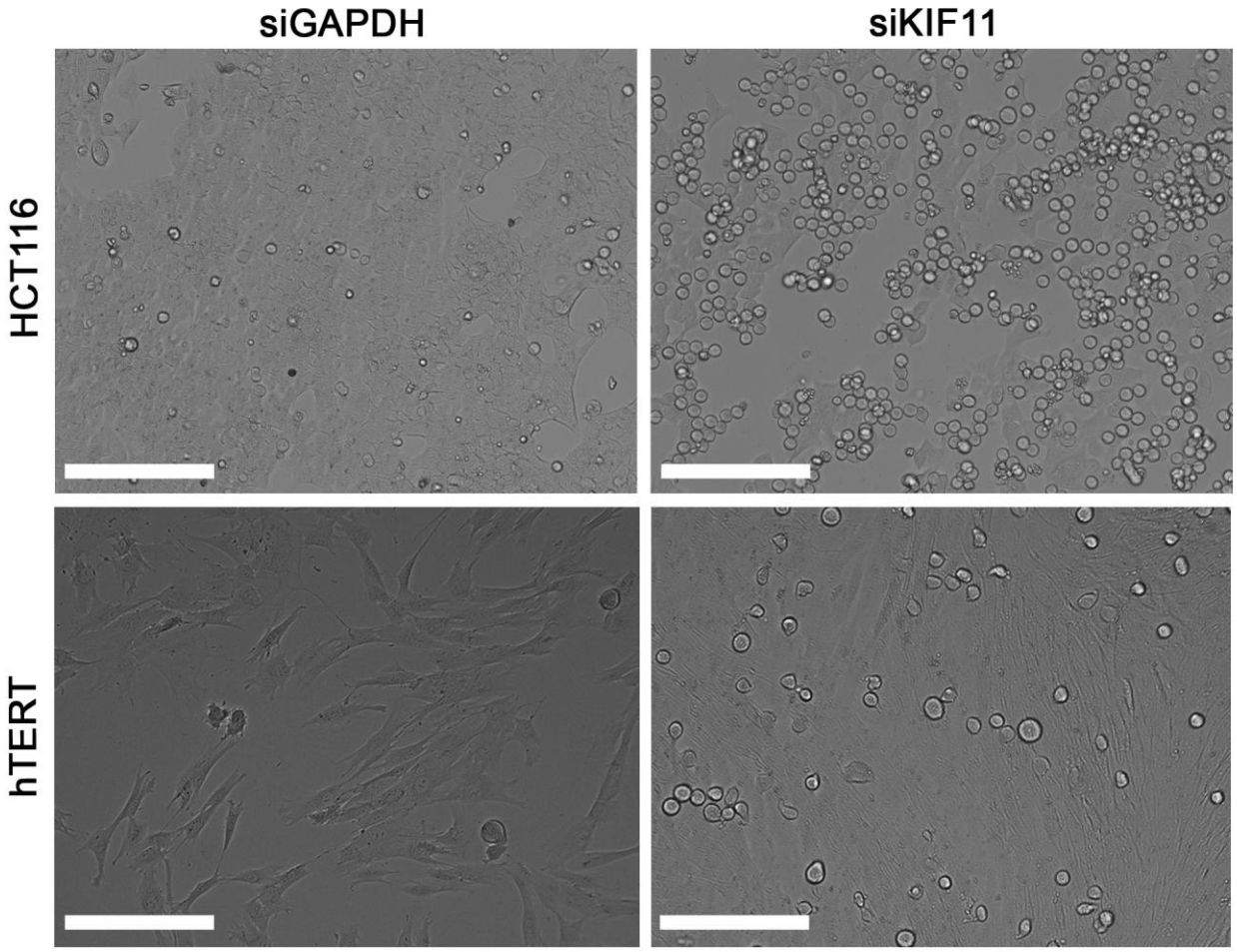

Figure 4-2: *KIF11* Silencing Induces Mitotic Arrest
Transmitted light microscopy reveals the effect of *KIF11* silencing (right panels) on the enrichment of HCT116 (top) and hTERT (bottom) cells in mitosis in comparison with the si*GAPDH* (left panels) negative control. (Scale bar = 200 μm). (time = 20 h post transfection with si*KIF11*).

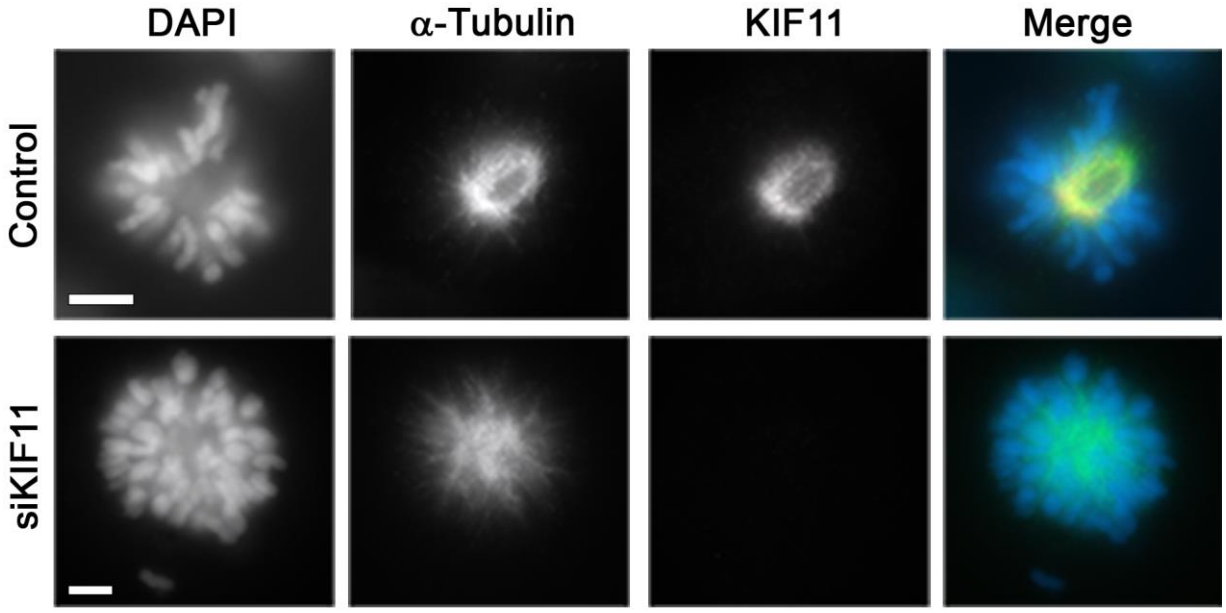

Figure 4-3: IIF Reveals a Decrease in *KIF11* Expression within *KIF11* Silenced Cells
Representative high-resolution IIF 2D images displaying KIF11 expression and localization within control (top panels) and silenced (bottom panels) HCT116 cells. DAPI, α-Tubulin, and KIF11 are pseudo-colored blue, green, and red, respectively, within the Merge. Qualitative comparisons can be made for the KIF11 channel as identical exposure times were employed. Note the extensive degree of colocalization occurring between KIF11 and α-Tubulin within the control cells resulting in the yellow color. (Scale bar = 5 μm).

4.1.2 *KIF11* Silencing is Associated with Increases in Nuclear Areas and Micronucleus Formation

Having identified the most efficient *KIF11* silencing duplexes, we now wished to determine the impact *KIF11* silencing has on two surrogate markers of CIN, namely NA and MN formation. Briefly, cells were transfected with si*KIF11*-Pool, si*KIF11*-1, si*KIF11*-3 or siGAPDH (control) and permitted to grow for five days, following which cells were fixed, permeablized, counterstained with DAPI, imaged and analyzed as detailed within Materials & Methods. To

compare changes in nuclear sizes between the various conditions, the areas of 100 interphase nuclei/condition were determined using automated imaging software (Figure 4-4).

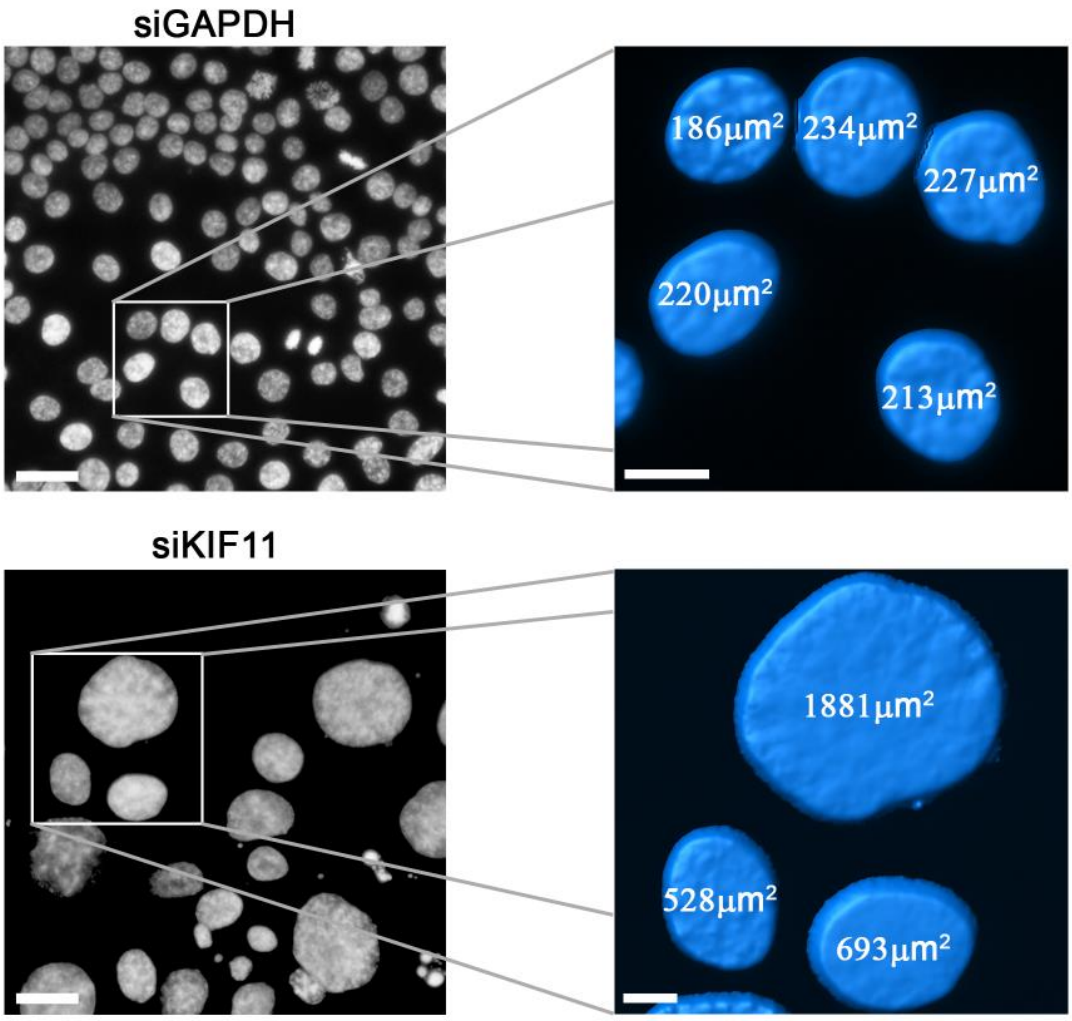

Figure 4-4: Increase in the Nuclear Area Following *KIF11* Silencing
Representative low-resolution 2D images depicting differences between the size of nuclei in control (si*GAPDH*; top panels) and *KIF11* silenced (si*KIF11*; bottom panels) HCT116 cells. All nuclei are counterstained with DAPI. Right panels present the software-generated surface renderings used to determine the NAs for the nuclei contained within the bounding boxes identified within the left panels (areas of individual nuclei are presented). Note the visual and quantitative increases in NAs within the si*KIF11* silenced cells relative to controls. Scale bars represent 30 μm and 10 μm within the left and right panels, respectively.

In agreement with the data from the preliminary screen, the overall NA ranges of HCT116 cells are both larger and dramatically increased following *KIF11* silencing relative to controls. Further, the mean NAs are approximately 1.5- to 3.0-fold larger within the si*KIF11*-Pool (556.6 μm^2), si*KIF11*-1 (688.8 μm^2), and si*KIF11*-3 (384.4 μm^2) treated cells relative to the negative control (si*GAPDH*; 213.0 μm^2). Subsequent Student's *t*-test revealed that these increases were all statistically significant (*p*-value < 0.0001), indicating that *KIF11* silencing is accompanied by increases in NAs within HCT116 cells (Figure 4-5; Table S6-1, pg. 119). In addition, *KIF11* silencing was also associated with an increase in the cumulative distribution frequency of NAs as evidenced by the striking right-ward shift of the distributions relative to the controls (Figure 4-6). Indeed, subsequent KS tests revealed these increases were all statistically significant (*p*-value < 0.0001; Table S6-2, pg. 120).

To confirm the increases in NA observed above are not restricted to HCT116 cells, similar experiments were performed within hTERT. In agreement with HCT116 data, the overall ranges of NAs were both larger and increased within the *KIF11* silenced conditions compared to controls. The mean NAs were 1.5 to 2.0-fold larger within the si*KIF11*-Pool (409.6 μm^2), si*KIF11*-1 (379.1 μm^2), and si*KIF11*-3 (491.9 μm^2) relative to the si*GAPDH* negative control (234.3 μm^2) that Student's *t*-test revealed were all statistically significant (*p*-value < 0.0001) (Figure 4-5; Table S6-1, pg. 119). In addition, the cumulative distribution frequency of NAs for the *KIF11* silenced cells were all right-shifted relative to controls indicating that *KIF11* silencing typically induced increases in NAs within those cellular populations (Figure 4-6). KS test confirmed these increases in NAs were highly statistically significant (*p*-value < 0.0001) (Table S6-5, pg. 123). Collectively, the above data show that *KIF11* silencing in either HCT116 or hTERT cells is associated with an overall increase in NAs.

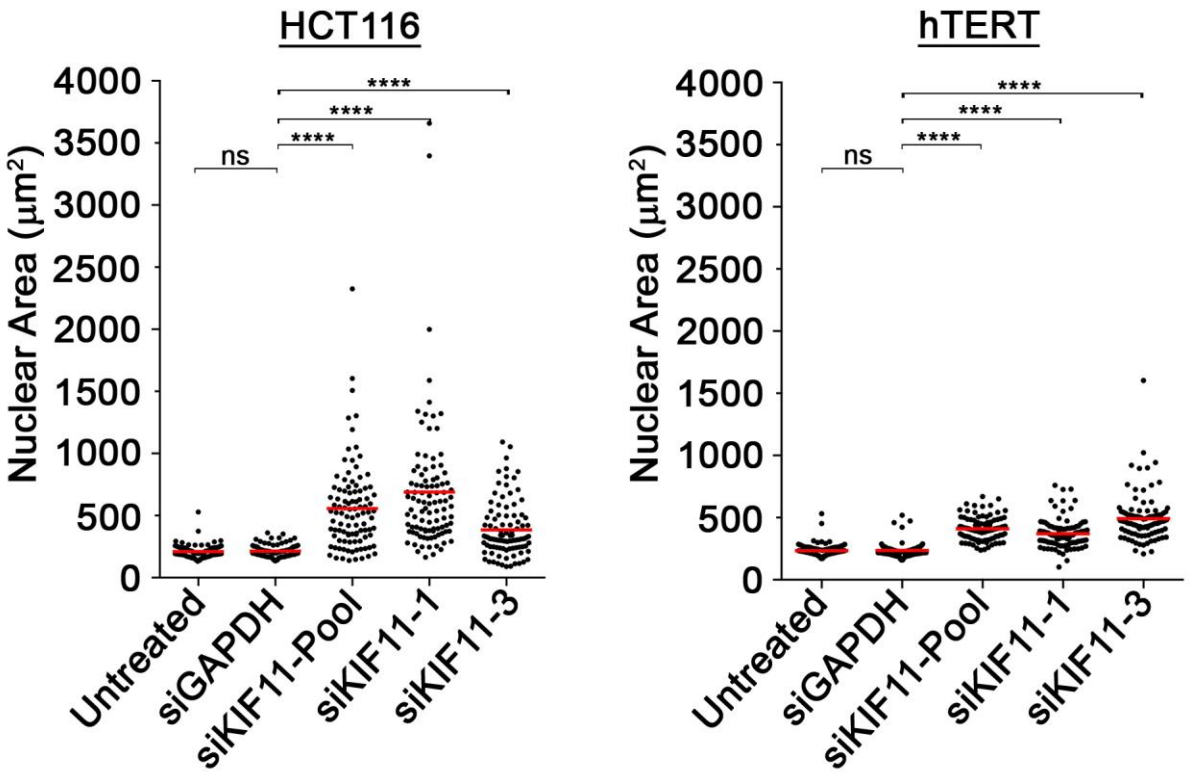

Figure 4-5: *KIF11* Silencing Induces Increases in Nuclear Area
Dot plots presenting the NAs of *KIF11* silenced cells relative to controls (Untransfected and si*GAPDH*) 5 days post-transfection within HCT116 (left) and hTERT (right) cells. The red bars identify the mean total NA for each condition. Student's *t*-tests reveal statistically significant increases in mean NA following *KIF11* silencing in both cell lines relative to controls. (****p-value < 0.0001; ns = non-significant; number of nuclei/condition = 100).

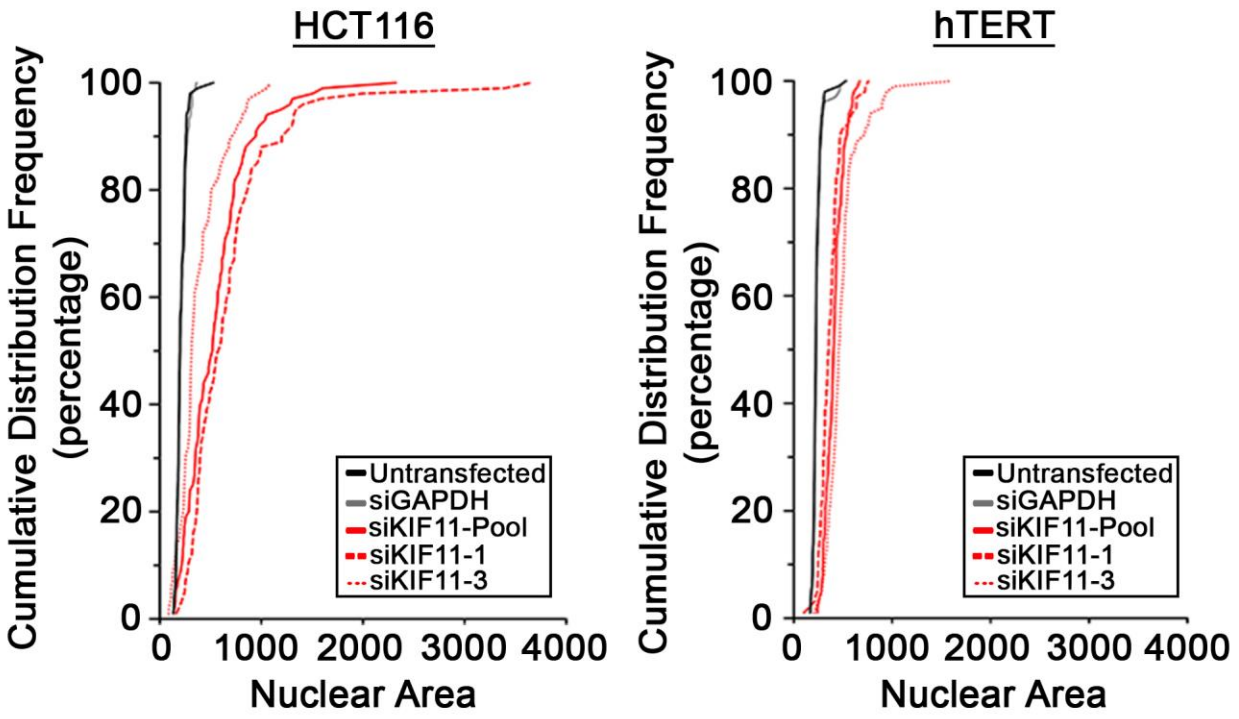

Figure 4-6: Cumulative Distribution Frequencies Reveal an Increase in the Nuclear Areas Distributions Following *KIF11* Silencing

Graphs presenting the cumulative distribution frequency profiles for NAs following *KIF11* silencing in HCT116 (left) and hTERT (right) cells relative to controls (Untransfected and si*GAPDH*). The right-ward shift of the distribution profiles for the *KIF11* silenced conditions relative to controls is indicative of an overall increase in NAs within those cellular populations. (number of nuclei/condition = 100).

Having established *KIF11* silencing induces increases in NAs, we now wished to determine whether *KIF11* silencing also induces increases in MN formation, a second hallmark of CIN[178]. Recall that micronuclei are small, extra nuclear bodies found outside the primary nucleus (Figure 4-7A). To quantify changes in the number of micronuclei following *KIF11* silencing, the number of micronuclei was enumerated within a minimum of 100 interphase nuclei/condition using automated imaging software (see Materials and Methods; *Section* 3.9.1, pg. 50), and the frequency of cells with micronuclei was determined (Figure 4-7B). Overall, there was a 32.1-, 31.1-, and 19.1-fold increase in the number of micronuclei observed within the si*KIF11*-Pool, -1, and -3 silenced populations, respectively, relative to *GAPDH* silenced HCT116 cells. Again, to extend these findings beyond the HCT116 cellular context, MN formation was also assessed within hTERT. Similar to HCT116 cells, *KIF11* silencing induced increases in MN formation within hTERT cells. Interesting however, the overall increases observed following *KIF11* silencing was smaller than that observed within the HCT116 cells, but was still substantial. More specifically, there was a 19.5-, 10.7-, and 28.1-fold increase in the number of micronuclei within the si*KIF11*-Pool, -1, and -3 silenced populations, respectively, relative to the si*GAPDH* control (Figure 4-7B). Taken together, these data show that *KIF11* silencing is associated with increases in MN formation in both HCT116 and hTERT cells.

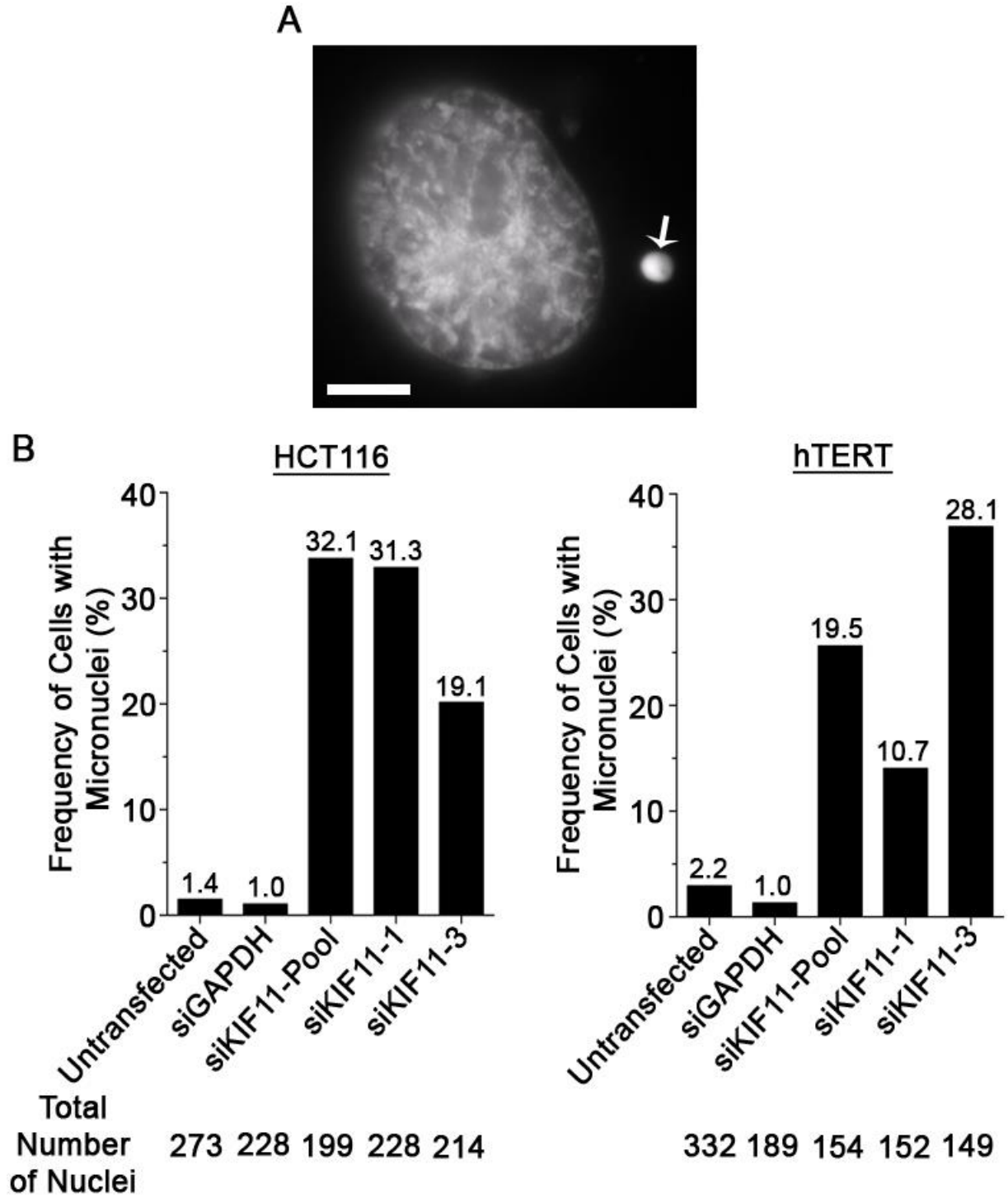

Figure 4-7: *KIF11* Silencing Induces Micronucleus Formation
(A) Representative high-resolution 2D image of a MN (arrow) contained within a HCT116 cell following *KIF11* silencing. (Scale bar = 10 μm). ***(B)*** Bar graphs presenting frequency of cells with micronuclei for each condition 5 days post-silencing in HCT116 (left) and hTERT (right) cells. The fold-increase relative to the si*GAPDH* negative control is indicated above each column. The total number of cells evaluated for each condition is shown below each column.

4.1.3 *KIF11* Silencing is Associated with Increases in DNA Content

The results obtained from the NA and MN formation assays suggest *KIF11* is a CIN gene, and further predict that *KIF11* silencing is associated with increases in DNA content. To assess this possibility, flow cytometry was performed and DNA content profiles were generated and compared for si*KIF11* silenced and control cells. Briefly, cells were transfected with appropriate siRNAs, and permitted to grow for five days, at which point cells were harvested, fixed, PI labeled and analyzed (see Materials and Methods; *Section* 3.10, pg. 51). Figure 4-8 presents the DNA content profiles for each condition and shows that *KIF11* silencing resulted in increases in the frequency of cells with 4C and > 4C DNA content relative to the controls (Table S6-3, pg. 121).

Since we typically observe increases in NA following KIF11 silencing, we focused our analyses on the population of cells with DNA contents beyond the prototypic diploid 2C peak rather than the subdiploid cells. In HCT116 control cells, ~70% of cells comprised 2C DNA content, whereas, this number is reduced to ~51.6% in *KIF11* silenced cells. Interestingly, there was a corresponding increase in the proportion of cells with DNA contents of 4C and > 4C. In HCT116, untransfected and negative control (siNon-targeting) cells 9.3 and 9.8% of cells comprised 4C DNA content respectively, whereas within the *KIF11* silenced cells, these numbers increased to ~18.0%. Moreover, proportion of cells with greater than 4C DNA content is increased from approximately ~0.5% in control cells to ~15.3% in *KIF11* silenced cells representing a ~29-fold increase (Figure 4-8; Table S6-3, pg. 121). Similar to HCT116 cells, more than 70% of hTERT control cells (untransfected and siNon-targeting) had a 2C DNA content, which dropped to ~10.9% within *KIF11* silenced cells. This drop is accompanied with increase of the population of cells with 4C DNA content from less than ~14.0% in control cells to ~64.1% in *KIF11* silenced cells. Furthermore, there was an increase of the proportion of cells with greater than a 4C DNA content

from ~1.5% in controls to ~12.6% in *KIF11* silenced hTERT cells (Figure 4-8; Table S6-3, pg. 121). Together, these data indicate that *KIF11* silencing in either HCT116 or hTERT cells is generally associated with an increase in DNA content, particularly within the >4C category.

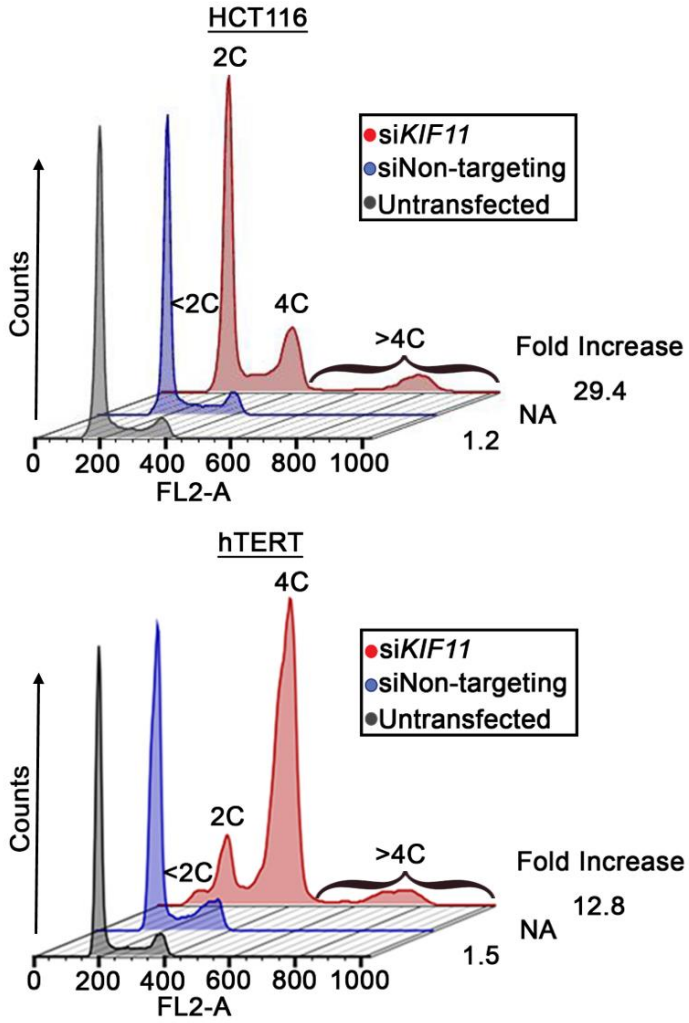

Figure 4-8: *KIF11* Silencing Induces Increases in DNA Content within HCT116 and hTERT Cells

HCT116 (top) and hTERT (bottom) cells were transfected with si*KIF11*-Pool (red) or siNon-targeting (blue), or were left untransfected (black). Five days post-transfection, asynchronous cells were fixed, labeled with PI and subjected to flow cytometry. For reference purposes, the prototypic DNA content is indicated above the *KIF11* silenced conditions (i.e. <2C, 2C, 4C, and >4C), with the brackets highlighting the >4C populations (i.e. increased DNA content). The fold increase within the >4C populations are indicated (right) and are presented relative to the control (siNon-targeting). Presented is a representative example of an experiment performed twice (N = 2).

4.1.4 *KIF11* Silencing Induces Increases in Chromosome Numbers

Having established *KIF11* silencing induces increases in the DNA content in both HCT116 and hTERT cells, we next wanted to determine whether these increases are associated with increases in chromosome numbers. Accordingly, mitotic chromosome spreads were generated for each condition (untransfected, si*GAPDH*, si*KIF11*-Pool, si*KIF11*-1, si*KIF11*-3) and chromosomes were counterstained (DAPI), imaged and manually enumerated from 100 mitotic chromosome spreads per condition. As predicted, large increases in mean chromosome numbers were observed following *KIF11* silencing relative to the controls (Table S6-4, pg. 122). Figure 4-9 presents representative examples mitotic chromosome spreads used for enumeration following *KIF11* and *GAPDH* silencing in both HCT116 and hTERT cells.

In general, *KIF11* silencing induced an overall increase in the total range of chromosome numbers compared to the untransfected and negative (si*GAPDH*) controls. In detail, the mean chromosome numbers of si*KIF11*-Pool (85.3), si*KIF11*-1 (77.1), and si*KIF11*-3 (79.5) are approximately 1.5- to 2.0-fold larger than the mean chromosome numbers of the negative control (siGAPDH; 45.6). Subsequent Student's *t*-test revealed these increases are all statistically significant (p-value < 0.0001; Table S6-4, pg. 122; Figure 4-10), indicating that *KIF11* silencing is accompanied by increases in the number of chromosomes in HCT116 cells.

Next, we compared the cumulative distribution frequencies for chromosome numbers between the various conditions. This comparison showed that *KIF11* silencing was associated with increases in the total distribution range of chromosome numbers as is evidenced by a right-ward shift in their distribution profiles (Figure 4-11). Subsequent KS test indicated these increases were statistically significant (p-value < 0.0001; Table S6-5, pg. 123). To evaluate the conserved nature of these observations, mitotic chromosome spreads were also generated and evaluated in hTERT

cells following *KIF11* silencing. In agreement with the HCT116 findings, the mean chromosome number of si*KIF11*-Pool (69.0), si*KIF11*-1 (54.5), and si*KIF11*-3 (66.6) were approximately 1.1 to 1.4-fold larger than the control (si*GAPDH*; 46.7). Subsequent Student's *t*-test and KS test both showed that all pairwise combinations were statistically different (*p*-value < 0.0001) with the exception of si*KIF11*-1 silenced condition that was shown to be only significant using Student's *t*-test (*p*-value 0.0210), but not by KS tests (*p*-value 0.0541) although there is a trend towards significance (Table S6-5, pg. 123). Collectively, the above data strongly suggest *KIF11* is a CIN gene.

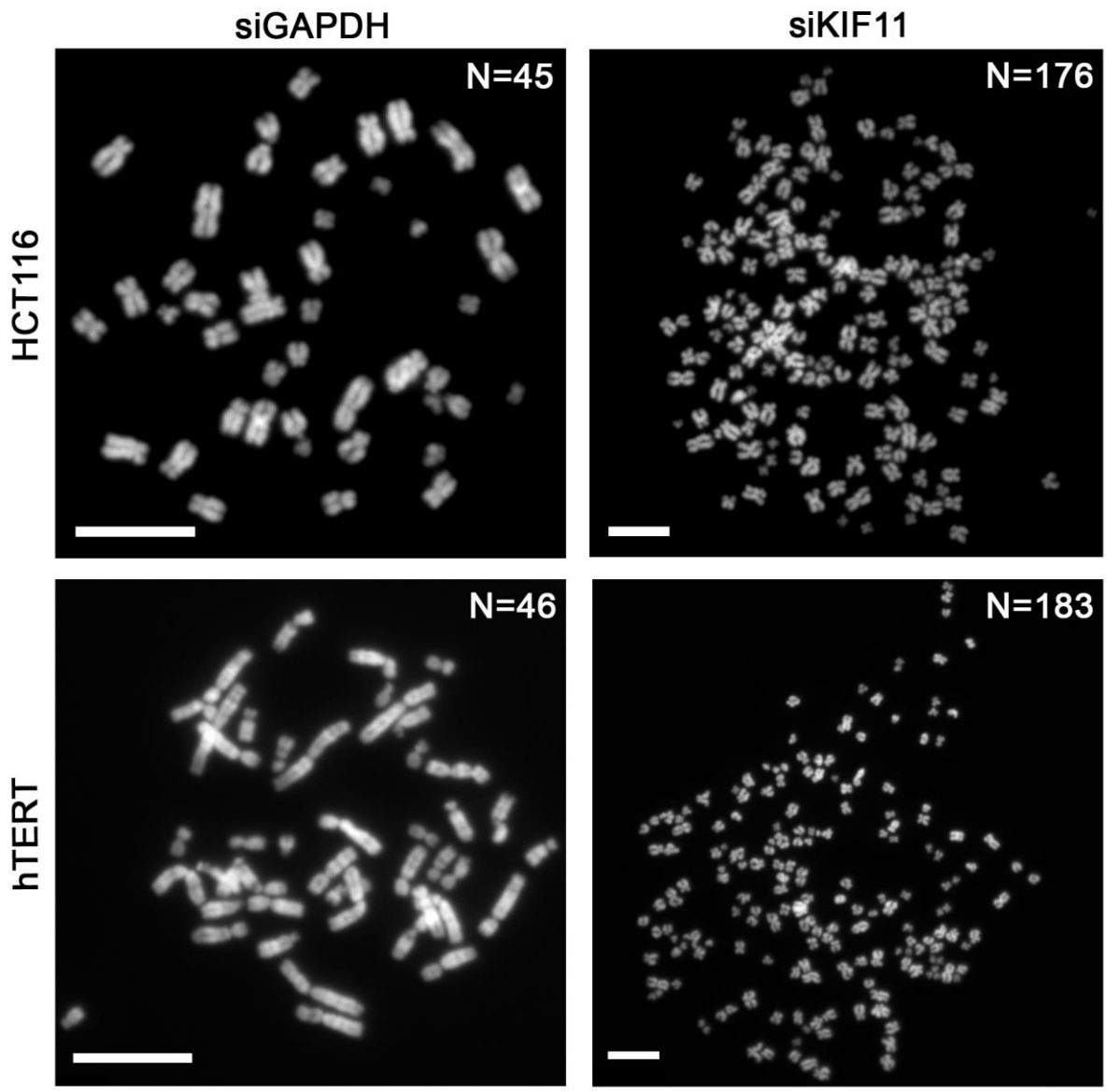

Figure 4-9: *KIF11* Silencing Induces Increases in Chromosome Numbers
Representative 2D images of mitotic chromosome spreads harboring increases in chromosome numbers in HCT116 (top; modal chromosome number = 45) and hTERT (bottom; modal chromosome number = 46) cells following *KIF11* silencing relative to the control (si*GAPDH*). (Scale bar = 10 μm).

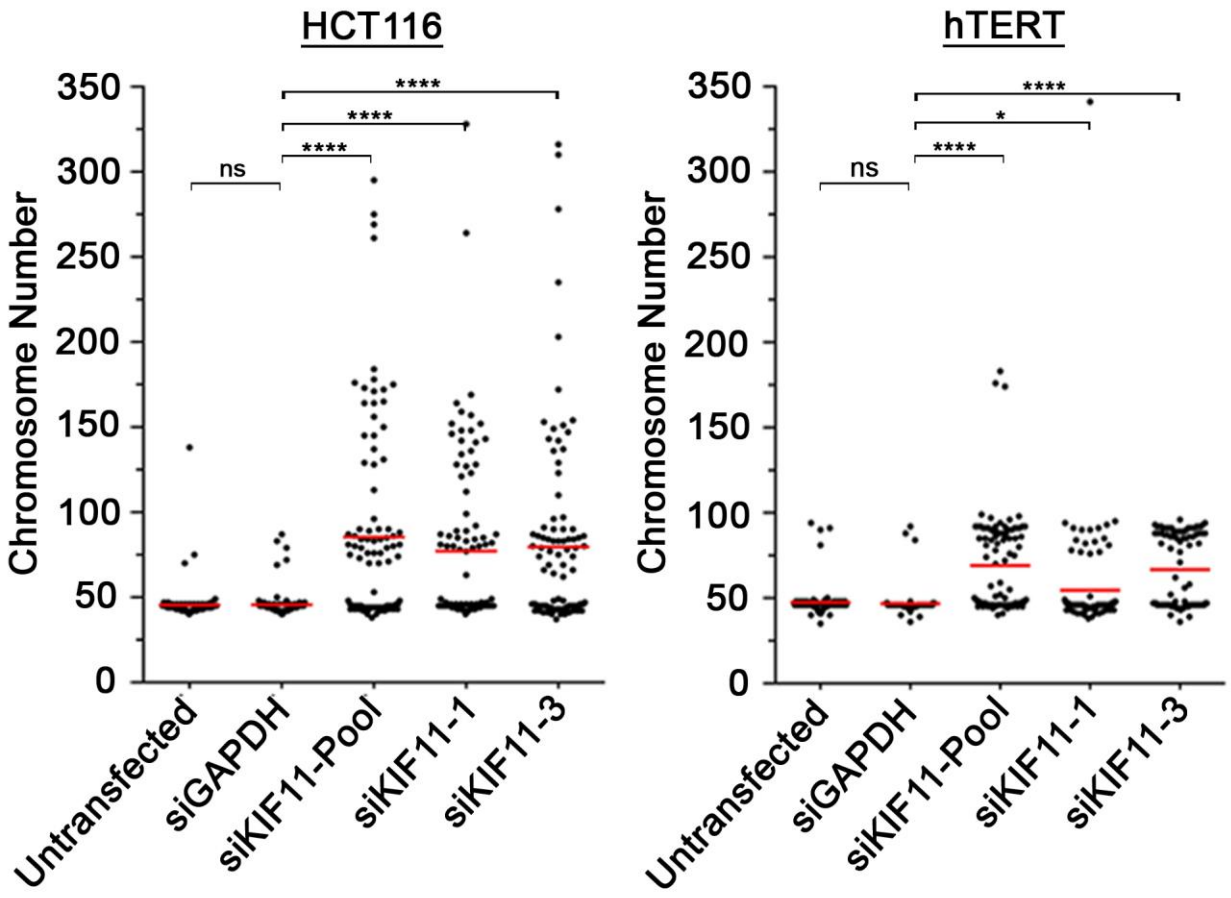

Figure 4-10: *KIF11* Silencing Underlies Increases in Chromosome Numbers
Dot plots presenting the number of chromosomes enumerated within mitotic chromosome spreads following *KIF11* silencing relative to si*GAPDH* control in HCT116 (left) and hTERT (right) cells. Red lines identify the mean number of chromosomes within each condition. Statistical significance was evaluated by Student's *t*-test and is presented above each column (****p-value < 0.0001; *p-value < 0.05; ns = not significant; number of spreads/condition = 100).

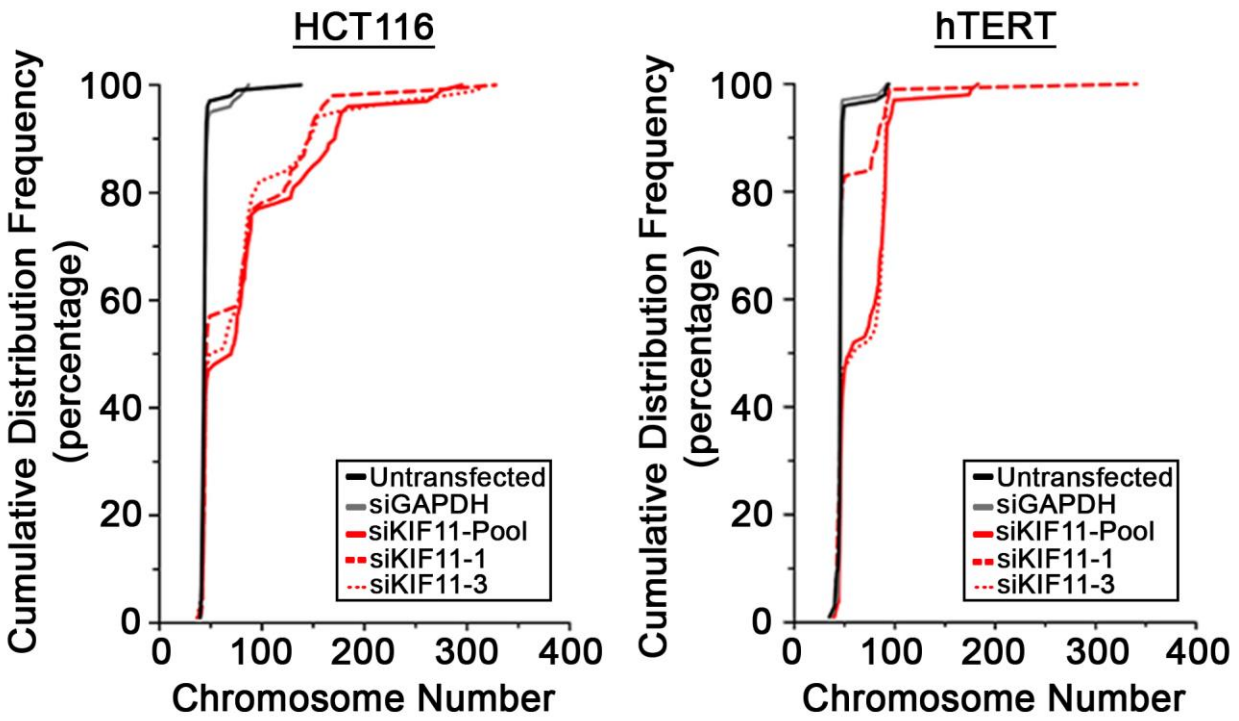

Figure 4-11: *KIF11* Silencing Induces Increases in the Distribution Frequencies of Chromosomes

Graphs presenting the cumulative distribution frequency profiles for the number of chromosomes under the various conditions evaluated (see key) in HCT116 (left) and hTERT (right) cells. KS tests reveal statistically significant differences in the overall distributions of chromosomes within *KIF11* silenced cells relative to controls (*GAPDH*-silenced and Untransfected). (number of spreads/condition = 100).

4.2 Aim 2: To Evaluate the Impact KIF11 Inhibition has on Chromosome Instability.

Having established *KIF11* silencing induces CIN in our cell-based models, we next wished to determine whether KIF11 inhibition also induces CIN thus validating *KIF11* as a CIN gene. To do so, monastrol, a selective KIF11 inhibitor[183], was employed in both HCT116 and hTERT cells. Following KIF11 inhibition, a similar series of experiments to those presented above were performed including assessments of NAs and MN formation, and mitotic chromosome spreads. Finally, to assess the potential impact diminished KIF11 function may have in oncogenesis, real-time cellular analyses were performed to evaluate whether KIF11 inhibited cells have the ability to proliferate.

4.2.1 Identifying the Optimal Concentration of Monastrol for Cell-based Assays

Prior to studying the effect KIF11 inhibition by monastrol has on CIN, it was first necessary to identify the optimal inhibitor concentration to employ. Exploring other manuscripts, we identified 100 μM as a concentration commonly used in many different cell-based studies[174,175,176,177]. To determine whether this concentration was effective in our cell models, a quick visual analysis was performed. As was described in *Section* 4.1.1 (pg. 55), *KIF11* silencing and inhibition typically induces a mitotic, prometaphase-like arrest that is easily assessed using conventional transmitted light microscopy and visualized as rounded-up cells (Figure 4-2). Accordingly, cells were treated with a 10-fold serial dilution of monastrol ranging from 1 μM to 1000 μM and were monitored for changes in their morphology. The highest concentration (1000 μM) was deemed excessive as it caused extensive cell death, while the lowest concentration (1.0 μM) failed to produce the expected phenotype as was essentially identical to the DMSO treated control. Both 10 μM and 100 μM concentrations of monastrol induced mitosis enrichment,

however, more cells harbored the rounded-up phenotype following treatment with 100 μM. Thus, 100 μM was selected for all subsequent work.

4.2.2 KIF11 Inhibition Induces Increases in Nuclear Area and Micronucleus Formation

Having identified the optimal monastrol concentration (100 μM), we next assessed whether a single or double dose of monastrol was sufficient to induce CIN over the 5 day time course of the experiments. To do so, cells were seeded into 96-well culture plates, permitted to attach and grow for 24 h prior to being treated with either monastrol or DMSO. For the double dose condition, cells were treated a second time with monastrol ~48 h after the first treatment. Overall, cells were allowed to grow for 5 days after the initial treatment, at which point they were fixed, counterstained (Hoechst 33342), and their NAs were analysed. Figure 4-12 shows that both conditions induced statistically significant increases in the mean NA of both HCT116 and hTERT cells relative to the DMSO control (*p*-value < 0.0001; Table S6-6, pg. 124). In fact, KIF11 inhibition induced a 1.5- and 1.9-fold increase in the mean NA of HCT116 cells treated with single and double doses of monastrol, respectively. Interestingly, both single and double doses of monastrol induced a 1.8-fold increase in mean NAs within hTERT cells. Accordingly, the single dose treatment was identified as the optimal treatment to be employed in all subsequent studies.

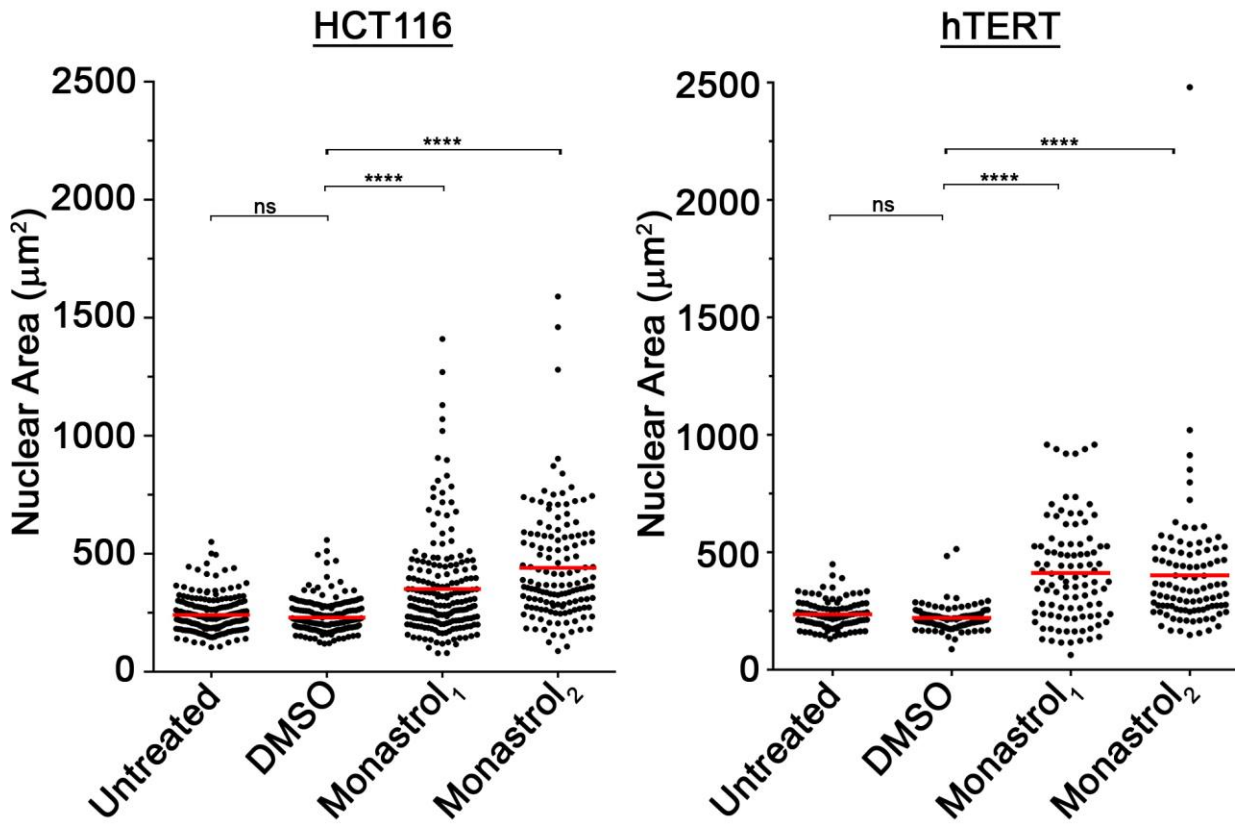

Figure 4-12: Both Single and Double Doses of Monastrol Induce Increases in Nuclear Area
Dot plots presenting the NAs 5 days post-treatment (monastrol = 100µM) relative to controls (DMSO and Untreated) in HCT116 (left) and hTERT (right) cells. (****p-value < 0.0001; ns = non-significant; number of nuclei/condition = 100). Red lines indicate the mean NAs for each condition. ($monastrol_1$ = single dose treatment of cells with monastrol). ($monastrol_2$ = double dose treatment of cells with monastrol).

Having established that the single monastrol treatment induced increases in NAs, we repeated the experiment using the optimized conditions. In agreement with the above findings, a single dose of monastrol resulted in an overall increase in mean NA within both HCT116 and hTERT cells relative to vehicle control alone (DMSO) (Figure 4-13). Similar to the *KIF11* silenced conditions, monastrol treatments was associated with increases in the overall NA ranges and mean NAs relative to controls. More specifically, the mean NA of monastrol treated HCT116 and

hTERT cells were 422.3 and 411.8 μm^2 respectively, which are ~2-fold larger than the corresponding controls (220.7 and 220.8 μm^2, respectively). Subsequent Student's *t*-test revealed these increases were statistically significant with *p*-values < 0.0001 for both cell lines (Table S6-7, pg. 125). Furthermore, KIF11 inhibition was associated with increases in the total distribution range of NAs as is evidenced by a right-ward shift in the distribution profiles of both cell lines (Figure 4-14). Subsequent KS test indicated these increases were statistically significant (*p*-value < 0.0001; Table S6-8, pg. 126).

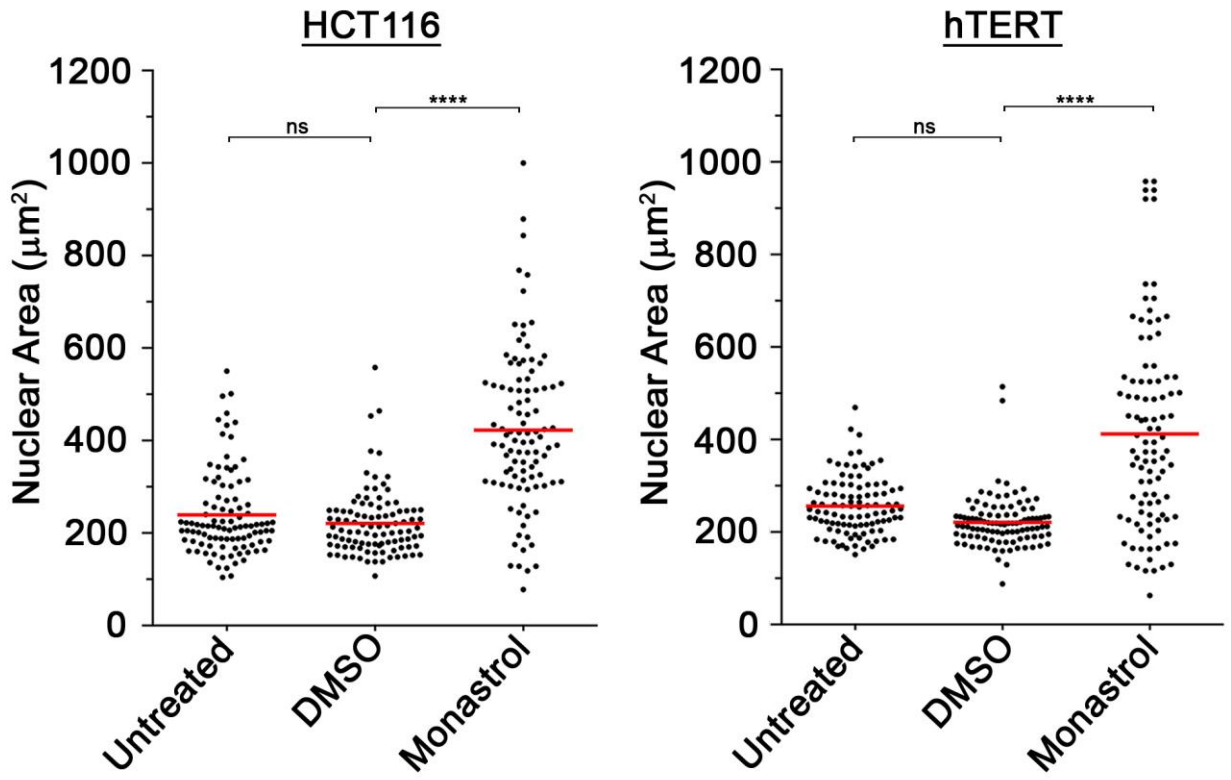

Figure 4-13: KIF11 Inhibition Results in Increases in Nuclear Areas
Dot plots presenting the NAs 5 days post-treatment (monastrol = 100µM) relative to controls (DMSO and Untreated) in HCT116 (left) and hTERT (right) cells. (****p-value< 0.0001; ns=non-significant; number of nuclei/condition = 100). Red lines indicate the mean NAs for each condition.

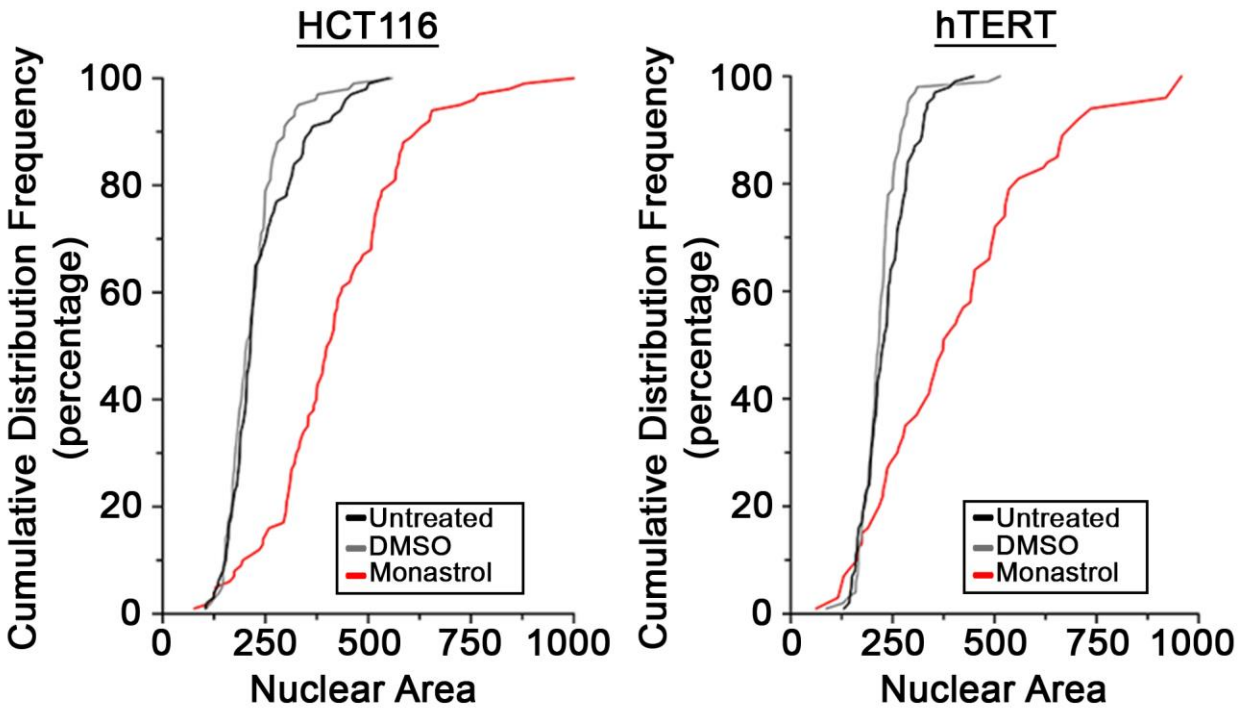

Figure 4-14: KIF11 Inhibition Increases Nuclear Area Distributions
Graphs presenting the cumulative distribution frequency profiles for the NAs under the various conditions evaluated (see key) in HCT116 (left) and hTERT (right) cells. KS tests reveal statistically significant differences in the distributions of NAs within KIF11 inhibited cells relative to the DMSO control. (number of nuclei/condition = 100).

Next, MN formation assays were performed to determine whether monastrol treatments induced increases similar to those observed following *KIF11* silencing. As presented in Figure 4-15, monastrol treatment induced a 10.9-fold increase in MN formation HCT116 cells relative to the vehicle control. Interestingly, although monastrol treatment also induced a 4.9-fold increase within hTERT, it was not as large as observed within the HCT116 cells. Thus, in agreement with the silencing data, KIF11 inhibition is associated with increases in NAs and MN formation within both HCT116 and hTERT cells.

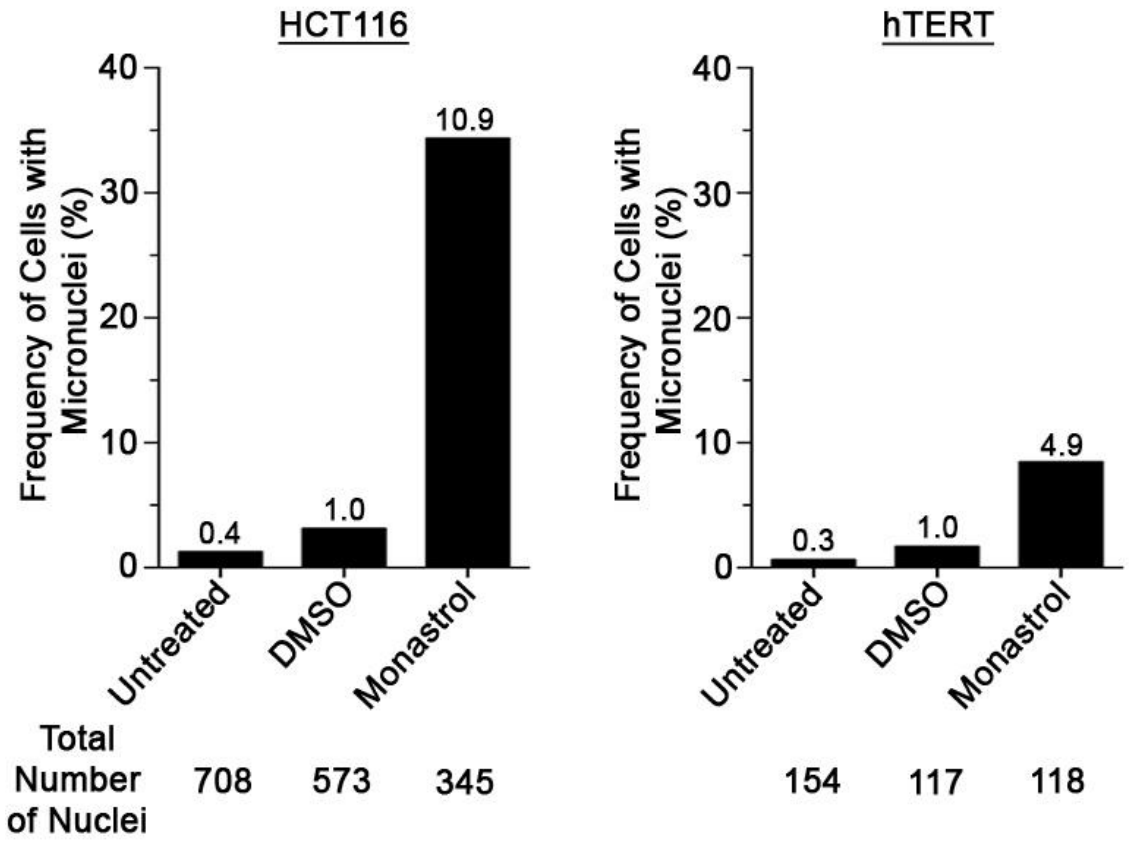

Figure 4-15: KIF11 Inhibited Cells Exhibited Increases in the Micronucleus Formation
Bar graphs presenting the frequency of cells with micronuclei for each condition 5 days post monastrol treatment in HCT116 (left) and hTERT (right) cells. The fold-increase relative to the negative control is indicated above each column. The total number of cells for each condition is shown below each column.

4.2.3 KIF11 Inhibition Induces Increases in Chromosomes Numbers

Having established that monastrol treatment induces increases in NAs and MN formation, we next investigated whether these increases are due to increases in the chromosome numbers as observed with *KIF11* silencing. Accordingly, mitotic chromosome spreads were generated for monastrol and vehicle control (DMSO) treated cells. As presented in Figure 4-16, there is an increase in the overall ranges and mean chromosome numbers observed within the monastrol treated samples relative to the controls. More specifically, the mean number of chromosomes following monastrol treatment in HCT116 (93.9) and hTERT (61.1) are 1.3- and 2.0-fold larger, respectively, than those of the corresponding controls (45.0 and 46.2, respectively). Subsequent Student's *t*-test revealed that these increases were statistically significant (*p*-value < 0.0001;Table S6-9, pg. 127).

Next, the cumulative distribution frequencies of chromosome numbers were compared between conditions and showed that monastrol treatments were associated with increases in the distribution profiles as evidenced by a right-ward shift in both cell lines (Figure 4-16). Subsequent KS test indicated these increases were statistically significant (*p*-value < 0.0001; Table S6-10, pg. 128) in HCT116 and hTERT cells. The above data are in agreement with those observed following *KIF11* silencing, and collectively indicate *KIF11* is a CIN gene.

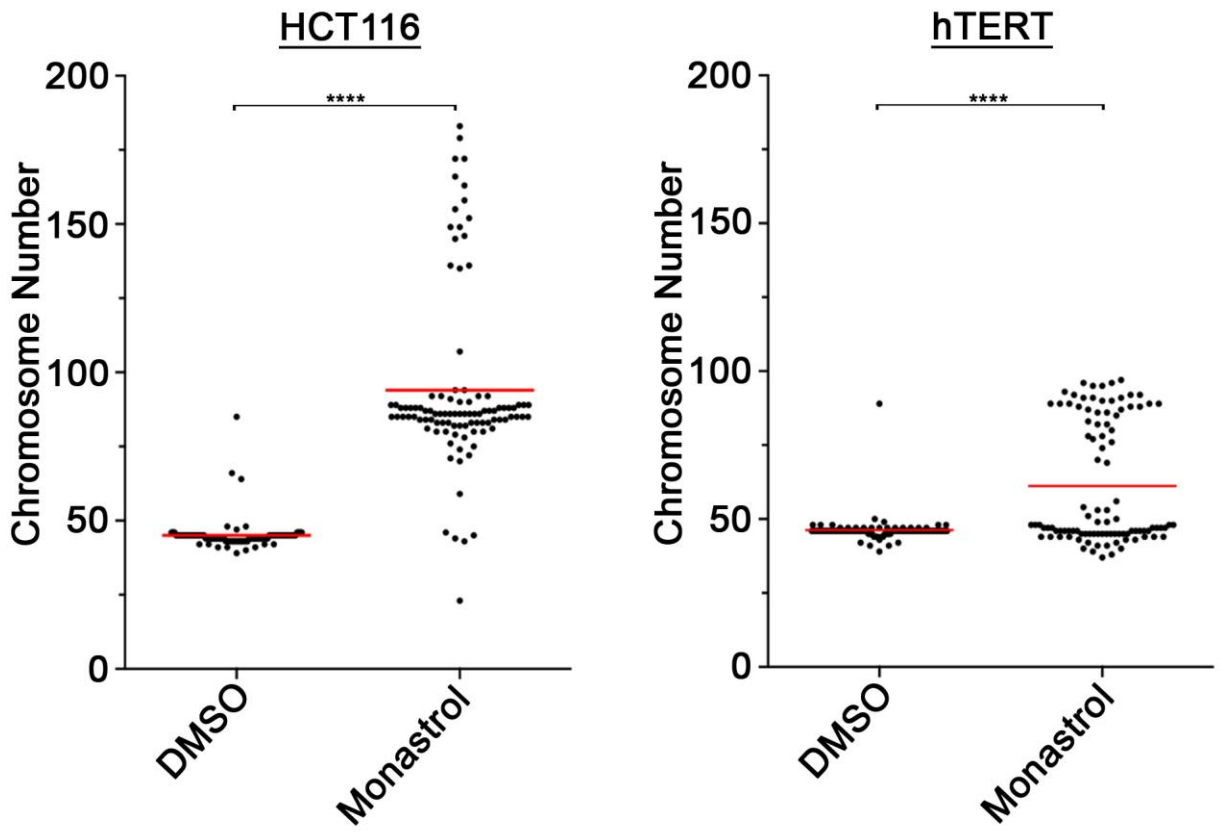

Figure 4-16: Increases in Chromosome Numbers Following Monastrol Treatment
Dot plots presenting the number of chromosomes enumerated within mitotic chromosome spreads following KIF11 inhibition relative to DMSO control in HCT116 (left) and hTERT (right) cells. Red lines indicate the mean number of chromosomes within each condition. Statistical significance was evaluated by Student's *t*-test (*****p*-value < 0.0001; number of spreads/condition = 100).

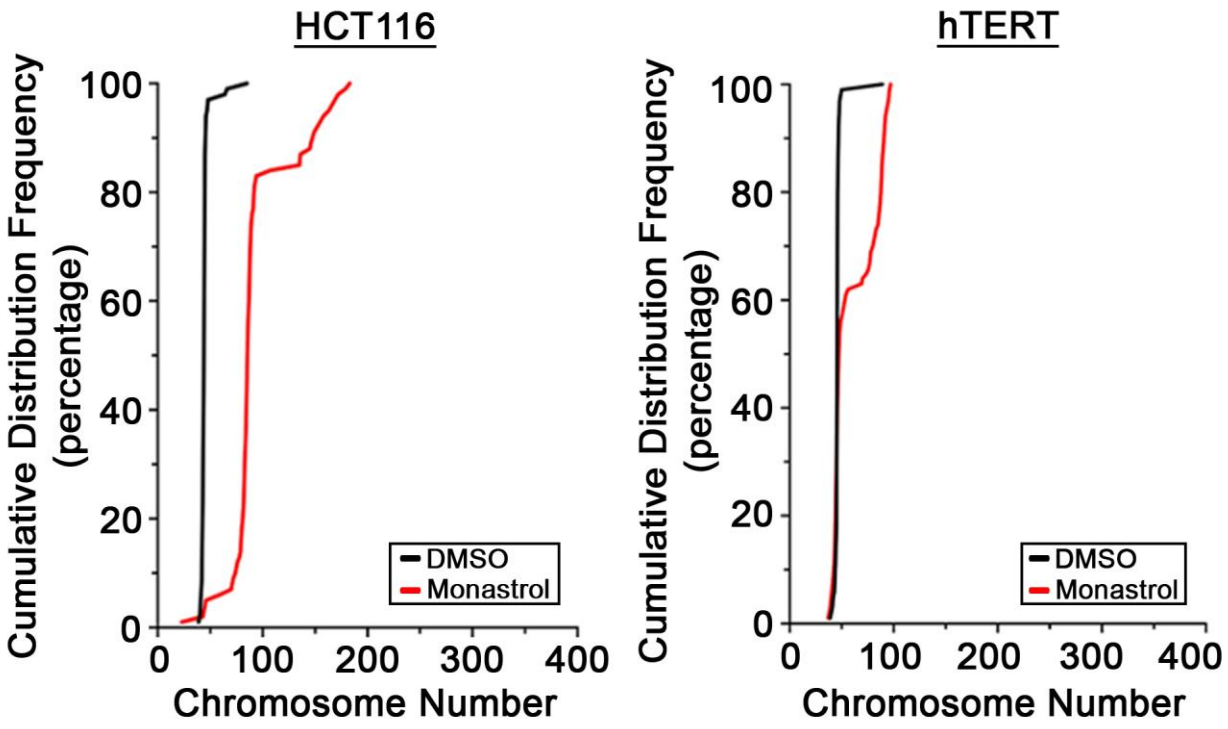

Figure 4-17: Cumulative Distribution Frequencies Indicate that KIF11 Inhibition Significantly Increases the Overall Chromosome Distribution

Graphs presenting the cumulative distribution frequency profiles for the number of chromosomes per cell under the various conditions evaluated (see key) in HCT116 (left) and hTERT (right) cells. KS tests reveal statistically significant differences in the distributions of chromosomes within KIF11 inhibited cells relative to DMSO control. (number of spreads/condition = 100).

4.2.4 KIF11 Inhibited Cells Can Proliferate

Having established that monastrol treatment induces CIN in cell-based models, we next sought to determine the effect KIF11 inhibition has on cellular proliferation relative to untreated and DMSO controls. Conceptually, if *KIF11* is a CIN gene that contributes to oncogenesis, then cells with diminished KIF11 function must be able to proliferate. Accordingly, we wished to determine whether monastrol treated cells are permanently arrested in mitosis (i.e. in a prometaphase-like state), or whether a subset of cells can escape the arrest, re-enter the cell cycle and continue to proliferate.

RTCA analyses were performed and cells were monitored for up to 5 days following monastrol treatment. In brief, the RTCA-DP system employs microelectrodes at the bottom of each well to measure increases or decreases in electrical impedance (termed cell index) that reflect increases or decreases in cells numbers, respectively. Accordingly, the RTCA can easily discern between altered proliferation patterns stemming from cell cycle arrests (i.e. stationary phase identified by a plateau) or cytotoxicity (i.e. a sharp decline). Figure 4-18 presents that the proliferation profiles generated from the control cells (untreated and DMSO) were nearly indistinguishable, while the proliferation curves of the monastrol treated cells are different from controls with a smaller slope during exponential growth in both cell lines (Figure 4-18), and is indicative of a slower proliferation rate. In HCT116 cells, monastrol treated cells remain in lag phase (i.e. phase that cells adjust to the environment) for ~12 h longer than the controls, however, they do appear to re-enter the cell cycle and begin to proliferate, but at much slower rate. Interestingly, KIF11 inhibition in hTERT appears to induce a longer lag phase that lasts up to ~3 days. However, after these 3 days, cells appear to re-enter the cell cycle and begin to proliferate with almost the same proliferation rate as observed with the monastrol inhibited HCT116 cells

(Figure 4-18). Based on our previous observations and findings within the literature (see Introducton), this extended lag phase is consistent with a prolonged mitotic (prometaphase-like) arrest. Nevertheless, these data show that cells treated with monastrol can proliferate but at a slower rate suggesting that certain hypomorphic *KIF11* mutations may also have the ability to proliferate.

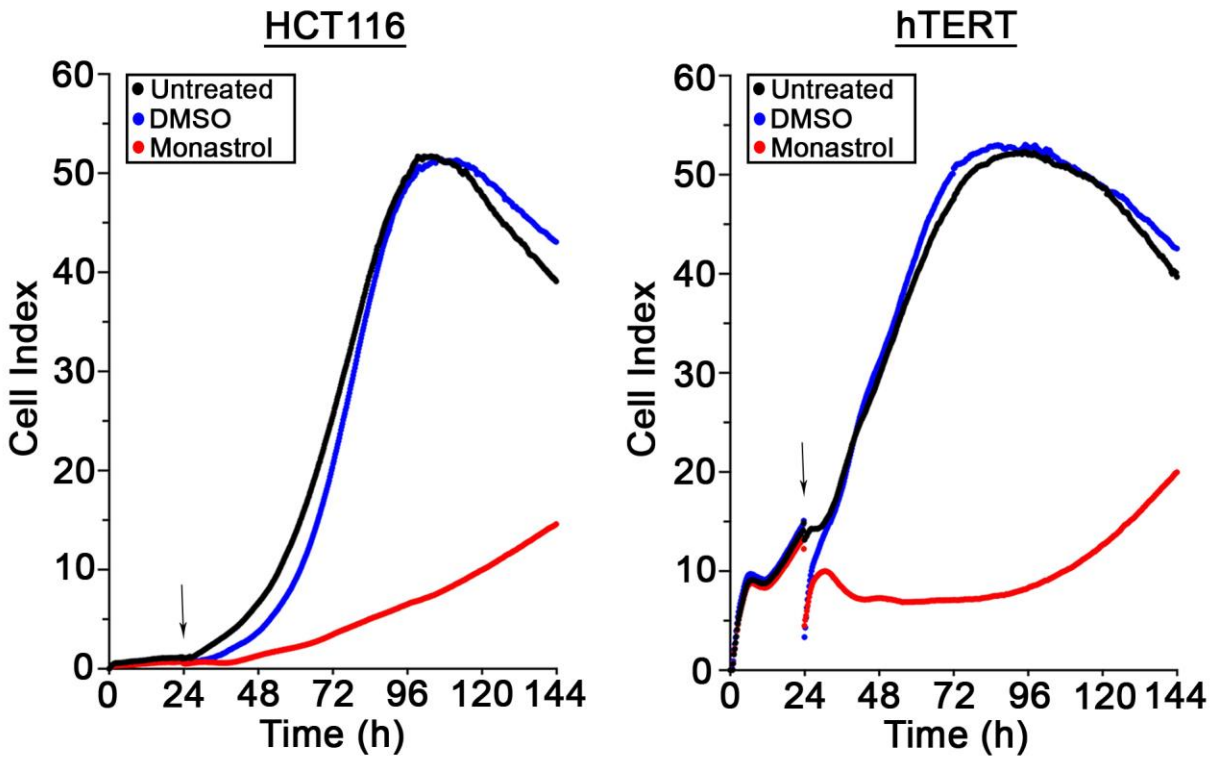

Figure 4-18: Monastrol Treated Cells Continue to Proliferate
RTCA proliferation curves for controls (untreated [black] and DMSO [blue]) and monastrol treated (red) HCT116 (left) and hTERT (right) cells. Arrow identifies the time-point of monastrol or DMSO addition. Note that the monastrol treated cell lines (red) exhibit a decrease in proliferation, but that they do continue to proliferate after an initial arrest. Presented are single representative examples of experiments performed twice each (N = 2; n = 4).

CHAPTER 5: CONCLUSIONS AND DISCUSSION

5.1 Conclusions

To determine whether *KIF11* is a *bona fide* CIN gene in humans, I examined whether *KIF11* silencing and/or inhibition induced CIN in two distinct human cell lines. Using HCT116 cells, a karyotypically stable, CRC cell line, I show that *KIF11* silencing is associated with increases in NAs and MN formation (*Section* 4.1.2, pg. 58), along with increases in DNA content (*Section* 4.1.3, pg. 65). Using mitotic chromosome spreads, I show that these increases likely result from underlying increases in chromosome numbers (*Section* 4.1.4, pg. 67). To extend our findings beyond the HCT116 cellular context, similar experiments were performed in a second karyotypically stable cell line, hTERT, with very similar findings. More specifically, we show that *KIF11* silencing in hTERT cells increases NAs, MN formation, DNA content and chromosome numbers. Thus, these results strongly suggest *KIF11* is an evolutionarily conserved CIN gene in human cells.

To firmly establish *KIF11* is a CIN gene, we next sought to determine whether KIF11 inhibition (*i.e.* diminished KIF11 function) also induces CIN phenotypes. In order to determine the effects KIF11 inhibition has on CIN, monastrol (a selective inhibitor of KIF11) was employed in both HCT116 and hTERT cells. Following KIF11 inhibition, we performed a similar series of experiments to those employed above and noted similar increases in NA and MN formation (*Section* 4.2.2, pg. 73), that were also accompanied by increases in chromosome numbers (*Section* 4.2.3, pg. 78) relative to DMSO treated controls. Collectively, these data show KIF11 silencing and inhibition induce increases in phenotypes associated with CIN (i.e. NAs, MN formation, and DNA content), along with increases in chromosome numbers in both HCT116 and hTERT cells, and thus identify *KIF11* as a *bone fide* CIN gene in humans.

Armed with the knowledge that *KIF11* is deleted and somatically altered in numerous cancer types including CRC[169,170] (Table 2-1, pg.35), and having established *KIF11* is a novel CIN gene, we wanted to begin to assess its potential contribution to the development and progression of cancer. Accordingly, we assessed the impact diminished KIF11 function (*i.e.* KIF11 inhibition) has on cellular proliferation, as it has been shown that KIF11 inhibition induces mitotic arrests[151], and only cells that proliferate can contribute to cancer development and progression. Accordingly, RTCA was performed and the proliferation rates of controls and KIF11 inhibited cells were compared. As expected, KIF11 inhibition was associated with a transient mitotic arrest in both cell lines, with a slightly longer arrest observed in hTERT, following which the cells appear to escape the mitotic checkpoint and re-entered the cell cycle (*Section* 4.2.4, pg. 81). Thus, these data show that diminished KIF11 function underlies CIN in human cells, and that those cells continue to proliferate suggesting aberrant KIF11 expression and function may contribute to oncogenesis.

5.2 HCT116 are Hypersensitive to *KIF11* Silencing and Inhibition Relative to hTERT

Results presented in this thesis show that *KIF11* silencing and inhibition induces CIN phenotypes in both HCT116 and hTERT cells. In general, *KIF11* silencing and inhibition consistently produced stronger phenotypes within the HCT116 cells relative to the hTERT cells. For example, silencing of *KIF11* with si*KIF11*-Pool induced 2.6-fold increase in mean NA of HCT116 cells, whereas it was only 1.7-fold increase in hTERT (*Section* 4.1.2). Similarly, KIF11 inhibition induced 10.9-fold increase in MN formation within HCT116 and only 4.9-fold increase within hTERT cells (*Section* 4.2.2).

There are a variety of underlying mechanisms that may account for the more pronounced phenotypes within the HCT116 cells. A strong possibility that may contribute to the more severe CIN phenotypes observed within HCT116 are the different genetic and cellular contexts (*i.e.*

differential gene expression patterns) of the two cell lines. For example, HCT116 is a CRC cell line with a MMR defect that stems from *MLH1*-deficiency. This deficiency results in the accumulation of small mutations (typically 1-3 base pairs) throughout the genome, particularly within highly repetitive sequences, which may include tumor suppressor genes and oncogenes[184]. Thus, due to the existence of additional background mutations, HCT116 may be more genetically predisposed to develop CIN following *KIF11* silencing or inhibition. For example, it is possible HCT116 may accrue background mutations conferring a selective growth advantage that weakens the mitotic checkpoint that is induced following *KIF11* silencing or inhibition. It is conceivable that mutations in SAC genes may render the cells more amendable checkpoint escape, thus allowing them to more readily re-enter the cell cycle.

On the other hand, hTERT cells are a non-malignant cell line immortalized through the integration and re-expression of *TERT*, the human telomerase reverse transcriptase gene. Interestingly, others have shown that *hTERT* re-expression enhances genome stability and DNA repair, albeit typically at telomeres[185], potentially rendering these cells more resistant to CIN. In addition, and in contrast to HCT116, hTERT are MMR proficient, and are expected to better preserve genome integrity through a combination of *TERT* re-expression and an intact MMR pathway, thus limiting CIN following *KIF11* silencing or inhibition. In agreement with this possibility, the RTCA data show that HCT116 cells tend to re-enter the cell cycle more rapidly than hTERT (Figure 4-18, pg. 82). More specifically, following monastrol treatment, HCT116 appear to arrest for ~12 h prior to re-entering the cell cycle and beginning their exponential proliferation phase, whereas hTERT appear to arrest for ~72 h prior to re-entering the cell cycle. Accordingly, due to a longer mitotic arrest, hTERT cells will undergo fewer cellular divisions and replicative cycles (i.e. S-phase), which could account for the less severe phenotypes.

Cell doubling times may also impact the severity of the CIN phenotypes observed within the HCT116 relative to the hTERT cells. Recall that the doubling time of HCT116 cells is ~22 h whereas doubling time of hTERT cells is ~36 h, which indicates that over the course of a typical 5-day (120 h) experiment, HCT116 cells will typically undergo ~5.5 cellular divisions, while hTERT cells will only undergo ~3.5. Thus, HCT116 cells have ~2 additional cell cycles in which the underlying mechanism(s) may induce CIN and thus exhibit stronger CIN phenotypes. To test this possibility, future experiments could be performed in which hTERT cells are grown for longer periods of time (e.g. 8 days instead of 5 days) so that similar numbers of cellular division could occur. However, the transient nature of the siRNAs and re-expression of KIF11 may impact the results. Thus, to address this caveat, cells could be transfected or inhibited for a second time ~2-3 days following the first treatment. Alternatively, stable silencing could be introduced by generating a shRNA expressing model using a lentivirus-based system. However, a major limitation of stably silencing cells with shRNA is the time-consuming nature of developing a homogenous population of cells expressing the desired shRNA, particularly in the context of a condition that is expected to induce CIN. Although the above examples describe putative mechanisms accounting for the enhanced CIN phenotypes within the HCT116 cells, the actual mechanism(s) accounting for the differences remain to be determined.

5.3 Potential Mechanisms Accounting for CIN Following *KIF11* Silencing or Inhibition

Although the data presented in this thesis indicate that *KIF11* silencing and inhibition induces CIN, the precise underlying mechanisms accounting for the induced changes in chromosome numbers remain to be elucidated. *KIF11* silencing or inhibition is associated with an initial monopolar spindle formation, which is not observed at later points. This observation suggests that these cells are capable of escaping mitotic arrest (*i.e.* the SAC) and continuing to

proliferate as indicated by RTCA (Figure 4-18, pg.82). Although the transient nature of siRNAs and inhibitors can also contribute to escaping the mitotic arrest, the strong silencing showed by analysis of KIF11 expression through either Western blot (Figure 4-1, pg.56) or IIF microscopy (Figure 4-3, pg.58) 5 days post transfection suggest this is unlikely the case for *KIF11* silenced cells. In addition, recall there were no overt differences observed in NAs following single or dual treatments with monastrol. Therefore, the most likely explanation accounting for the existence of CIN and continued proliferation is that the cells somehow adapt and escape the SAC. Below are some potential explanations of how *KIF11* silenced or inhibited cells may escape cell cycle checkpoint arrests, especially the SAC, and continue to proliferate and induce CIN phenotypes following *KIF11* silencing or inhibition.

5.3.1 Potential Mechanisms Accounting for Increases in Nuclear Area, DNA Content, and Chromosome Numbers

Fundamental research studies in human cell lines have shown that *KIF11* silencing and inhibition induces mitotic arrest[186,151], a transient phenotype also observed within the current study. Recall that KIF11 functions in early prophase to ensure the separation of centrosomes and bipolar spindle formation. In *KIF11* silenced or inhibited cells lack of KIF11 function leads to unsuccessful separation of centrosomes and formation of a monopolar spindle. Monopolar spindles incapable of generating the required tension between kinetochores located on sister chromatids, and thus will result in activation of the SAC. The SAC is required to maintain mitotic fidelity, as it ensures the accurate segregation of genetic material (i.e. chromosomes) to daughter cells during mitosis[34]. An active SAC will transiently arrest cells in mitosis until a bipolar spindle and tension is induced. However, if the SAC maintains for an extended period of time, cells typically either induce apoptosis or escape the checkpoint and re-enter the cell cycle without completing mitosis

and thus not having properly segregated the DNA[187] (Figure 5-1). The process of escaping the mitotic arrest in the presence of an unsatisfied SAC is called SAC adaptation or mitotic slippage. It is suggested that escaping mitotic arrest with a functional SAC requires the gradual degradation of Cyclin B to a point below the threshold needed to maintain the mitotic arrest[140]. Therefore, the fate of cells arrested in mitosis depends on the balance between the rate of Cyclin B degradation and accumulation of death signals, typically pro-apoptotic signals[187]. In the other words, a cell will survive if it escapes mitotic arrest prior to death signals reaching the arbitrary threshold required to trigger apoptosis. To investigate whether Cyclin B degradation is the mechanism of the SAC adaptation in *KIF11* silenced or inhibited cells, changes in the level of Cyclin B expression can be regularly (e.g. every 6 hours) examined following *KIF11* silencing or inhibition through western blot analysis. In addition to Cyclin B, the expression and localization of other proteins required for the SAC function, such as CDK1, APC/C, and MAD2 can be also evaluated. Thus to induce mitotic slippage and based on the function of these proteins (see *Section* 1.3.1.3, pg. 9), it is predicted to see that CDK1 and MAD2 could be downregulated, whereas APC/C could be overexpressed.

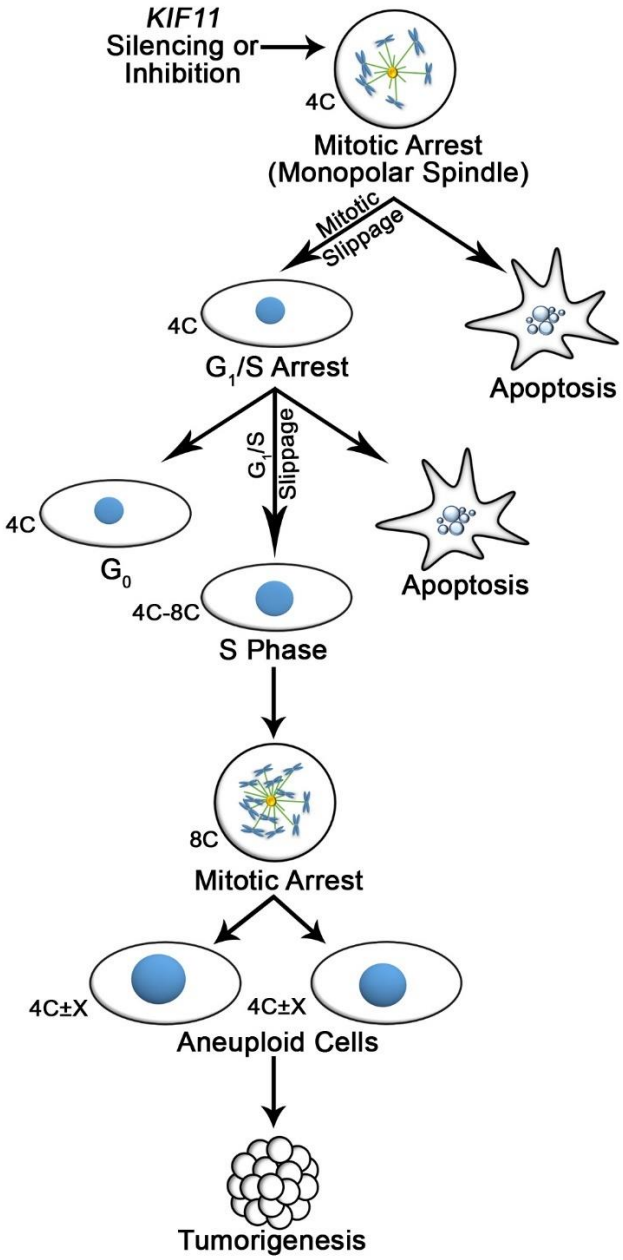

Figure 5-1: The Fate of *KIF11* Silenced or Inhibited Cells
Schematic depicting a model describing the steps at which *KIF11* silenced or inhibited cells escape mitotic arrest to form aneuploid cells and promote oncogenesis. Following *KIF11* silencing or inhibition due to the lack of tension on sister chromatids, cells are arrested in mitosis. Arrested cells either undergo apoptosis and die or escape the mitotic arrest and survive as cells with 4C DNA content. Cells survived prolonged mitotic arrest may be arrested in G1/S checkpoint due to the high level of DNA damage. Therefore, these cells either undergo apoptosis, remains in G0, or proceed through cell cycle. Cells survived the G1/S checkpoint replicate their DNA and form cells with 8C DNA content. Octoploid cells enter the next cell cycle may be arrested in mitosis due to the lack of *KIF11* expression or function. However, the presence of aneuploidy in these cells may help them to rapidly adjust to the situation and undergo cell division. Aneuploid cells formed through this pathway may continue to proliferate to induce oncogenesis.

Cells escaping prolonged mitotic arrest are suggested to become arrested at the following cell cycle checkpoint (i.e. G1/S checkpoint) due to extensive amount of DNA damage[188,189,190]. During mitosis, DNA damage response proteins are not normally recruited to the site of DNA damage (e.g. DSBs) apparently due to the extensive level of compaction observed within mitotic chromosomes[188,191]. Lack of DNA repair protein recruitment will lead to the accumulation of DNA errors and may contribute to CIN. Thus, *KIF11* silenced or inhibited cells that escape the SAC may become arrested at G1/S-phase checkpoint due to the presence of DNA damage. Cells arrested at this checkpoint may undergo senescence (i.e. enter G0), die through apoptosis, or alternatively escape the G1 checkpoint and continue to proliferate[192]. In fact, the presence of cells with more than 4N DNA content (e.g. octoploid cells) following *KIF11* silencing or inhibition suggests that at least a subset of cells is capable of proceeding through S phase and replicating their DNA. Although the presence of octoploid or near octoploid cells is consistent with cells replicating their DNA (going through S phase), this possibility was not formally tested. Cells replicating their DNA content during S phase may then enter mitosis, where due to the lack of *KIF11* function, they may active the SAC once more. Polyploid cells are known to be genetically unstable, which allows them to survive high level of gains of chromosomes[193,194]. Therefore, these cells are expected to escape the mitotic arrest much more rapidly but in a less accurate manner and perhaps through cell division to form aneuploid cells and induce CIN. CIN in turn changes the rate of loss of tumor suppressors and gain of oncogenes and therefore promotes oncogenesis[16].

5.3.2 Potential Mechanisms Accounting for Increases in MN Formation

Although the above information provides a possible explanation for increases in NAs, DNA content, and chromosome numbers, they do not necessarily account for the increases in MN formation we observe. Recall, micronuclei are chromosomes or large chromosomal fragments that

typically arise due to aberrant mitoses stemming from DSBs or lagging chromosomes (i.e. missegregated chromosomes)[195]. As noted above, mitotic cells are generally incapable of recruiting DNA damage response proteins to the condensed chromosomes, and thus DSBs are not typically repaired during mitosis[188,191]. Large DNA fragments resulting from DSBs may lack centromeric sequences and therefore are unable to assemble a kinetochore that captures microtubules. Accordingly, these acentric chromosome fragments are not adequately segregated, which may prevent them from being included within the primary nucleus as the nuclear envelope reforms at the end of mitosis resulting in the formation of a MN (Figure 5-2). Although data presented in this thesis indicate that *KIF11* silencing or inhibition increases MN formation, we did not specifically look for increases in DSBs in our models. However, increases in DSBs does not appear to be the principal mechanism accounting for increases in MN formation as we did not frequently observe chromosome breaks within the mitotic chromosome spreads. Nevertheless, DNA DSBs were not quantitatively assessed and thus it may still contribute, at least in part, to the development of micronuclei following KIF11 silencing or inhibition. Accordingly, to assess this possibility, DSBs could be quantified using IIF and a surrogate marker of breaks, namely γ-H2AX[196].

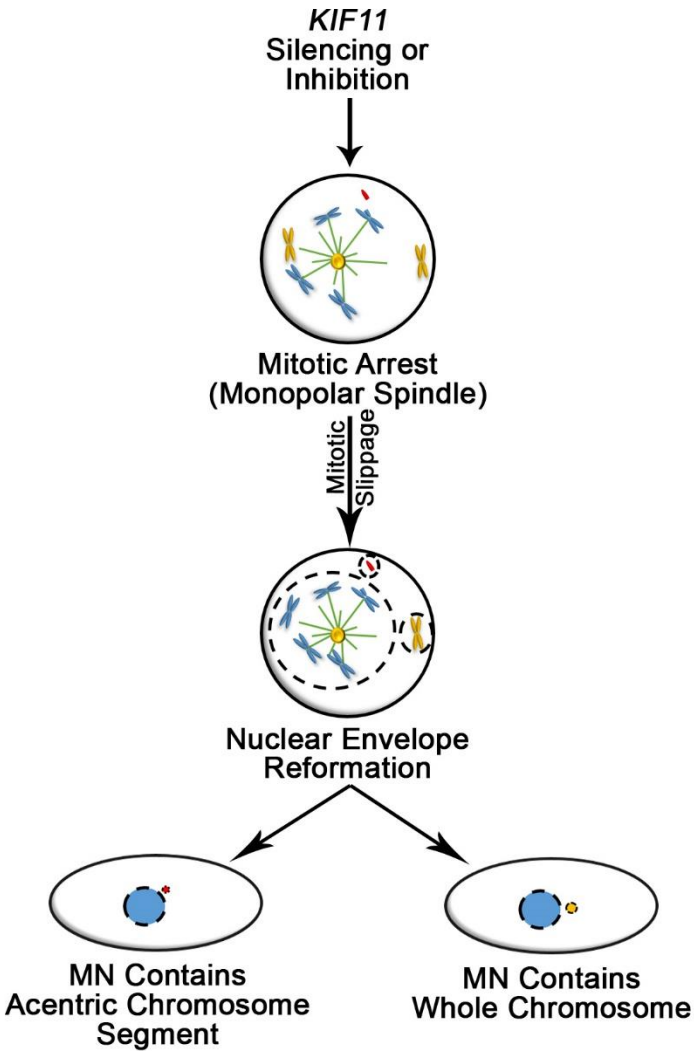

Figure 5-2: Potential Mechanisms of MN Formation in *KIF11* Silenced or Inhibited Cells
Schematic illustrating models of MN formation following *KIF11* silencing or inhibition. Prolonged mitotic arrest following *KIF11* silencing or inhibition may result in DSB. Unrepaired DSBs through mitotic arrest may cause acentric chromosomes that are incapable of capturing kinetochore microtubules. Thus, these fragments may be excluded from the primary nucleus during nuclear envelope reformation and form micronuclei. Alternatively, whole chromosomes lacking kinetochore attachment may induce MN formation. Unattached chromosomes and acentric chromosome segments are shown in yellow and red respectively. Nuclear envelopes are shown with dashes.

A second possible mechanism accounting for the increases in micronuclei observed following *KIF11* silencing and inhibition is through whole chromosome missegregation. Recall that during mitosis and in the absence of sister chromatid tension, Aurora B functions by phosphorylating targets within the outer kinetochore to destabilize incorrect kinetochore attachments to facilitate kinetochores reorientation[68]. Therefore, it is possible that in *KIF11* silenced or inhibited cells, lack of tension on sister chromatids leads to destabilization of the kinetochore attachments by Aurora B. Unattached kinetochores may or may not recapture the microtubules and therefore would not migrate to monopolar spindle poles (centrosome). As a result, if cells escape the mitotic arrest, these chromosomes may be excluded from the primary nucleus during nuclear envelope formation and form micronuclei (Figure 5-2). To investigate this possibility, live cell imaging can be performed using HCT116 or hTERT cells designed to express histone H2B-GFP (green florescent protein) and tubulin-RFP (red florescent protein). KIF11 can be either silenced or inhibited in these cells and images can be acquired frequently (e.g. every 15-30 min). Study of these images may allow to determine the potential mechanism accounting for MN formation following *KIF11* silencing or inhibition.

5.4 Therapeutically Exploiting *KIF11* Deficiencies in Cancer

CIN, which is a characteristic of most cancers[197], plays role in cancer development and tumor adaptation to the environmental stresses through tumor heterogeneity and clonal evolution[198,199]. Cancers exhibiting CIN are associated with aggressive tumors[19], multidrug resistance[20], and consequently poor patient prognosis[21]. Therefore, therapeutic strategies and drug targets that exploit the molecular origins of CIN are urgently needed to deliver precision-based medicine approaches. Recall that despite the various clinical trials testing the effect of KIF11 inhibitors on different cancers, to date there are limited benefits reported for patients using these

anticancer agents. Although, the underlying reason(s) for the apparent failure of KIF11 inhibitors remains to be elucidated, the results of the current study suggest that the ability of cells to continue to proliferate following KIF11 inhibition could be a potential explanation. In fact, our data suggests that a subset of cells inhibited by monastrol (and perhaps other KIF11 inhibitors) can survive an initial mitotic arrest, continue to proliferate, and contribute to oncogenesis through CIN and clonal evolution.

Although KIF11 inhibition might not be effective in cancer therapy, exploiting *KIF11* deficiencies found in cancer (Table 2-1, pg. 35) may be possible using synthetic lethal (SL) approaches. Synthetic lethality is defined as a rare and lethal combination of two independently viable mutations[200]. Two genes are SL if their mutation or deletion alone does not affect cell viability, but their simultaneous mutation or deletion is lethal for the cell[201]. In the context of cancer, identifying a SL interactor of a gene mutated or deleted in cancer (e.g. *KIF11*) can be beneficial to develop precision medicine-based drug targets to preferentially kill cancer cells within a cancer patient. There are studies from yeast to human identifying SL interactors of genes encoding critical functions important for accurate chromosome segregation and stability that can be exploiting in cancers exhibiting CIN[202,203,165]. Recall that *CIN8* is the yeast ortholog of human *KIF11*[204], and like KIF11, Cin8 is a kinesin motor protein whose absence induces CIN in yeast[167]. Accordingly, SL datasets for *CIN8* may help identify conserved SL interactors (i.e. drug targets) capable of exploiting *KIF11* defects occurring in human cancers. In this regard, Geiser et al.[205] identified 17 SL interactors of *CIN8*, many of which have human orthologs (Table 5-1). Accordingly, we propose these genes are candidate SL interactors of *KIF11* that could be explored in future direct SL tests. Briefly, dual silencing of *KIF11* and candidate SL interactors could be performed and the residual number of cells remaining following dual silencing could be compared

with those remaining following KIF11 silencing alone. A putative SL interactor would be identified based on fewer remaining cells within KIF11 silenced cells relative to controls. Alternatively, other than siRNAs, additional approaches such as small molecular inhibitors could be employed to validate these candidate SL interactions identified (detailed in *Section* 5.5).

Table 5-1: Human Orthologs of the *CIN8* SL Interactors

Yeast Gene[A]	Human Ortholog[B]	Human Protein Function[C]
ARP1	*ACTR1B*	subunit of dynactin complex
BIK1	*CLIP1*	linker of endocytic vesicles to microtubules
CIN1	*TNPO1*	beta subunit of the karyopherin receptor complex
DYN1	*DYNC1H1*	cytoplasmic dynein
KIP1	*KIF13A*	kinesin
PAC1	*PAFAH1B1*	subunit of platelet-activating factor acteylhydrolase enzyme
PAC2	*TBCE*	β-Tubulin folding cofactor
JNM1	*CLIP1*	linker of endocytic vesicles to microtubules
CDC20	*CDC20*	cell cycle regulatory factor
BUB2	*TBC1D1*	cell growth and differentiation regulatory factor
MOS1	*TLK1*	kinase involved in chromatin assembly regulation
BUB3	*BUB3*	involved in spindle assembly checkpoint
PAC10	*VBP1*	Von Hippel-Lindau binding protein
PAC11	*DYNC1I1*	cytoplasmic dynein
NUM1	*GCC2*	peripheral membrane protein
NIP100	*CLIP2*	linker of dendritic lamellar body to microtubules
IPL1	*AURKC*	aurora subfamily of serine/threonine protein kinases

[A]SL interactors of *CIN8* identified by Geiser et al.[205]
[B] Data adapted from Ensembl (version 85)[206] and Protein Blast (NCBI)[204]
[C] Data adapted from GeneCards[207]

5.5 Future Experimental Directions

This thesis indicates *KIF11* expression and function are normally required to maintain chromosome stability in HCT116 and hTERT cells, and therefore *KIF11* silencing or inhibition induces CIN. Although data presented in this thesis show *KIF11* is a CIN gene in conventional 2D (two-dimensional) culture systems, a major limitation of 2D cell cultures is that they do not accurately reflect the 3D growth and microenvironmental factors contained within tumors[208]. Therefore, the next logical step in the validation of *KIF11* as a CIN gene would be to evaluate the impact diminished KIF11 expression and function has in animal models. Homozygous deletion of *KIF11* has been found to be embryonic lethal[209], therefore, genetically engineered mouse models with traditional *KIF11* knockout are not an option for this study. However, conditional *KIF11* knockout, where only selected tissues are targeted for the knockout, could potentially circumvent this concern. In this strategy, germline cells are modified for the target gene, but the gene is only inactivated in selected cells (e.g. colonic epithelial cells)[210]. Although the loss of *KIF11* alone is not predicted to induce oncogenesis immediately, the CIN induced following the loss of KIF11 expression and function may over time, drive oncogenesis within these mice. Alternatively, the conditional *KIF11* knockout mice could be genetically crossed with *p53*-deficient mice. As *p53*-deficient mice are highly susceptible to tumor formation[211], tumor development, latency and metastasis could be compared between those in which *KIF11* has been conditionally knocked out with those in which it remains.

An alternative study could involve the use of immunocompromised mouse xenograft models (for tumor establishment and growth studies) with subcutaneous injection of HCT116 cells in which *KIF11* has been stably silenced (e.g. using shRNAs). Mouse HCT116 xenograft models with normal *KIF11* expression could also be used as controls. Comparison of the growth of *KIF11*

silenced tumors and control tumors, by measuring tumor volume or tumor weight, would allow to investigate the effect of *KIF11* diminished expression on tumor latency and development. If tumor latency is reduced in *KIF11* silenced xenografts, it would be supportive of diminished *KIF11* expression and function being a contributing pathogenic event in the etiology of cancer. However, a more representative model would be colonic injection of HCT116 cells to immunocompromised mouse. Although these models would more accurately imitates the microenvironments and 3D architecture of CRCs, colonic xerograph models are technically more challenging to be generated.

KIF11 has been found somatically deleted or mutated in numerous cancer types[169,170] (Table 2-1, pg.35). Although gene homozygous deletion results in eliminated protein expression, mutations within a gene are not necessarily representative of protein expression or function loss. To investigate whether loss of KIF11 expression is commonly found in CRC, immunohistochemical analysis against KIF11 could be performed in CRC tumor microarrays. Only once KIF11 found downregulated in human CRC tumors, this study can migrate to identify novel therapeutic approaches that exploit these origins. Presence of *KIF11* mutations or diminished expression in cancers as well as its role in maintaining chromosome stability, make *KIF11* a strong candidate to be exploited therapeutically. For example, as indicated above (*Section* 5.4, pg. 93) SL interactors of *KIF11* could be identified and be targeted in CRC as well as other relevant cancers. Initially, a siRNA-based screen could be performed to confirm SL interaction of genes indicated in Table 5-1 (pg. 95) with *KIF11*. In this screen, dual silencing could be performed in which both KIF11 and its potential interactors (Table 5-1, pg. 95) would either individually or simultaneously be silenced in desired cell lines. Following, the effect of dual silencing of KIF11 and candidate SL interactors on residual number of remaining cells could be compared with KIF11 silencing alone. To evaluate the conserved SL interaction of these genes with *KIF11,* this experiment can also be

performed using small molecule inhibitors. Next, the effect of these drugs can be studied on more promising and physically relevant models such as animal models. Similar to above, mouse xenograft models in which *KIF11* has been stably silenced could be developed and be targeted with *KIF11* SL interactors identified within basic science models. Only once these interactions have been identified therapeutically effective in animal models, will it be possible to migrate the most promising SL interactors to cancer clinical trials. Alternatively, as some of these potential KIF11 interactors such as *TNPO1* and *GCC2* are somatically mutated in cancers[169,170], another therapeutic approach could be the use of KIF11 inhibitors as drug targets in cancers with mutations of these genes.

5.6 Conclusions and Significances

In summary, *KIF11* diminished expression and function was shown to induce CIN in two karyotypically stable cell lines (HCT116 and hTERT). Based on our understanding that *KIF11* is somatically altered in a number of different human cancers[169,170], the data generated from this thesis likely has implications for the pathogenesis of many cancer types including CRC (Table 2-1, pg. 35). However, the role of KIF11 in normally maintaining chromosome stability and how its aberrant expression and function may contribute to cancer development and progression has not been elucidated. Once a greater understanding of the role KIF11 has in oncogenesis is achieved novel therapeutic strategies could be developed that exploit the underlying defects. Since *KIF11* is somatically altered in a number of different cancer types[169,170], therapeutic strategies designed to exploit defects in *KIF11* may benefit a large number of cancer patients (Table 2-1, pg. 35). For example, each year ~5,000 Americans and ~1,000 Canadians are diagnosed with CRC that may benefit from a KIF11-specific therapeutic approach. Finally, the findings of the current thesis are

likely to have etiological implications in many additional cancer contexts, such as prostate, uterine, and lung (Table 2-1, pg. 35).

CHAPTER 6: REFERENCES

1. Cahill, D. P., Kinzler, K. W., Vogelstein, B. & Lengauer, C. Genetic instability and darwinian selection in tumours. *Trends Biochem. Sci.* 24, 57–60 (1999).
2. Lengauer, C., Kinzler, K. W. & Vogelstein, B. Genetic instability in colorectal cancers. *Nature* 386, 623–627 (1997).
3. Wooster, R. *et al.* Instability of short tandem repeats (microsatellites) in human cancers. *Nat Genet* 6, 152–6. (1994).
4. Michor, F. Chromosomal instability and human cancer. 631–635 (2005). doi:10.1098/rstb.2004.1617
5. Dunican, D. S., McWilliam, P., Tighe, O., Parle-McDermott, A. & Croke, D. T. Gene expression differences between the microsatellite instability (MIN) and chromosomal instability (CIN) phenotypes in colorectal cancer revealed by high-density cDNA array hybridization. *Oncogene* 21, 3253–3257 (2002).
6. Sinicrope, F. A. & Sargent, D. J. Molecular pathways: Microsatellite instability in colorectal cancer: Prognostic, predictive, and therapeutic implications. *Clin. Cancer Res.* 18, 1506–1512 (2012).
7. Esteller, M., Levine, R., Baylin, S. B., Ellenson, L. H. & Herman, J. G. MLH1 promoter hypermethylation is associated with the microsatellite instability phenotype in sporadic endometrial carcinomas. *Oncogene* 17, 2413–2417 (1998).
8. Kohlmann, W. & Gruber, S. B. Hereditary non-polyposis colon cancer. *GeneReviews* 98, 1 (2004).
9. Modrich, P. Mechanisms in Eukaryotic Mismatch Repair. *J. Biol. Chem.* 281, 30305–30309 (2006).
10. Kunkel, T. & Erie, D. Dna Mismatch Repair*. *Annu. Rev. Biochem.* 74, 681–710 (2005).
11. Genschel, J., Littman, S. J., Drummond, J. T. & Modrich, P. Isolation of MutSbeta from human cells and comparison of the mismatch repair specificities of MutSbeta and MutSalpha. *J Biol Chem* 273, 19895–19901 (1998).
12. Pukkila, P. J., Peterson, J., Herman, G., Modrich, P. & Meselson, M. Effects of high levels of DNA adenine methylation on methyl-directed mismatch repair in Escherichia coli. *Genetics* 104, 571–582 (1983).
13. Polosina, Y. Y., Mui, J., Pitsikas, P. & Cupples, C. G. The Escherichia coli mismatch repair protein MutL recruits the Vsr and muth endonucleases in response to DNA damage. *J. Bacteriol.* 191, 4041–4043 (2009).
14. Holmes, J., Clark, S. & Modrich, P. Strand-specific mismatch correction in nuclear extracts of human and Drosophila melanogaster cell lines. *Proc. Natl. Acad. Sci. U. S. A.* 87, 5837–5841 (1990).
15. Bayani, J. *et al.* Genomic mechanisms and measurement of structural and numerical instability in cancer cells. *Semin. Cancer Biol.* 17, 5–18 (2007).
16. Chi, Y. H. & Jeang, K. T. Aneuploidy and cancer. *J. Cell. Biochem.* 102, 531–538 (2007).
17. Torres, E. M., Williams, B. R. & Amon, A. Aneuploidy: Cells losing their balance. *Genetics* 179, 737–746 (2008).
18. Nowell, P. The clonal evolution of tumor cell populations. *Science (80-.).* 194, 23–28 (1976).
19. Carter, S. L., Eklund, A. C., Kohane, I. S., Harris, L. N. & Szallasi, Z. A signature of chromosomal instability inferred from gene expression profiles predicts clinical outcome in

multiple human cancers. *Nat Genet* 38, 1043–1048 (2006).
20. Duesberg, P., Stindl, R. & Hehlmann, R. Explaining the high mutation rates of cancer cells to drug and multidrug resistance by chromosome reassortments that are catalyzed by aneuploidy. *Proc. Natl. Acad. Sci. U. S. A.* 97, 14295–14300 (2000).
21. McGranahan, N., Burrell, R. A., Endesfelder, D., Novelli, M. R. & Swanton, C. Cancer chromosomal instability: therapeutic and diagnostic challenges. *EMBO Rep* 13, 528–538 (2012).
22. Lengauer, C., Kinzler, K. W. & Vogelstein, B. Genetic instabilities in human cancers. *Nature* 396, 643–649 (1998).
23. Cherry, J. M. *et al.* Saccharomyces Genome Database: The genomics resource of budding yeast. *Nucleic Acids Res.* 40, 700–705 (2012).
24. Stirling, P. C. *et al.* The complete spectrum of yeast chromosome instability genes identifies candidate cin cancer genes and functional roles for astra complex components. *PLoS Genet.* 7, 9–13 (2011).
25. Pennisi, E. ENCODE Project Writes Eulogy for Junk DNA. *Science (80-.).* 337, 1159–1161 (2012).
26. Weaver, B. A. & Cleveland, D. W. Does aneuploidy cause cancer? *Curr. Opin. Cell Biol.* 18, 658–667 (2006).
27. Michel, L. S. *et al.* MAD2 haplo-insufficiency causes premature anaphase and chromosome instability in mammalian cells. *Nature* 409, 355–359 (2001).
28. Spruck, C. H., Won, K. a & Reed, S. I. Deregulated cyclin E induces chromosome instability. *Nature* 401, 297–300 (1999).
29. Fukasawa, K. Centrosome amplification, chromosome instability and cancer development. *Cancer Lett.* 230, 6–19 (2005).
30. Putkey, F. R. *et al.* Unstable kinetochore-microtubule capture and chromosomal instability following deletion of CENP-E. *Dev. Cell* 3, 351–365 (2002).
31. Sajesh, B. V, Lichtensztejn, Z. & McManus, K. J. Sister chromatid cohesion defects are associated with chromosome instability in Hodgkin lymphoma cells. *BMC Cancer* 13, 391 (2013).
32. Mathieu, N., Pirzio, L., Freulet-Marrière, M. A., Desmaze, C. & Sabatier, L. Telomeres and chromosomal instability. *Cell. Mol. Life Sci.* 61, 641–656 (2004).
33. Rosario, C. O. *et al.* Plk4 is required for cytokinesis and maintenance of chromosomal stability. *Proc. Natl. Acad. Sci. U. S. A.* 107, 6888–6893 (2010).
34. Musacchio, A. & Salmon, E. D. The spindle-assembly checkpoint in space and time. *Nat. Rev. Mol. Cell Biol.* 8, 379–93 (2007).
35. Peters, J.-M. & Nishiyama, T. Sister chromatid cohesion. *Cold Spring Harb. Perspect. Biol.* 4, 1–18 (2012).
36. Bertoli, C., Skotheim, J. M. & de Bruin, R. A. M. Control of cell cycle transcription during G1 and S phases. *Nat. Rev. Mol. Cell Biol.* 14, 518–28 (2013).
37. Dasika, G. K. *et al.* DNA damage-induced cell cycle checkpoints and DNA strand break repair in development and tumorigenesis. *Oncogene* 18, 7883–99 (1999).
38. Malmanche, N., Maia, A. & Sunkel, C. E. The spindle assembly checkpoint: Preventing chromosome mis-segregation during mitosis and meiosis. *FEBS Lett.* 580, 2888–2895 (2006).
39. Zetterberg, A., Larsson, O. & Wiman, K. G. What is the restriction point? *Curr. Opin. Cell Biol.* 7, 835–842 (1995).

40. Weinberg, R. A. The retinoblastoma protein and cell cycle control. *Cell* 81, 323–330 (1995).
41. Dimova, D. K. & Dyson, N. J. The E2F transcriptional network: old acquaintances with new faces. *Oncogene* 24, 2810–2826 (2005).
42. Yang, K., Hitomi, M. & Stacey, D. W. Variations in cyclin D1 levels through the cell cycle determine the proliferative fate of a cell. *Cell Div.* 1, 32 (2006).
43. Ohtani, K., DeGregori, J. & Nevins, J. R. Regulation of the cyclin E gene by transcription factor E2F1. *Proc. Natl. Acad. Sci. U. S. A.* 92, 12146–12150 (1995).
44. Bartek, J. & Lukas, J. Mammalian G1- and S-phase checkpoints in response to DNA damage. *Curr. Opin. Cell Biol.* 13, 738–747 (2001).
45. Coverley, D., Laman, H. & Laskey, R. a. Distinct roles for cyclins E and A during DNA replication complex assembly and activation. *Nat. Cell Biol.* 4, 523–528 (2002).
46. Shiotani, B. & Zou, L. Single-Stranded DNA Orchestrates an ATM-to-ATR Switch at DNA Breaks. *Mol. Cell* 33, 547–558 (2009).
47. Carroll, J. & Marangos, P. The DNA damage response in mammalian oocytes. *Front. Genet.* 4, 1–9 (2013).
48. Wade Harper, J., Adami, G. R., Wei, N., Keyomarsi, K. & Elledge, S. J. The p21 Cdk-interacting protein Cip1 is a potent inhibitor of G1 cyclin-dependent kinases. *Cell* 75, 805–816 (1993).
49. Massagué, J. G1 cell-cycle control and cancer. *Nature* 432, 298–306 (2004).
50. Lindqvist, A., Rodríguez-Bravo, V. & Medema, R. H. The decision to enter mitosis: feedback and redundancy in the mitotic entry network. *J. Cell Biol.* 185, 193–202 (2009).
51. Stark, G. R. & Taylor, W. R. Control of the G2/M transition. *Mol. Biotechnol.* 32, 227–248 (2006).
52. Santos, S. D. M., Wollman, R., Meyer, T. & Ferrell, J. E. Spatial positive feedback at the onset of mitosis. *Cell* 149, 1500–1513 (2012).
53. Kellogg, D. R. Wee1-dependent mechanisms required for coordination of cell growth and cell division. *J. Cell Sci.* 116, 4883–4890 (2003).
54. Zitouni, S., Nabais, C., Jana, S. C., Guerrero, A. & Bettencourt-Dias, M. Polo-like kinases: structural variations lead to multiple functions. *Nat Rev Mol Cell Biol* 15, 433–452 (2014).
55. Gavet, O. & Pines, J. Progressive Activation of CyclinB1-Cdk1 Coordinates Entry to Mitosis. *Dev. Cell* 18, 533–543 (2010).
56. Raleigh, J. M. & O'Connell, M. J. The G(2) DNA damage checkpoint targets both Wee1 and Cdc25. *J. Cell Sci.* 113 (Pt 1, 1727–1736 (2000).
57. Sanchez, Y. *et al.* Conservation of the Chk1 checkpoint pathway in mammals: linkage of DNA damage to Cdk regulation through Cdc25. *Science* 277, 1497–501 (1997).
58. Boutros, R., Lobjois, V. & Ducommun, B. CDC25 phosphatases in cancer cells: key players? Good targets? *Nat. Rev. Cancer* 7, 495–507 (2007).
59. Clute, P. & Pines, J. Temporal and spatial control of cyclin B1 destruction in metaphase. *Nat. Cell Biol.* 1, 82–87 (1999).
60. Glotzer, M., Murray, A. W. & Kirschner, M. W. Cyclin is degraded by the ubiquitin pathway. *Nature* 349, 132–138 (1991).
61. Zachariae, W. & Nasmyth, K. Whose end is destruction: cell division and the anaphase-promoting complex. *Genes Dev.* 13, 2039–2058 (1999).
62. Fang, G., Yu, H. & Kirschner, M. W. Direct binding of CDC20 protein family members activates the anaphase-promoting complex in mitosis and G1. *Mol Cell* 2, 163–171 (1998).
63. Nasmyth, K. Disseminating the genome: joining, resolving, and separating sister chromatids

during mitosis and meiosis. *Annu. Rev. Genet.* 35, 673–745 (2001).
64. Rieder, C. L., Schultz, A., Cole, R. & Sluder, G. Anaphase onset in vertebrate somatic cells is controlled by a checkpoint that monitors sister kinetochore attachment to the spindle. *J. Cell Biol.* 127, 1301–1310 (1994).
65. Lara-Gonzalez, P., Westhorpe, F. G. & Taylor, S. S. The Spindle Assembly Checkpoint. *Curr. Biol.* 22, R966–R980 (2012).
66. Sudakin, V., Chan, G. K. T. & Yen, T. J. Checkpoint inhibition of the APC/C in HeLa cells is mediated by a complex of BUBR1, BUB3, CDC20, and MAD2. *J. Cell Biol.* 154, 925–936 (2001).
67. Stern, B. M. & Murray, A. W. Lack of tension at kinetochores activates the spindle checkpoint in budding yeast. *Curr. Biol.* 11, 1462–1467 (2001).
68. Lampson, M. A. & Cheeseman, I. M. Sensing centromere tension: Aurora B and the regulation of kinetochore function. *Trends Cell Biol.* 21, 133–140 (2011).
69. Alushin, G. M. *et al.* Multimodal microtubule binding by the Ndc80 kinetochore complex. *Nat. Struct. Mol. Biol.* 19, 1161–7 (2012).
70. Suzuki, A. *et al.* Spindle microtubules generate tension-dependent changes in the distribution of inner kinetochore proteins. *J. Cell Biol.* 193, 125–140 (2011).
71. Godek, K. M., Kabeche, L. & Compton, D. A. Regulation of kinetochore-microtubule attachments through homeostatic control during mitosis. *Nat. Rev. Mol. Cell Biol.* 16, 57–64 (2015).
72. Cimini, D. *et al.* Merotelic kinetochore orientation is a major mechanism of aneuploidy in mitotic mammalian tissue cells. *J. Cell Biol.* 152, 517–527 (2001).
73. Marjanovic, M. The cell cycle and cancer cell. *2009 Nano-Biophotonics Summer Sch. Univ.* 1–20 (2009).
74. Muller, P. A. J., Vousden, K. H., Patricia, A. J. M. & Karen, H. V. P53 Mutations in Cancer. *Nat. Cell Biol.* 15, 2–8 (2013).
75. Forbes, S. A. *et al.* COSMIC: Exploring the world's knowledge of somatic mutations in human cancer. *Nucleic Acids Res.* 43, D805–D811 (2015).
76. Trust Sanger Institute. Cosmic: catalogue of somatic mutations in cancer. at <cancer.sanger.ac.uk>
77. Hernando, E. *et al.* Rb inactivation promotes genomic instability by uncoupling cell cycle progression from mitotic control. *Nature* 430, 797–802 (2004).
78. Sotillo, R. *et al.* Mad2 Overexpression Promotes Aneuploidy and Tumorigenesis in Mice. *Cancer Cell* 11, 9–23 (2007).
79. Cahill, D. P. *et al.* Mutations of mitotic checkpoint genes in human cancers. *Nature* 392, 300–303 (1998).
80. Kitajima, T. S., Kawashima, S. a & Watanabe, Y. The conserved kinetochore protein shugoshin protects centromeric cohesion during meiosis. *Nature* 427, 510–517 (2004).
81. Karamysheva, Z., Diaz-Martinez, L. A., Crow, S. E., Li, B. & Yu, H. Multiple anaphase-promoting complex/cyclosome degrons mediate the degradation of human sgo1. *J. Biol. Chem.* 284, 1772–1780 (2009).
82. Nasmyth, K. Segregating sister genomes: the molecular biology of chromosome separation. *Science* 297, 559–565 (2002).
83. Barber, T. D. *et al.* Chromatid cohesion defects may underlie chromosome instability in human colorectal cancers. *Proc. Natl. Acad. Sci. U. S. A.* 105, 3443–3448 (2008).
84. Barber, T. D. *et al.* Chromatid cohesion defects may underlie chromosome instability in

human colorectal cancers. *Proc. Natl. Acad. Sci. U. S. A.* 105, 3443–8 (2008).
85. Barbero, J. Cohesins and cohesin-regulators: Role in Chromosome Segregation/Repair and Potential in Tumorigenesis. *Atlas Genet. Cytogenet. Oncol. Haematol.* 16, 157–164 (2012).
86. Sjogren, C., Nasmyth, K. & Sjögren, C. Sister chromatid cohesion is required for postreplicative double-strand break repair in Saccharomyces cerevisiae . *Curr. Biol.* 11, 991–995 (2001).
87. Mannini, L., Menga, S. & Musio, A. The expanding universe of cohesin functions: A new genome stability caretaker involved in human disease and cancer. *Hum. Mutat.* 31, 623–630 (2010).
88. Warner, F. D. & Satir, P. The Substructure of Ciliary Microtubules. *J. Cell Sci.* 12, 313–326 (1973).
89. Bergen, L. & Borisy, G. Head-to-tail polymerization of microtubules in vitro. Electron microscope analysis of seeded assembly. *Electron Microsc. Anal. Seeded Assem.* 84, 141–150 (1980).
90. Brinkley, B. R. Microtubule Organizing Centers. *Ann. Rev. Cell Biol* 145–172 (1985). doi:10.1146/annurev.cellbio.1.1.145
91. Moritz, M. *et al.* Structure of the gamma-tubulin ring complex: a template for microtubule nucleation. *Nat Cell Biol* 2, 365–370 (2000).
92. Morris, R. L. Axonal transport of mitochondria along microtubules and F-actin in living vertebrate neurons. *J. Cell Biol.* 131, 1315–1326 (1995).
93. Compton, D. A. Spindle Assembly in Animal Cells. *Annu. Rev. Biochem.* 69, 95–114 (2000).
94. Sablin, E. P. *et al.* Direction determination in the minus-end-directed kinesin motor ncd. *Nature* 395, 813–6 (1998).
95. Hirokawa, N., Noda, Y. & Okada, Y. Kinesin and dynein superfamily proteins in organelle transport and cell division. *Curr. Opin. Cell Biol.* 10, 60–73 (1998).
96. Lawrence, C. J. *et al.* A standardized kinesin nomenclature. *J. Cell Biol.* 167, 19–22 (2004).
97. Exertier, P. *et al.* Impaired angiogenesis and tumor development by inhibition of the mitotic kinesin Eg5 ABSTRACT : *Oncotarget* 4, 2302–2316 (2013).
98. Goshima, G. Cell Cycle-dependent Dynamics and Regulation of Mitotic Kinesins in Drosophila S2 Cells. *Mol. Biol. Cell* 16, 3896–3907 (2005).
99. Hirokawa, N., Noda, Y., Tanaka, Y. & Niwa, S. Kinesin superfamily motor proteins and intracellular transport. *Nat. Rev. Mol. Cell Biol.* 10, 682–696 (2009).
100. Wojcik, E. J. *et al.* Kinesin-5: Cross-bridging mechanism to targeted clinical therapy. *Gene* 531, 133–149 (2013).
101. Ensembl. Gene: KIF11 (ENSG00000138160) - Orthologues - Homo sapiens - Ensembl genome browser 86. at <http://uswest.ensembl.org/Homo_sapiens/Gene/Compara_Ortholog?db=core;g=ENSG00000138160;r=10:92593286-92655395;t=ENST00000260731>
102. Le Guellec, R., Paris, J., Couturier, a, Roghi, C. & Philippe, M. Cloning by differential screening of a Xenopus cDNA that encodes a kinesin-related protein. *Mol. Cell. Biol.* 11, 3395–3398 (1991).
103. National Center for Biotechnology Information. KIF11 kinesin family member 11 [Homo sapiens (human)] - Gene - NCBI. at <http://www.ncbi.nlm.nih.gov/gene/3832>
104. Sun, X. *et al.* Dimethylenastron suppresses human pancreatic cancer cell migration and invasion in vitro via allosteric inhibition of mitotic kinesin Eg5. *Acta Pharmacol. Sin.* 32,

1543–1548 (2011).
105. Weizmann Institute of Science. KIF11 Gene - GeneCards | KIF11 Protein | KIF11 Antibody. at <http://www.genecards.org/cgi-bin/carddisp.pl?gene=KIF11&keywords=kif11>
106. El-Nassan, H. B. Advances in the discovery of kinesin spindle protein (Eg5) inhibitors as antitumor agents. *Eur. J. Med. Chem.* 62, 614–631 (2013).
107. Case, R. B., Rice, S., Hart, C. L., Ly, B. & Vale, R. D. Role of the kinesin neck linker and catalytic core in microtubule-based motility. *Curr. Biol.* 10, 157–160 (2000).
108. Sarli, V. & Giannis, A. Targeting the kinesin spindle protein: Basic principles and clinical implications. *Clin. Cancer Res.* 14, 7583–7587 (2008).
109. Hariharan, V. & Hancock, W. O. Insights into the Mechanical Properties of the Kinesin Neck Linker Domain from Sequence Analysis and Molecular Dynamics Simulations. *Cell. Mol. Bioeng.* 2, 177–189 (2009).
110. Valentine, M. T., Fordyce, P. M. & Block, S. M. Eg5 steps it up! *Cell Div.* 1, 31 (2006).
111. Turner, J. *et al.* Crystal Structure of the Mitotic Spindle Kinesin Eg5 Reveals a Novel Conformation of the Neck-linker. *J. Biol. Chem.* 276, 25496–25502 (2001).
112. Cross, R. a. & McAinsh, A. Prime movers: the mechanochemistry of mitotic kinesins. *Nat. Rev. Mol. Cell Biol.* 15, 257–271 (2014).
113. A Non-Motor Microtubule Binding Site In Kinesin-5 Is Required For Filament Crosslinking And Sliding. *Changes* 29, 997–1003 (2012).
114. Kashina, A. ., Rogers, G. . & Scholey, J. . The bimC family of kinesins: essential bipolar mitotic motors driving centrosome separation. *Biochim. Biophys. Acta - Mol. Cell Res.* 1357, 257–271 (1997).
115. Blangy, A. *et al.* Phosphorylation by p34cdc2 regulates spindle association of human Eg5, a kinesin-related motor essential for bipolar spindle formation in vivo. *Cell* 83, 1159–1169 (1995).
116. Acar, S. *et al.* The bipolar assembly domain of the mitotic motor kinesin-5. *Nat. Commun.* 4, 1343 (2013).
117. Scholey, J. E., Nithianantham, S., Scholey, J. M. & Al-Bassam, J. Structural basis for the assembly of the mitotic motor kinesin-5 into bipolar tetramers. *Elife* 2014, 1–19 (2014).
118. Kapitein, L. C. *et al.* Microtubule cross-linking triggers the directional motility of kinesin-5. *J. Cell Biol.* 182, 421–428 (2008).
119. Shang, Z. *et al.* High-resolution structures of kinesin on microtubules provide a basis for nucleotide-gated force-generation. *Elife* 3, e04686 (2014).
120. Rosenfeld, S. S., Xing, J., Jefferson, G. M. & King, P. H. Docking and rolling, a model of how the mitotic motor Eg5 works. *J. Biol. Chem.* 280, 35684–95 (2005).
121. ALberts, B. *et al. Molecular Biology of THE CELL*. (Garland science, Taylor & Francis Group, 2008).
122. Verhey, K. J. & Hammond, J. W. Traffic control: regulation of kinesin motors. *Nat. Rev. Mol. Cell Biol.* 10, 765–777 (2009).
123. Kaseda, K., McAinsh, A. D. & Cross, R. a. Walking, hopping, diffusing and braking modes of kinesin-5. *Biochem. Soc. Trans.* 37, 1045–1049 (2009).
124. Agircan, F. G., Schiebel, E. & Mardin, B. R. Separate to operate: control of centrosome positioning and separation. *Philos. Trans. R. Soc. Lond. B. Biol. Sci.* 369, 20130461- (2014).
125. Cross, R. A. & Mcainsh, A. Prime movers : the mechanochemistry of mitotic kinesins. *Nat. Publ. Gr.* 15, 257–271 (2014).
126. vanHeesbeen, R. G. H. P., Tanenbaum, M. E. & Medema, R. H. Balanced activity of three

mitotic motors is required for bipolar spindle assembly and chromosome segregation. *Cell Rep.* 8, 948–956 (2014).
127. Raaijmakers, J. A. *et al.* Nuclear envelope-associated dynein drives prophase centrosome separation and enables Eg5-independent bipolar spindle formation. *EMBO J.* 31, 4179–4190 (2012).
128. Tanenbaum, M. E. *et al.* Kif15 Cooperates with Eg5 to Promote Bipolar Spindle Assembly. *Curr. Biol.* 19, 1703–1711 (2009).
129. Wittmann, T., Boleti, H., Antony, C., Karsenti, E. & Vernos, I. Localization of the kinesin-like protein Xklp2 to spindle poles requires a leucine zipper, a microtubule-associated protein, and dynein. *J. Cell Biol.* 143, 673–685 (1998).
130. Drechsler, H., McHugh, T., Singleton, M. R., Carter, N. J. & McAinsh, A. D. The Kinesin-12 Kif15 is a processive track-switching tetramer. *Elife* 2014, 1–17 (2014).
131. Myers, K. a. & Baas, P. W. Kinesin-5 regulates the growth of the axon by acting as a brake on its microtubule array. *J. Cell Biol.* 178, 1081–1091 (2007).
132. Nadar, V., Lin, S. & Baas, P. Microtubule redistribution in growth cones elicited by focal inactivation of kinesin-5. 32, 5783–5794 (2012).
133. Falnikar, A., Tole, S. & Baas, P. W. Kinesin-5, a mitotic microtubule-associated motor protein, modulates neuronal migration. *Mol. Biol. Cell* 22, 1561–1574 (2011).
134. Bartoli, K. M., Jakovljevic, J., Woolford, J. L. & Saunders, W. S. Kinesin molecular motor Eg5 functions during polypeptide synthesis. *Mol. Biol. Cell* 22, 3420–3430 (2011).
135. Ferhat, L. *et al.* Expression of the mitotic motor protein Eg5 in postmitotic neurons: implications for neuronal development. *J. Neurosci.* 18, 7822–7835 (1998).
136. Mardin, B. R., Agircan, F. G. & Lange, C. Plk1 Controls the Nek2A-PP1 g Antagonism in Centrosome Disjunction. *Curr. Biol.* 21, 1145–1151 (2011).
137. Mardin, B. R. & Schiebel, E. Breaking the ties that bind: New advances in centrosome biology. *J. Cell Biol.* 197, 11–18 (2012).
138. Bertran, M. T. *et al.* Nek9 is a Plk1-activated kinase that controls early centrosome separation through Nek6/7 and Eg5. *EMBO J.* 30, 2634–47 (2011).
139. Lawo, S. Centrosome and Mitotic Spindle Organization in Human Cells. (2013). at <https://tspace.library.utoronto.ca/handle/1807/43651>
140. Brito, D. A. & Rieder, C. L. Mitotic Checkpoint Slippage in Humans Occurs via Cyclin B Destruction in the Presence of an Active Checkpoint. *Curr. Biol.* 16, 1194–1200 (2006).
141. Gruss, O. J. *et al.* Ran induces spindle assembly by reversing the inhibitory effect of importin alpha on TPX2 activity. *Cell* 104, 83–93 (2001).
142. Ma, N., Titus, J., Gable, A., Ross, J. L. & Wadsworth, P. TPX2 regulates the localization and activity of Eg5 in the mammalian mitotic spindle. *J. Cell Biol.* 195, 87–98 (2011).
143. Gable, a. *et al.* Dynamic reorganization of Eg5 in the mammalian spindle throughout mitosis requires dynein and TPX2. *Mol. Biol. Cell* 23, 1254–1266 (2012).
144. Mayer, T. U. *et al.* Small molecule inhibitor of mitotic spindle bipolarity identified in a phenotype-based screen. *Science* 286, 971–4 (1999).
145. Klein, E., Debonis, S., Thiede, B. & Skoufias, D. A. New chemical tools for investigating human mitotic kinesin Eg5. 15, 6474–6488 (2007).
146. Kapoor, T. M., Mayer, T. U., Coughlin, M. L. & Mitchison, T. J. Probing spindle assembly mechanisms with monastrol, a small molecule inhibitor of the mitotic kinesin, Eg5. *J. Cell Biol.* 150, 975–988 (2000).
147. Hanahan, D. & Weinberg, R. a. Hallmarks of cancer: The next generation. *Cell* 144, 646–

674 (2011).
148. Jordan, M. A. & Wilson, L. MIicrotubules as a Target for Anticancer Drugs. 4, 253–265 (2004).
149. Van Vuuren, R. J., Visagie, M. H., Theron, A. E. & Joubert, A. M. Antimitotic drugs in the treatment of cancer. *Cancer Chemother. Pharmacol.* 76, 1101–1112 (2015).
150. Jackson, J. R., Patrick, D. R., Dar, M. M. & Huang, P. S. Targeted anti-mitotic therapies: can we improve on tubulin agents? *Nat. Rev. Cancer* 7, 107–17 (2007).
151. Mayer, T. U. *et al.* Small molecule inhibitor of mitotic spindle bipolarity identified in a phenotype-based screen. *Science* 286, 971–974 (1999).
152. Gartner, M. *et al.* Development and biological evaluation of potent and specific inhibitors of mitotic kinesin Eg5. *ChemBioChem* 6, 1173–1177 (2005).
153. Huszar, D., Theoclitou, M.-E., Skolnik, J. & Herbst, R. Kinesin motor proteins as targets for cancer therapy. *Cancer Metastasis Rev.* 28, 197–208 (2009).
154. Talapatra, S. K., Schuttelkopf, A. W. & Kozielski, F. The structure of the ternary Eg5-ADP-ispinesib complex. *Acta Crystallogr. Sect. D Biol. Crystallogr.* 68, 1311–1319 (2012).
155. U.S. National Institutes of Helath. ClinicalTrials.gov. at <https://clinicaltrials.gov/>
156. Lee, C. W. *et al.* A phase II study of ispinesib (SB-715992) in patients with metastatic or recurrent malignant melanoma: A National Cancer Institute of Canada Clinical Trials Group trial. *Invest. New Drugs* 26, 249–255 (2008).
157. Tang, P. A. *et al.* Phase II study of ispinesib in recurrent or metastatic squamous cell carcinoma of the head and neck. *Invest. New Drugs* 26, 257–264 (2008).
158. Beer, T. M. *et al.* Southwest Oncology Group phase II study of ispinesib in androgen-independent prostate cancer previously treated with taxanes. *Clin. Genitourin. Cancer* 6, 103–9 (2008).
159. Beekman, K. W. *et al.* University of Chicago Consortium phase II study of ispinesib (SB-715992) in patients (pts) with advanced renal cell carcinoma (RCC). *J. Clin. Oncol.* 25, 15573 (2007).
160. Shahin, M. S. *et al.* A phase II, open-label study of ispinesib (SB-715992) in patients with platinum/taxane refractory or resistant relapsed ovarian cancer. *J. Clin. Oncol.* 25, 5562 (2007).
161. El-Khoueiry, A. B. *et al.* A randomized phase II non-comparative study of Ispinesib given weekly or every three weeks in metastatic colorectal cancer. A California Cancer Consortium Study (CCC-P). *J. Clin. Oncol.* 24, 3595 (2006).
162. Theoclitou, M.-E. *et al.* Discovery of (+)- N -(3-Aminopropyl)- N -[1-(5-benzyl-3-methyl-4-oxo-[1,2]thiazolo[5,4- d]pyrimidin-6-yl)-2-methylpropyl]-4-methylbenzamide (AZD4877), a Kinesin Spindle Protein Inhibitor and Potential Anticancer Agent. *J. Med. Chem.* 54, 6734–6750 (2011).
163. ClinicalTrials.gov. at <https://clinicaltrials.gov/>
164. Thompson, L. L. & McManus, K. J. A Novel Multiplexed, Image-Based Approach to Detect Phenotypes That Underlie Chromosome Instability in Human Cells. *PLoS One* 10, e0123200 (2015).
165. Sajesh, B. V., Bailey, M., Lichtensztejn, Z., Hieter, P. & McManus, K. J. Synthetic Lethal Targeting of Superoxide Dismutase 1 Selectively Kills RAD54B-Deficient Colorectal Cancer Cells. *Genetics* 195, 757–767 (2013).
166. HT-1080 [HT1080] (ATCC ® CCL-121™). at <https://www.atcc.org/Products/All/CCL-121.aspx#characteristics>

167. Yuen, K. *et al.* Systematic genome instability screens in yeast and their potential relevance to cancer. *Proc. Natl. Acad. Sci. U. S. A.* 104, 3925–3930 (2007).
168. The Cancer Genome Atlas - Cancer Genome - TCGA. at <https://cancergenome.nih.gov/>
169. Cerami, E. *et al.* The cBio cancer genomics portal: an open platform for exploring multidimensional cancer genomics data. *Cancer Discov.* 2, 401–4 (2012).
170. Gao, J. *et al.* Integrative analysis of complex cancer genomics and clinical profiles using the cBioPortal. *Sci. Signal.* 6, pl1 (2013).
171. Canadian Cancer Society. Canadian Cnacer Statistics, 2016. (2016).
172. American Cancer Society. Cancer Facts & Figures 2016. *Cancer Facts Fig. 2016* 1–9 (2016). doi:10.1097/01.NNR.0000289503.22414.79
173. Cogan, N. *et al.* Mutation Research / Fundamental and Molecular Mechanisms of Mutagenesis DNA damaging bystander signalling from stem cells , cancer cells and fibroblasts after Cr (VI) exposure and its dependence on telomerase. 683, 1–8 (2010).
174. Zhu, H., Fang, K. & Fang, G. FAM29A, a target of Plk1 regulation, controls the partitioning of NEDD1 between the mitotic spindle and the centrosomes. *J. Cell Sci.* 122, 2750–2759 (2009).
175. Thompson, S. L. & Compton, D. A. Examining the link between chromosomal instability and aneuploidy in human cells. *J. Cell Biol.* 180, 665–72 (2008).
176. Kapoor, T. M., Mayer, T. U., Coughlin, M. L. & Mitchison, T. J. Probing spindle assembly mechanisms with monastrol, a small molecule inhibitor of the mitotic kinesin, Eg5. *J. Cell Biol.* 150, 975–88 (2000).
177. Heilman, S. a, Nordberg, J. J., Liu, Y., Sluder, G. & Chen, J. J. Abrogation of the postmitotic checkpoint contributes to polyploidization in human papillomavirus E7-expressing cells. *J. Virol.* 83, 2756–64 (2009).
178. McManus, K. J. & Thompson, L. L. A novel multiplexed, image-based approach to detect phenotypes that underlie chromosome instability in human cells. *PLoS One* 10, (2015).
179. Geigl, J. B., Obenauf, A. C., Schwarzbraun, T. & Speicher, M. R. Defining 'chromosomal instability'. *Trends Genet.* 24, 64–69 (2008).
180. Rajagopalan, H. *et al.* Inactivation of hCDC4 can cause chromosomal instability. *Nature* 428, 77–81 (2004).
181. Fodde, R. *et al.* Mutations in the APC tumour suppressor gene cause chromosomal instability. *Nat. Cell Biol.* 3, 433–438 (2001).
182. Tillement, V. *et al.* Spindle assembly defects leading to the formation of a monopolar mitotic apparatus. *Biol. Cell* 101, 1–11 (2009).
183. Maliga, Z. & Mitchison, T. J. Small-molecule and mutational analysis of allosteric Eg5 inhibition by monastrol. *BMC Chem. Biol.* 6, 2 (2006).
184. Kolodner, R. D. *et al.* Structure of the Human MLH1 Locus and Analysis of a Large Hereditary Nonpolyposis Colorectal Carcinoma Kindred for mlh1 Mutations Structure of the Human MLH1 Locus and Analysis of a Large Hereditary Nonpolyposis Colorectal Carcinoma Kindred for mihi Mutat. 242–248 (1995).
185. Sharma, G. G. *et al.* hTERT associates with human telomeres and enhances genomic stability and DNA repair. *Oncogene* 22, 131–46 (2003).
186. Kittler, R. *et al.* An endoribonuclease-prepared siRNA screen in human cells identifies genes essential for cell division. *Nature* 432, 1036–1040 (2004).
187. Topham, C. H. & Taylor, S. S. Mitosis and apoptosis: How is the balance set? *Curr. Opin. Cell Biol.* 25, 780–785 (2013).

188. Dalton, W. B., Nandan, M. O., Moore, R. T. & Yang, V. W. Human cancer cells commonly acquire DNA damage during mitotic arrest. *Cancer Res.* 67, 11487–11492 (2007).
189. Quignon, F. *et al.* Sustained mitotic block elicits DNA breaks: one-step alteration of ploidy and chromosome integrity in mammalian cells. *Oncogene* 26, 165–172 (2007).
190. Hain, K. O., Colin, D. J., Rastogi, S., Allan, L. A. & Clarke, P. R. Prolonged mitotic arrest induces a caspase-dependent DNA damage response at telomeres that determines cell survival. *Sci. Rep.* 6, 26766 (2016).
191. Huang, X., Tran, T., Zhang, L., Hatcher, R. & Zhang, P. DNA damage-induced mitotic catastrophe is mediated by the Chk1-dependent mitotic exit DNA damage checkpoint. *Proc. Natl. Acad. Sci. U. S. A.* 102, 1065–70 (2005).
192. Rieder, C. L. & Maiato, H. Stuck in Division or Passing through. *Dev. Cell* 7, 637–651 (2004).
193. Roschke, A. V. & Rozenblum, E. Multi-Layered Cancer Chromosomal Instability Phenotype. *Front. Oncol.* 3, 1–13 (2013).
194. Storchova, Z. & Pellman, D. From polyploidy to aneuploidy, genome instability and cancer. *Nat. Rev. Mol. Cell Biol.* 5, 45–54 (2004).
195. Fenech, M. *et al.* Molecular mechanisms of micronucleus, nucleoplasmic bridge and nuclear bud formation in mammalian and human cells. *Mutagenesis* 26, 125–132 (2011).
196. KUO, L. J. & YANG, L.-X. γ-H2AX - A Novel Biomarker for DNA Double-strand Breaks. *Vivo* 22, 305–309 (2008).
197. Nowak, M. A. *et al.* The role of chromosomal instability in tumor initiation. *Proc. Natl. Acad. Sci. U. S. A.* 99, 16226–31 (2002).
198. Gordon, D. J., Resio, B. & Pellman, D. Causes and consequences of aneuploidy in cancer. *Nat. Rev. Genet.* 13, 189–203 (2012).
199. Gerlinger, M. & Swanton, C. How Darwinian models inform therapeutic failure initiated by clonal heterogeneity in cancer medicine. *Br. J. Cancer* 103, 1139–1143 (2010).
200. Sajesh, B. V., Guppy, B. J. & McManus, K. J. Synthetic genetic targeting of genome instability in cancer. *Cancers (Basel).* 5, 739–761 (2013).
201. Kaelin, W. G. The concept of synthetic lethality in the context of anticancer therapy. *Nat. Rev. Cancer* 5, 689–98 (2005).
202. Measday, V. *et al.* Systematic yeast synthetic lethal and synthetic dosage lethal screens identify genes required for chromosome segregation. *Proc. Natl. Acad. Sci. U.S.A.* 102, 13956–13961 (2005).
203. Baetz, K., Measday, V. & Andrews, B. Revealing hidden relationships among yeast genes involved in chromosome segregation using systematic synthetic lethal and synthetic dosage lethal screens. *Cell Cycle* 5, 592–595 (2006).
204. Altschul, S. F. *et al.* Gapped BLAST and PSI-BLAST: A new generation of protein database search programs. *Nucleic Acids Res.* 25, 3389–3402 (1997).
205. Geiser, J. R. *et al.* Saccharomyces cerevisiae genes required in the absence of the CIN8-encoded spindle motor act in functionally diverse mitotic pathways. *Mol. Biol. Cell* 8, 1035–1050 (1997).
206. Yates, A. *et al.* Ensembl 2016. *Nucleic Acids Res.* 44, D710–D716 (2016).
207. Weizmann Institute of Science. GeneCards - HUMAN GENE DATABASE. at <http://www.genecards.org/>
208. Imamura, Y. *et al.* Comparison of 2D- and 3D-culture models as drug-testing platforms in breast cancer. *Oncol. Rep.* 33, 1837–1843 (2015).

209. Chauvière, M., Kress, C. & Kress, M. Disruption of the mitotic kinesin Eg5 gene (Knsl1) results in early embryonic lethality. *Biochem. Biophys. Res. Commun.* 372, 513–519 (2008).
210. Hofker, M. H. & van Deursen, J. M. *Transgenic Mouse Methods and Protocols*. *Methods in Molecular Biology* 693, (2011).
211. Donehower, L. A. The p53-deficient mouse: a model for basic and applied cancer studies. *Semin. Cancer Biol.* 7, 269–278 (1996).

APPENDIX A: SOLUTIONS

CELL CULCURE

10×PBS (Stock Solution)

Name	Amount
NaCl	80.0 g
KCl	2.0 g
Na_2HPO_4	14.4 g
KH_2PO_4	2.4 g
ddH_2O	800.0 mL
Titrate	
ddH_2O	Up to 1.0 L total volume
Total Volume	1.0 L

-titrate to pH 7.4

1×PBS

Name	Amount
10×PBS (stock)	100.0 mL
ddH_2O	900.0 mL
Total Volume	1.0 L

PROTEIN SILENCING

1×siRNA Buffer

Name	Amount
5×siRNA Buffer	100.0 μL
DEPC-treated Water	40.0 μL
Total Volume	500.0 μL

WESTERN BLOT

Modified RIPA Buffer

Name	Amount
50 mM Tris Base – pH 8.0	5.0 mL
150 mM NaCl	7.5 mL
0.1% SDS	500.0 μL
0.5% Sodium Deoxycholate	0.5 g
1% NP40	1.0 mL
Milli-Q water	up to 100.0 mL total volume
Total Volume	100.0 mL

5× SDS/DTT Sample Buffer

Name	Amount
Glycerol	12.0 mL
Dithiothreitol	1.5 g
SDS	2.0 g
2M Tris-HCl – pH 6.8	2.5 mL
Bromophenol Blue	until desired colour is reached
Milli-Q water	up to 20.0 mL total volume
Total Volume	20.0 mL

10× Running Buffer

Name	Amount
Tris Base	30.0 g
Glycine	144.0 g
SDS	10.0 g
Milli-Q water	up to 1.0 L total volume
Total Volume	1.0 L

1× Running Buffer

Name	Amount
10× Running Buffer	100.0 mL
Milli-Q water	900.0 mL
Total Volume	1.0 L

Transfer Buffer

Name	Amount
10× Running Buffer	50.0 mL
Methanol	100.0 mL
Milli-Q water	350.0 mL
Total Volume	500.0 mL

Copper phthalocyanine 3,4′,4″,4‴-tetrasulfonic acid tetrasodium salt (CPTS)

Name	Amount
CPTS	50.0 mg
HCl	1.0 mL
Milli-Q water	899.0 mL
Total Volume	1.0 L

5% None-fat Milk

Name	Amount
Skimmed Milk Powder (Carnation)	5.0 g
TBST	100.0 mL
Total Volume	100.0 mL

TBS-Tween20 (TBST)

Name	Amount
10× TBS	100.0 mL
Tween-20	1.0 mL
Milli-Q water	899.0 mL
Total Volume	1.0 L

10× Tris Buffered Saline (TBS)

Name	Amount
NaCl	80.0 g
KCl	2.0 g
1 M Tris pH – 7.5	250.0 mL
Milli-Q water	up to 1.0 L total volume
Total Volume	1.0 L

INDIRECT IMMUNOFLUORESCENCE LABELLING

4% Paraformaldehyde

Name	Amount
Paraformaldehyde (VWR Canlab)	0.4 g
1×PBS	up to 10.0 mL total volume
Total Volume	1.0 L

-bring to slight boil with mixing
-allow to cool prior to use

PBS 0.5% Triton X-100

Name	Amount
Triton X-100	5.0 mL
1×PBS	995.0 mL
Total Volume	1.0 L

PBS 0.1% Triton X-100

Name	Amount
Triton X-100	1.0 mL
1×PBS	999.0 mL
Total Volume	1.0 L

Mounting Media + DAPI

Name	Amount
Vectashield Mounting Media	1.0 mL
DAPI (50 μg/mL)	10.0 μL
Total Volume	1.0 mL

FLOW CYTOMETRY

Propidium Iodide (Stock Solution)

Name	Amount
Propidium Iodide (Fisher Scientific)	1.0 mg
Milli-Q water	1.0 mL
Total Volume	1.0 mL

-store at -20ºC away from light

70% Ethanol (Fixative)

Name	Amount
95% Ethanol	737.0 mL
ddH_2O	263.0 mL
Total Volume	1.0 L

RNase A (Stock Solution)

Name	Amount
RNase A (Fisher Scientific)	1.0 mg
Milli-Q water	1.0 mL
Total Volume	1.0 mL

-store at -20ºC

MITOTIC CHROMOSOME SPREAD

1M KCl (Stock Solution)

Name	Amount
KCl	7.5 g
ddH_2O	up to 100.0 mL total volume
Total Volume	10.0 mL

75mM KCl (Hypotonic Solution)

Name	Amount
1M KCl	750.0 μL
ddH_2O	up to 10.0 mL total volume
Total Volume	10.0 mL

3:1 Methanol:Acetic Acid (Fixative)

Name	Amount
Methanol	3.0 mL
Acetic Acid	1.0 mL
Total Volume	4.0 L

APPENDIX B: SUPPLEMENTRY TABLES

Table S6-1: Student's *t*-tests Identifying Statistical Differences in the Nuclear Area of Cells Following *KIF11* Silencing Relative to the Controls

			Nuclear Area (μm^2)			
Cell Line	**siRNA Treatment**	**N[A]**	**Mean**	**SD[B]**	**Fold Increase[C]**	**p-value[D]**
HCT116	Untransfected	100	209.9	52.3	0.9	0.6636
	si*GAPDH*	100	213.0	47.0	N/A	N/A
	si*KIF11*-Pool	100	556.6	345.8	2.6	< 0.0001
	si*KIF11*-1	100	688.8	527.1	3.2	< 0.0001
	si*KIF11*-3	100	384.4	220.0	1.8	< 0.0001
hTERT	Untransfected	100	233.2	48.3	0.9	0.8774
	si*GAPDH*	100	234.3	55.7	N/A	N/A
	si*KIF11*-Pool	100	409.6	92.7	1.7	< 0.0001
	si*KIF11*-1	100	370.1	115.9	1.5	< 0.0001
	si*KIF11*-3	100	491.9	189.9	2.0	< 0.0001

[A]Number of nuclei analyzed = N
[B]Standard Deviation = SD
[C]Fold increase in mean NA relative to the si*GAPDH* negative control (N/A; not applicable)
[D]*p*-values calculated for each condition relative to si*GAPDH* with *p*-values < 0.05 are considered statistically significant

Table S6-2: KS Test Reveals Statistical Significant Increases in the Total Distribution Range of Nuclear Areas Following *KIF11* Silencing Relative to si*GAPDH*

Cell Line	Treatment	si*GAPDH*	si*KIF11*-Pool	si*KIF11*-1	si*KIF11*-3
HCT116	Untransfected	0.6994	< 0.0001	< 0.0001	< 0.0001
	si*GAPDH*	N/A	< 0.0001	< 0.0001	< 0.0001
	si*KIF11*-Pool		N/A	0.2106	< 0.0001
	si*KIF11*-1			N/A	< 0.0001
hTERT	Untransfected	0.9671	< 0.0001	< 0.0001	< 0.0001
	si*GAPDH*	N/A	< 0.0001	< 0.0001	< 0.0001
	si*KIF11*-Pool		N/A	0.0023	0.0002
	si*KIF11*-1			N/A	< 0.0001

Presented are the *p*-values calculated from two-treatment KS tests for the indicated pairs with *p*-values < 0.05 are considered statistically significant

Table S6-3: Changes in DNA Content Following *KIF11* Silencing Relative to the Controls

Cell Line	siRNA Treatment	DNA Content (percentage)				
		<2C	**2C**	**2C<x>4C**	**4C**	**>4C**
HCT116	Untransfected	1.87	74.40	13.80	9.34	0.64
	siNon-targeting	3.16	69.20	17.10	9.82	0.52
	si*KIF11*	1.45	51.60	13.60	18.0	15.3
hTERT	Untransfected	0.04	75.10	12.30	11.30	0.75
	siNon-targeting	0.60	73.40	12.60	13.40	0.98
	si*KIF11*	3.56	10.90	8.66	64.10	12.6

Table S6-4: Student's *t*-tests Identifying Statistical Differences in the Number of Chromosomes Following *KIF11* Silencing Relative to the Controls

			Chromosome Number			
Cell Line	**siRNA Treatment**	**N[A]**	**Mean**	**SD[B]**	**Fold Increase[C]**	**p-value[D]**
HCT116	Untransfected	100	45.5	10.2	0.9	0.9199
	si*GAPDH*	100	45.6	7.8	N/A	N/A
	si*KIF11*-Pool	100	85.3	57.6	1.8	< 0.0001
	si*KIF11*-1	100	77.1	49.9	1.6	< 0.0001
	si*KIF11*-3	100	79.5	55.7	1.7	< 0.0001
hTERT	Untransfected	100	47.5	8.8	1.0	0.5174
	si*GAPDH*	100	46.7	7.4	N/A	N/A
	si*KIF11*-Pool	100	69.0	28.1	1.4	< 0.0001
	si*KIF11*-1	100	54.5	32.6	1.1	0.0210
	si*KIF11*-3	100	66.6	21.4	1.4	< 0.0001

[A]Number of nuclei analyzed = N
[B]Standard Deviation = SD
[C]Fold increase in mean NA relative to the si*GAPDH* negative control (N/A; not applicable)
[D]*p*-values calculated for each condition relative to si*GAPDH* with *p*-values < 0.05 are considered statistically significant

Table S6-5: KS Test Reveals Statistical Significant Changes in Cumulative Distribution Frequency of Chromosomes Following *KIF11* Silencing Relative to si*GAPDH*

Cell Line	Treatment	si*GAPDH*	si*KIF11*-Pool	si*KIF11*-1	si*KIF11*-3
HCT116	Untransfected	> 0.9999	< 0.0001	< 0.0001	< 0.0001
	si*GAPDH*	N/A	< 0.0001	< 0.0001	< 0.0001
	si*KIF11*-Pool		N/A	0.6994	0.8127
	si*KIF11*-1			N/A	0.6994
hTERT	Untransfected	0.0541	< 0.0001	0.2809	< 0.0001
	si*GAPDH*	N/A	< 0.0001	0.0541	< 0.0001
	si*KIF11*-Pool		N/A	< 0.0001	0.6994
	si*KIF11*-1			N/A	< 0.0001

Presented are the *p*-values calculated from two-treatment KS tests for the indicated pairs with *p*-values < 0.05 are considered statistically significant

Table S6-6: Comparing the Effect of Single Dose and Double Dose Monastrol Treatment on the Nuclear Area of HCT116 and hTERT Cells Relative to the Controls

			Nuclear Area (μm^2)			
Cell Line[A]	**Treatment**	**N[B]**	**Mean**	**SD[C]**	**Fold Increase[D]**	**p-value[E]**
HCT116	Untreated	200	240.6	76.2	1.0	0.1384
	DMSO	200	229.7	70.7	N/A	N/A
	$Monastrol_1$	200	350.7	210.8	1.5	< 0.0001
	$Monastrol_2$	140	440.4	235.5	1.9	< 0.0001
hTERT	Untreated	100	235.7	62.1	1.0	0.0747
	DMSO	100	220.8	55.7	N/A	N/A
	$Monastrol^1$	100	411.8	214.7	1.8	< 0.0001
	$Monastrol_2$	100	401.8	268.2	1.8	< 0.0001

[A]H = HCT116, h = hTERT
[B]Number of nuclei analyzed = N
[C]Standard Deviation = SD
[D]Fold increase in mean NA relative to the DMSO negative control (N/A; not applicable)
[E]*p*-value of each condition relative to DMSO

Table S6-7: Statistical Changes in the Nuclear Area of Monastrol Treated Cells Compared to the Controls Identified Through Student's *t*-test

			Nuclear Area (μm^2)			
Cell Line[A]	**Treatment**	**N[B]**	**Mean**	**SD[C]**	**Fold Increase[D]**	**p-value[E]**
HCT116	Untreated	100	239.3	91.48	1.0	0.1106
	DMSO	100	220.7	71.47	N/A	N/A
	Monastrol	100	422.3	169.6	1.9	< 0.0001
hTERT	Untreated	100	235.7	62.1	1.0	0.0747
	DMSO	100	220.8	55.7	N/A	N/A
	Monastrol	100	411.8	214.7	1.8	< 0.0001

[A]H = HCT116, h = hTERT
[B]Number of nuclei analyzed = N
[C]Standard Deviation = SD
[D]Fold increase in mean NA relative to the DMSO negative control (N/A; not applicable)
[E]*p*-value of each condition relative to DMSO

Table S6-8: KS Test Reveals Statistical Significant Increases in the Total Distribution Range of Nuclear Areas Following KIF11 Inhibition Relative to DMSO

Cell Line	Treatment	DMSO	Monastrol
HCT116	Untreated	0.2809	< 0.0001
	DMSO	N/A	< 0.0001
hTERT	Untreated	0.0243	< 0.0001
	DMSO	N/A	< 0.0001

Presented are the *p*-values calculated from two-treatment KS tests for the indicated pairs with *p*-values < 0.05 are considered statistically significant

Table S6-9: Student's *t*-tests Identifying Statistical Differences in the Number of Chromosomes Following Monastrol Treatment Relative to the Controls

			Chromosome Number			
Cell Line	**siRNA Treatment**	**N[A]**	**Mean**	**SD[B]**	**Fold Increase[C]**	**p-value[D]**
HCT116	DMSO	100	45.0	5.1	N/A	N/A
	Monastrol	100	93.9	30.0	2.0	< 0.0001
hTERT	DMSO	100	46.2	4.5	N/A	N/A
	Monastrol	100	61.1	20.6	1.3	< 0.0001

[A]Number of nuclei analyzed = N

[B]Standard Deviation = SD

[C]Fold increase in mean NA relative to the DMSO negative control (N/A; not applicable)

[D]*p*-values calculated for each condition relative to DMSO with *p*-values < 0.05 are considered statistically significant

Table S6-10: KS test Reveals Statistical Significant Increases in the Distribution Range of Chromosomes in Monastrol Treated Cells Relative to DMSO

Cell Line	Treatment	DMSO	Monastrol
HCT116	DMSO	N/A	< 0.0001
hTERT	DMSO	N/A	< 0.0001

Presented are the *p*-values calculated from two-treatment KS tests for the indicated pairs with *p*-values < 0.05 are considered statistically significant